

**Modification of *Vibrio cholerae* Quorum Sensing Receptors
with Autoinducer Substrate Analogs**

Vineet Tyagi

Submitted in Partial Fulfillment
of the Requirements of the
Degree of
Bachelor of Arts

To the Department of Chemistry
of
Princeton University

April 18, 2011

© by Vineet Tyagi, 2011. All rights reserved.

I hereby declare that I am the sole author of this thesis, and that this thesis represents my own work in accordance with University regulations.

Signature

Acknowledgements

I would like to thank Martin Semmelhack for allowing me to join his lab group. His mentorship throughout my projects has been invaluable. I would also like to thank Lark Perez for his willingness to answer any and all questions; his desire to teach and impart knowledge is clear and I am glad to have been given the chance to work with him. I would also like to thank my fellow lab members, especially Eric Kim, for some memorable moments and humor which interspersed lab work. I would like to thank the Princeton University Department of Chemistry and the Semmelhack laboratory for funding for my work.

Most importantly, I would like to dedicate this thesis to my parents, who have continually shown their support for any and all of my endeavors.

Abstract

Quorum sensing is a cooperative behavior through which bacteria communicate with members of the same and other species. Using quorum sensing, these bacteria determine when to initiate biofilm formation, virulence, and defense responses. This mechanism depends upon the synthesis of signaling molecules which activate a pathway that causes the transcription of certain genes. *Vibrio cholerae*, which is pathogenic, employs this quorum sensing mechanism. Work has been done at Princeton University to determine the structure of the autoinducer used by these pathogens; the native autoinducer is known as cholera autoinducer-1 (CAI-1). This molecule consists of a polar head group and a long, non-polar alkyl chain. Efforts have been made to synthesize analogs of the molecule in order to induce interactions with amino acid side chains located in the quorum sensing receptor binding pockets; a particularly strong binding interaction might lead to agonist or antagonist activity. Another goal is the preparation of water soluble analogs, which may be more effective in the application of such agonists or antagonists in treating cholera infections. The primary goal of the project is to covalently modify a cysteine residue in the active site of the receptor to allow for irreversible binding and interference with the quorum sensing response. The synthesized analogs are designed to have an electrophilic group susceptible for bimolecular nucleophilic substitution by the sulfur of the cysteine side chain. A series of terminal epoxides, isothiocyanates, and one terminal bromide were synthesized and tested. Another goal of this project is to elucidate the structure of the CqsS receptor. This can be done by synthesizing molecules which are locked in a certain conformation using unsaturated alkyl chains. A series of alkyne and alkene chains were synthesized. These molecules will be used in the future to make analog molecules to be tested by bioassay.

Table of Contents

1 Introduction to Quorum Sensing	1
Bibliography	18
2 Introduction to Cholera	20
2.1 Background	20
2.2 Symptoms	20
2.3 Molecular Mechanisms of Infection	21
2.4 Treatment Options	22
2.4.1 Oral Rehydration Therapy	22
2.4.2 Antibiotics	24
2.4.3 Antidiarrheal Agents	26
Bibliography	28
3 Experimental Rationale	29
4 CqsS Receptor Structure Elucidation	33
4.1 Solid Phase Synthesis	33
4.2 Syntheses	34
4.2.1 Issues with <i>Z</i> -Alkene Formation	34
4.2.2 Issues with <i>E</i> -Alkene Formation	46
4.3 Results	49
4.4 Conclusion	50

4.5 Future Directions.....	50
5 Covalent Modification of <i>Vibrio cholerae</i> CqsS.....	52
5.1 Use of TBS Protection Groups	52
5.2 Issues with Bis-silylation.....	53
5.3 Syntheses	63
5.3.1 Synthesis of Terminal Alpha-Chloro Amide Analogs.....	64
5.3.2 Potential Alternate Synthesis of Terminal Bromide Molecules	72
5.4 Results	76
5.4.1 Bioassay Results	77
5.4.2 Drug-like Properties of Synthesized Molecules	80
5.5 Conclusion	83
5.6 Future Directions.....	84
6 Synthetic Procedures	88
6.1 CqsS Receptor Structure Elucidation Procedures	89
6.2 Covalent Modification of <i>Vibrio cholerae</i> CqsS Procedures	96
Appendices.....	102
Appendix A: CqsS Receptor Structure Elucidation Spectra	102
Appendix B: Covalent Modification of <i>Vibrio cholerae</i> CqsS Spectra.....	121

List of Figures, Charts, and Tables

Chapter 1: Introduction to Quorum Sensing

Figure 1.1: AI-2 Signal Transduction Pathway	2
Figure 1.2: Pathway Proposed by Schauder and Bassler	4
Figure 1.3: Activity of Fe-substituted Enzyme	9
Figure 1.4: Potent Inhibitors of LuxS Activity	12
Figure 1.5: Cholera Quorum Sensing at Low Cell Density	15
Figure 1.6: Cholera Quorum Sensing at High Cell Density	16

Chapter 2: Introduction to Cholera

Chapter 3: Experimental Rationale

Figure 3.1: Structure of Native CAI-1 Molecule	29
Figure 3.2: General Esterification Mechanism Catalyzed by DMAP	30
Figure 3.3: Covalent Modification of Cysteine Residue in CqsS	31
Figure 3.4: (a) Straight Chain in CqsS (b) Folded Chain in CqsS	31

Chapter 4: CqsS Receptor Structure Elucidation

Figure 4.1: Synthesis of Alkyne Molecules	34
Figure 4.2: 2-Z-Isomer Formation from 2-Alkyne	34
Figure 4.3: Potential Acetylation of 2-Z-Alkene	35
Figure 4.4: Potential Alkene Shift followed by Tautomerization	35
Figure 4.5: Overlap of 2 Hour Reaction Mixture and Pure 2-E-octen-1-ol	37

Figure 4.6: Alkyne Reduction to form Z-Isomer	42
Figure 4.7: Step Motif on Surface of Lindlar Catalyst	43
Figure 4.8: Alternate Synthesis for 2-Z-Isomer.....	45
Figure 4.9: Alternate Synthesis for 3-E-Alkene	50
Figure 4.10: Transesterification Sequence	51
Chart 4.1: Alkyne Fraction as a Function of Sodium Equivalents	47
Table 4.1: Reduction Reaction Mixtures for Various Time Points	39
Table 4.2: Alpha-Hydroxyl Methylene Peaks for Time Series Reactions	40
Table 4.3: Reduction Reaction Mixtures for Various Sodium Equivalents	47
Table 4.4: Alkyne and Alkene Chains Available for Coupling	49
 Chapter 5: Covalent Modification of <i>Vibrio cholerae</i> CqsS	
Figure 5.1: Silylation Mechanism	52
Figure 5.2: Silyl Deprotection Mechanism Using TBAF	53
Figure 5.3: Procedure for Synthesis of Free, Mono-Silylated Carboxylic Acid	53
Figure 5.4a: Mixture of Bis-Silylated and Mono-Silylated Molecules.....	55
Figure 5.4b: NMR Peaks for Methine Protons in 4.2 ppm Range	56
Figure 5.4c: NMR Peaks for Carbons Bearing Methine Proton	57
Figure 5.5: Mixture of Products from Selective Deprotection Reaction	57
Figure 5.6: Alternative Synthesis Scheme for Free, Mono-Silylated Carboxylic Acid.	58
Figure 5.7: Ethyl Ester, with Characteristic Protons.....	59

Figure 5.8: Mixture of Attempted Selective Ethyl Ester Deprotection	60
Figure 5.9: Mechanism for Acid Chloride Formation	61
Figure 5.10: Attempted Synthesis Sequence for Alpha-Chloro Ester Analogs	63
Figure 5.11: Synthesis Sequence for Alpha-Chloro Amide Analogs	63
Figure 5.12: Synthesis Sequence for Terminal Epoxide Analogs	64
Figure 5.13: Synthesis Sequence for Terminal Isothiocyanate Analogs	64
Figure 5.14: Potential Mechanism for Terminal Hydroxyl Formation	67
Figure 5.15: Formation of Alpha-Chloro Analogs	68
Figure 5.16: Potential Folding of Terminal Hydroxyl Molecule	69
Figure 5.17: Protonation of Terminal Amine Molecule	72
Figure 5.18: Alternate Synthesis Sequence for Terminal Bromide Analogs	73
Figure 5.19: Mixture of Products from Convergent Synthesis Approach	74
Figure 5.20: Bioassay Results.....	77-78
Figure 5.21: Covalent Modification with Terminal Aziridine Analogs.....	85
Figure 5.22: Covalent Modification with Terminal Lactone Analogs	86
Table 5.1: Synthesized Molecules for Covalent Modification	76
Table 5.2: Chemical Properties of Synthesized Molecules	81

1 Introduction to Quorum Sensing

Bacteria, which comprise the oldest known life forms on Earth, were long thought to be isolated organisms that operated on an individual basis. This all changed with the discovery of *Vibrio harveyi*, a group of marine bacteria that exhibited bioluminescent characteristics. It is important to note, however, that clusters of bacteria only emitted light once a critical density was reached. This phenomenon, labeled quorum sensing, dispelled the once commonly accepted idea that bacteria had only limited communication with one another. The next step in the study of bacterial interactions was to find the mechanism by which the bacteria were communicating.

In the initial studies done on *Vibrio harveyi*, it was found that the bacteria were communicating using a molecule called autoinducer-1 (AI-1). The mechanism by which this molecule functioned was to activate a dephosphorylation cascade. This pathway triggered the repressor for the bioluminescence gene (LuxCDABE) to be deactivated, thus allowing light to be emitted. At first, it was thought that this was the primary mechanism through which this signaling occurred. To test this, the gene was inhibited, but the bacteria still demonstrated luminescent characteristics once a threshold cell density was reached. This indicated the possibility that there was an alternate pathway that could feed into the AI-1 system.^[1]

Another autoinducer, known as AI-2, was found to be the signaling molecule for this different mechanism. *S*-Ribosylhomocysteinase (LuxS) breaks a thioester bond in *S*-ribosylhomocysteine (SRH) and forms L-homocysteine and 4,5-dihydroxy-2,3-

pentanedione (DPD). DPD is thought to be a precursor to AI-2, which binds to the LuxP receptor protein located in the periplasm (between the inner cytoplasmic membrane and the outer phospholipid bilayer) of the cell. The AI-2/LuxP complex then binds to another protein, LuxQ, which is located inside the cell. Once this interaction occurs, LuxQ changes function and become a phosphatase (which breaks phosphate bonds) instead of a kinase (which phosphorylates molecules); this is essential because it can switch on the dephosphorylation pathway that is key to the AI-1 signal.^[2]

An important finding about AI-2 is that its use is conserved among a large range of bacterial species, indicating that it may be a “universal” signaling molecule. This implies that a process that somehow regulates AI-2 could have applications as a method of bacterial growth control. Figure 1.1 illustrates the mechanism by which AI-2 enters the cell and initiates a signal transduction pathway:

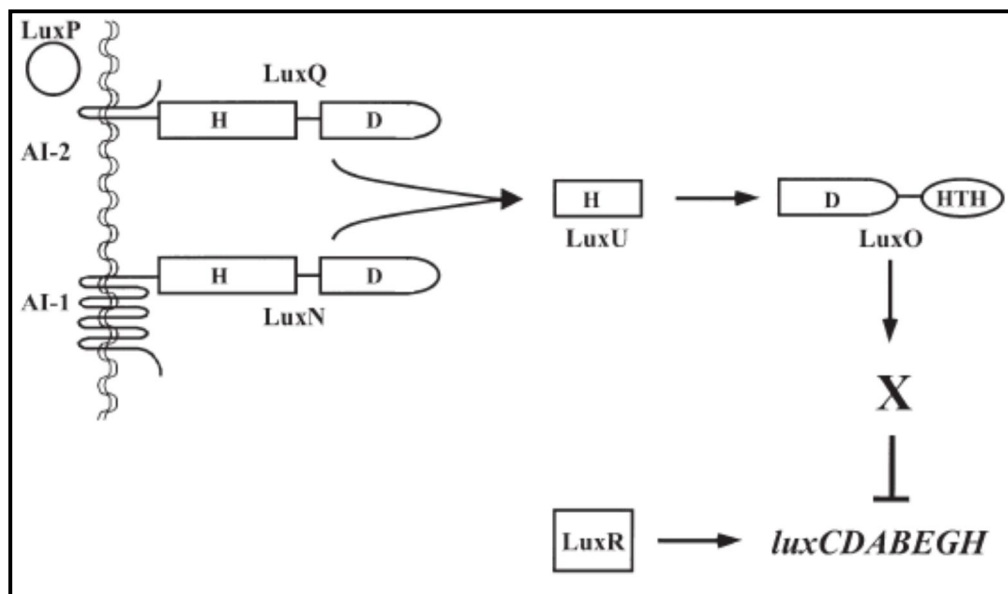


Figure 1.1: AI-2 Signal Transduction Pathway

Based on the knowledge of the biological pathway of AI-2, there seemed to be three options to prevent the signaling cascade that allowed quorum sensing by interfering with its critical steps. The first solution would be to prevent the binding of AI-2 to the LuxP receptor. This would completely prohibit the entrance of AI-2 into the cell, and thus avoid any possibly further interactions. Another possible solution would be to prevent binding of the AI-2/LuxP complex to LuxQ. This would also prevent the formation of the critical complex needed to begin the transduction pathway. The final solution would be to inhibit the function of LuxS, which is needed to produce AI-2. This can be done by either 1) deforming the enzyme itself so that its active site conformation no longer catalyzes the production of AI-2 or by 2) creating some kind of molecule that inhibits the binding of substrate to the LuxS protein.

A study was done at Princeton University by Stephan Schauder and Bonnie L. Bassler to determine the mechanism by which AI-2 was formed, which would be critical to somehow inhibiting AI-2 function. It was noted that the LuxS gene was not consistent in its location among chromosomes, but in one species (*Borrelia burgdorferi*), LuxS was found to be at the terminal position of a three gene sequence. Based on this, it was thought that LuxS might work in coordination with the two genes preceding it. These genes, *metK* and *pfs*, are known to be activated in the production of S-adenosylmethionine (SAM). SAM is used to methylate other molecules and subsequently forms S-adenosylhomocysteine (SAH). SAH prevents the use of SAM as a methylating agent, which is critical for several bacterial functions. The *pfs* gene then converts SAH to SRH, which is then further metabolized into DPD and homocysteine, as mentioned

above. The homocysteine can then be methylated to form methionine, which can be used to form SAM. SAM then undergoes a decarboxylation reaction to form methylthioadenosine (MTA), which reacts further with pfs to form methylthioribose (MTR). Schauder and Bassler figured that based on their genomic reasoning, LuxS could be part of the SAM to DPD series or part of the SAM to MTR reactions since metK and pfs were used in those pathways.

In order to determine which reaction set LuxS played a role in, Schauder and Bassler created two strains of *S. typhimurium*, one carrying the LuxS gene and one without; arabinose was added to the growth broth. The cells were then lysed and SAM, SAH, SRH, and MTA were added to the extract. To test for AI-2 activity, an assay which tested the luminescence of *Vibrio harveyi* was used. The results showed that MTA did not induce a large increase in light production, whereas SAM, SAH, and SRH did; the largest increase was seen in the addition of SRH to the lysate mixture. These results indicated that LuxS was a component in the SAM to DPD pathway. Figure 1.2 shows this pathway of LuxS proposed by Schauder and Bassler:

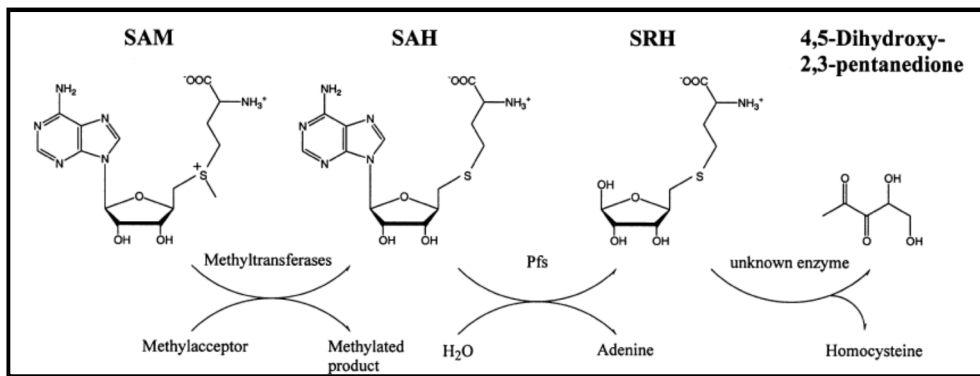


Figure 1.2: Pathway Proposed by Schauder and Bassler

Once this was confirmed, Schauder and Bassler continued their study to determine whether LuxS and pfs were the only enzymes needed to form DPD from SAH. To do so, various combinations of the enzymes and substrates were prepared. The controls consisted of the substrates with no enzymes added, and they yielded a fourfold increase in light production in the AI-2 bioassay. The largest increase was seen in the addition of pfs and LuxS to SAH (over eighty thousand fold). When SRH was added to pfs, a seventy fold increase was seen, as opposed to a twenty seven thousand fold increase when added to LuxS. This assay shows that LuxS is the major enzyme needed for the production of the AI-2 molecule.

Another problem related to studying LuxS is that it is unstable, and when exposed to air, denatures. Related to this problem is the inherent difficulty in assaying for LuxS activity. Based on the knowledge of the pathway of LuxS, it is known that DPD and homocysteine are formed. DPD is difficult to detect, but homocysteine could easily be detected because of its thiol group. Using the Ellman's test, Schauder and Bassler were able to determine the amount of homocysteine present in solution. To test for the concentration of homocysteine, Ellman's reagent [5,50-dithio-bis-(2-nitrobenzoic acid)] is added to the solution being tested; this reagent binds to free thiol groups, such as those on homocysteine, to form a colored product which optimally absorbs light at a wavelength of 412 nanometers. Based on a spectrophotometric approach, the concentration of homocysteine can be determined. This directly correlated to the amount of DPD produced, and therefore, to the level of activity of LuxS.^[3]

However, there are still difficulties in using homocysteine as an indirect indication of LuxS activity. As Bassler noted, homocysteine is unstable at temperatures near 37°C. This instability leaves room for error and slightly skewed results since this assay for LuxS activity relates directly to homocysteine concentrations. If homocysteine has degraded before the Ellman's test is performed, the reported levels of DPD production and LuxS activity would be lower than actual levels. Studies done by Dehua Pei of Ohio State University developed an alternate way to test for activity. In his work, Pei proposed using a fluorescence resonance energy transfer (FRET) sensor which would be attached to the LuxP receptor protein, which changes conformation when ligand, which in this case is DPD, binds to it. Once this structural alteration occurs, the amount of energy transferred between the two ends of the sensor decreases. This change in energy can be quantified, and used as a DPD detector. In the same manner that the Ellman's test relates homocysteine concentration to activity, the concentration of DPD can be directly related to the bioactivity of LuxS. This assay provided a quantitative method which could be used to understand quorum sensing.^[4] It is important to note a potential weakness of this tool. Because many small molecules can interact with the LuxP surface receptor, the conformation of the protein can change when binding to molecules other than AI-2 or DPD. This can cause false signals, known as background, which may give the impression that LuxS activity levels are higher than they truly are. This innovative assay illustrates the difficulties of accurately finding an effective method to find LuxS activity. Nevertheless, this assay provides valuable insight and is important to characterizing levels of LuxS activity.

In order to control the reactions facilitated by the LuxS protein, the mechanism of formation of AI-2 would need to be known. In 2001, Mark T. Hilgers and Martha L. Ludwig of the University of Michigan conducted experiments aimed to find the structure of the LuxS protein. In order to do so, they used a cloning and mutagenesis strategy intended to purify the protein so that its structure could be studied. First, the LuxS gene from *B. subtilis* was amplified by the polymerase chain reaction. DNA primers were included in the sequence so that it could be inserted into an expression vector, which was subsequently transformed into bacteria. The first attempt, which was unsuccessful, yielded a protein that did not crystallize. The following attempt to purify the protein was done without the coding for a hexahistidine tag at the C-terminus of the peptide chain. The vector with the PCR product was then inserted into competent *E. coli* cells, which were incubated at 37°C. The cells were then sonicated, and the protein products were eluted at various concentrations of potassium chloride salts.^[5]

This yielded several fractions of the LuxS protein, which were then further purified by another purification stage in a different buffer. The identity of the protein was confirmed to be LuxS by sodium dodecyl sulfate polyacrylamide gel electrophoresis (SDS-PAGE) and amino acid sequencing. Once the protein was purified and its identity confirmed, crystals were formed at 22°C and subjected to x-rays from a rotating source. The diffraction patterns were then studied to find the structure of the protein itself.^[6]

The results of this procedure showed that the quaternary structure of LuxS consisted of four β -sheets surrounded by five α -helices. Examinations of similar sequences done prior to structure analysis confirmed the findings that the folding pattern

of LuxS was novel. Hilgers and Ludwig also found that LuxS was a homodimer with two active sites, each of which had a relatively large area that was accessible to solvents.

Another important finding deals with the conservation of certain amino acids in the primary structure. The alignment of twenty six sequences of LuxS found that twenty three amino acids were conserved, which meant that these residues might be key to the active site, and thus, formation of AI-2. Analysis showed that a zinc cofactor is present and that the active site is highly polar. The reactive volume available to the substrate was found to be relatively low (approximately 90 \AA^3). This would mean that the reactive functional groups of AI-2 would have to be small enough to enter the active site in the proper conformation and were probably polar as well. It seemed from the findings of Hilgers and Ludwig that the catalytic formation of AI-2 was dependent on a zinc ion.

Studies done by Pei of Ohio State University then found largely contrasting results. According to his study, Pei used techniques similar to those in the previous study to isolate and purify the LuxS protein. A metal affinity column was used to separate the protein fraction from the lysate, followed by SDS-PAGE to collect the portions with significant quantities of LuxS. LuxS proteins substituted with Zn (II), Co(II), and Fe(II) were also synthesized. An assay was then run to test for the relative inactivity levels of each of LuxS in the presence of enzymes with substituted cofactors. SRH was mixed with each LuxS/substitute and at various time points, a portion of the solution was removed to be tested in a UV-VIS spectrophotometer.^[7]

Tests were also done by Pei to analyze the relation between the ferrous iron content and the activity of LuxS. Iron-substituted LuxS was incubated at room temperature in the presence of atmospheric oxygen in order to allow oxidation to occur. At various timepoints, solution was withdrawn and tested for ferrous iron content as well as catalytic activity. To test for the content of ferrous and ferric iron, absorbance readings were taken in a UV-VIS spectrophotometer at 510 nm and 480 nm, respectively. Figure 1.3 shows the activity of the FE-substituted enzyme as a function of time, as well as the relative content of both forms of ionic iron:

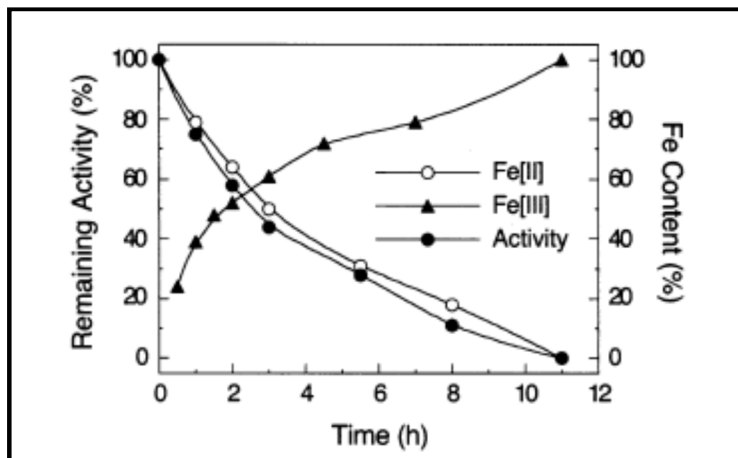


Figure 1.3: Activity of Fe-substituted Enzyme

If Fe(II) was the necessary cofactor, activity should have decreased as oxidation time increased (converting more ferrous iron to ferric iron). It was found that the activity of the iron-substituted LuxS and the native LuxS were similar. As time progressed and ferrous iron content decreased, activity of both enzymes followed the same downward pattern. The cobalt substituted LuxS enzyme did not have any decrease in activity over time. This indicated that the critical metal cofactor was Fe(II), rather than zinc, which the University of Michigan study concluded. This finding also confirmed the earlier

observations that LuxS becomes unstable when purified and that a cysteine residue in the active site region was oxidized when crystallography was attempted. Pei's findings shed some light on the nature of the structure of the LuxS protein, which is critical to understanding the mechanism by which it functions.

With a general idea about the system of LuxS, the next step in the process of controlling quorum sensing would be to effectively control LuxS. A recent study done by Fang Wang in the Chinese Academy of Sciences found that LuxS can be regulated using ethR, which is a transcription regulator. It is known that *Edwardsiella tarda* makes use of the *E. tarda* hemolysin (Eth) system, which consists of ethA and ethB, as part of its virulence. The expression of ethB is controlled by a ferric uptake regulator and ethR, which represses the promoter of the ethB sequence. To test for effects of this regulator on LuxS, the sequence of ethR in *E. tarda* was disrupted using the complementary RNA sequence, which was inserted into the cells via a plasmid. This set (TX1/pJRI) modeled underexpression of the sequence. Plasmids containing the ethR sequence were inserted into another set of cells (TX1/pJER) to model overexpression. The regular levels of expression were modeled by cells in the set TX1/JRA. To test for AI-2 activity, an assay based on bioluminescence was performed. The two sets of cells were grown overnight; for various time points, solution was taken from the cell cultures and centrifuged to obtain supernatant fluid containing no cells. This fluid from each set was transferred to different cultures of *V. harveyi*, which were then tested for light production. It was found that the AI-2 levels in the overexpressed TX1/pJER were approximately twice as high as those in TX1/JRA. Levels in the underexpressed set TX1/JRI were roughly one-third

those of the control set. This suggested that ethR expression related positively to LuxS expression, and thus, AI-2 activity.^[8]

The study done by Wang also tested the difference of LuxS expression in vitro versus in vivo. To do so, TX1/pJER and TX1/pJRA were injected into the kidneys of flounder. RNA was then extracted from the kidney and analyzed by qRT-PCR. It was found that LuxS expression for TX1/pJER in vivo was 10.6 times as much as expression for X1/pJRA. This indicates a differential for LuxS production when in a host, which means that quorum sensing is much more pronounced in vivo.

A significant amount of knowledge has been gained regarding the mechanism of action of LuxS. With this knowledge, it was proposed that the pathway could be inhibited by preventing LuxS from reacting. Pei had shown with UV-VIS spectroscopy and X-ray crystallography that the iron center was key to stabilizing the intermediates in their enediolate state. The idea behind inhibition of LuxS aimed to prevent the iron cofactor from being able to bond with the key intermediates, thus precluding the formation of DPD, the precursor to AI-2. Pei had done similar work with other iron-centered enzymes that relied on the divalent form of the metal for stabilization of intermediates. Pei believed that replacing the enediolate with a hydroxamate group, which is often used as a chelating agent. In doing so, the SRH analog would be able to effectively bind to the divalent iron center of LuxS, which would reduce its ability to form AI-2. Pei also crystallized LuxS when it was bound to an intermediate. The results indicated that the enzyme was binding to the ends of the molecule; the amino and carboxyl groups of the homocysteine on the molecule were binding to a site opposite the iron ion, which bound

to ribose. To develop an analog based on this, Pei designed a set of molecules which had an amino acid group on one end and a chelating agent on the other; these groups were connected by chains of different lengths to account for the distance between the active site and region where homocysteine was binding.

After assaying for LuxS activity, it was found that the following compounds, shown in Figure 1.4, were the most potent inhibitors.

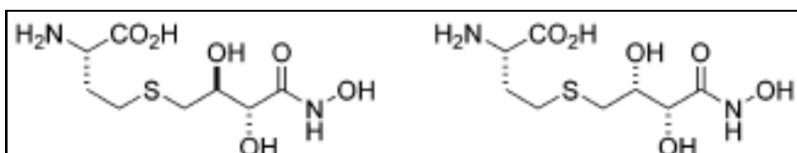


Figure 1.4: Potent Inhibitors of LuxS Activity

The study also found that the K_i value (inhibitor dissociation constant) for the analogs could be related to the K_m values for enzymes. This indicated that the effectiveness of the inhibition of LuxS was related to the affinity of the enzyme for its normal substrate. This demonstrates that the analogs fit into the active site of LuxS well. These analogs prevent turnover of the enzyme by competitively inhibiting binding of substrate to the active site. However, Pei noted that tests of these inhibitors with zinc and cobalt substituted forms of LuxS showed weaker inhibition levels. Nevertheless, this work shows that potent inhibitors for the native form of LuxS can be synthesized based on the knowledge of the mechanism of activity.^[9]

The next step in the process would be to create an effective pharmaceutical application of the enzyme analogs so that they can be used to reduce bacterial virulence in organisms. This is more difficult than it seems because most analogs of AI-2 are based

on amino acids. These inhibitors are much too ionic to readily diffuse through bilayer plasma membranes, which required active transport for most charged compounds. This means that the analogs will not readily be taken up by the bacteria, and therefore, are rendered ineffective. There may be certain techniques to circumvent this problem. For example, according to Howell and Chauhan, it may be possible to use liposomes, which are simply vesicles formed out of nonpolar lipid bilayers.^[10] The surfaces of liposomes can be marked by receptors which may allow bacteria to recognize them and possibly allow the liposomes to fuse to the bacteria. It may be possible that the bacteria can then intake the contents of the vesicle, allowing the analog inhibitors to enter the bacterial cytoplasm. Another possible method which would allow pharmacological applications of the analog system would be to transform the inhibitors so that they are able to diffuse across the bacterial membranes.^[11] This would require that the analogs return to their original form by reacting with the reducing cytosol environment inside the cell. This, of course, is easier said than done; much more research is needed before the use of substrate analogs can become a realistic medicinal possibility. The work done so far, however, does show that control of bacteria in many situations is possible. Once efficient inhibitors of LuxS can be effectively delivered, the applications of quorum sensing control are truly limitless.

The cholera quorum sensing pathway is of interest because cholera can bind to human intestines after ingestion of contaminated water or food. The result of this is diarrhea, which can lead to dehydration and eventually death if left untreated. Analysis

has shown that a system similar to the *Vibrio harveyi* AI-2 path was present, in addition to another parallel circuit.^[12]

The major cholera system of interest makes use of cholera autoinducer 1 (CAI-1), the synthesis of which is dependent upon activation of the quorum sensing pathway via the CqsS sensor. When the concentration of CAI-1 is low, the LuxU integrator protein is phosphorylated; the phosphate group comes from the CqsS and LuxP/Q sensors. The phosphate group is then transferred to LuxO, which then activates the sigma-54 repressor. This suppresses expression of the hapR gene, which is the cholera analogue of the gene responsible for luminescence in *Vibrio harveyi*. This system of phosphorylation is reversed at high cell density. In this case, LuxO is inactivated via dephosphorylation. This allows HapR to be expressed, causing biofilm formation, as well as potential toxicity, to cease through inactivation of virulence genes.^[13]

Figures 1.5 and 1.6 illustrate the cholera quorum sensing pathway at low and high cell densities, respectively.^[14]

a *V. cholerae* LCD

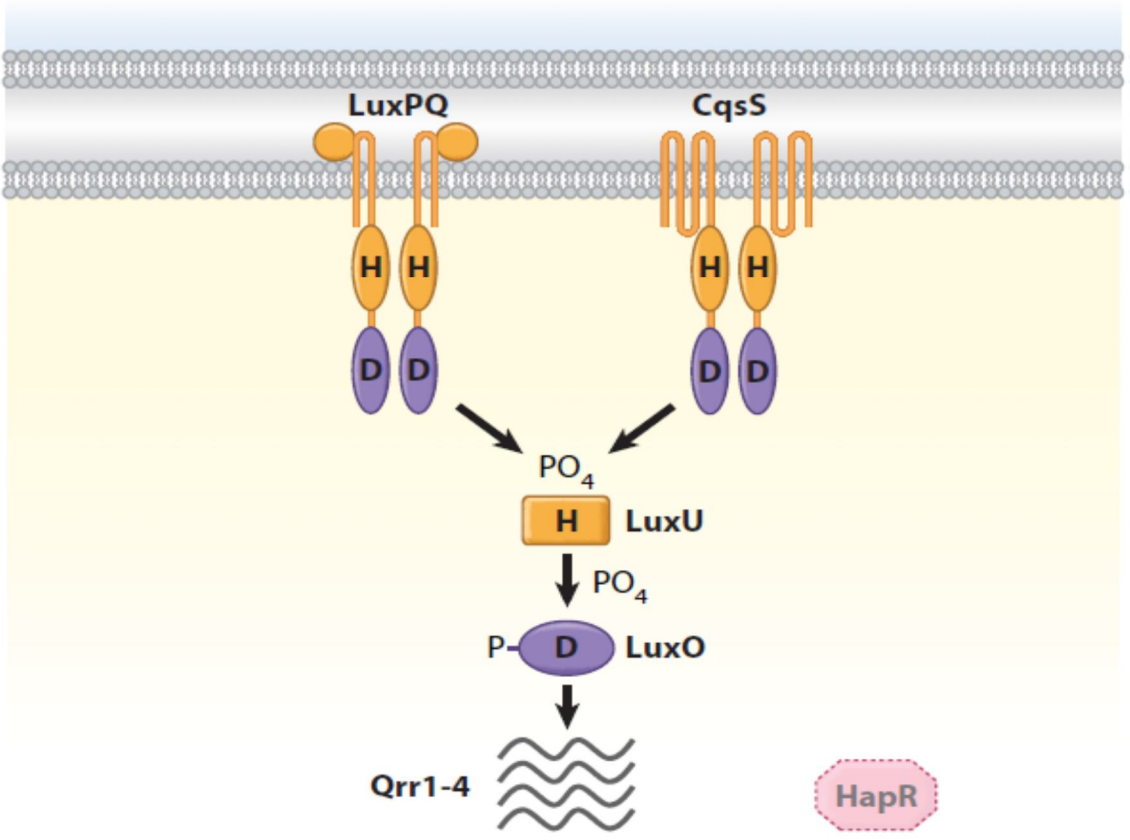


Figure 1.5: Cholera Quorum Sensing at Low Cell Density

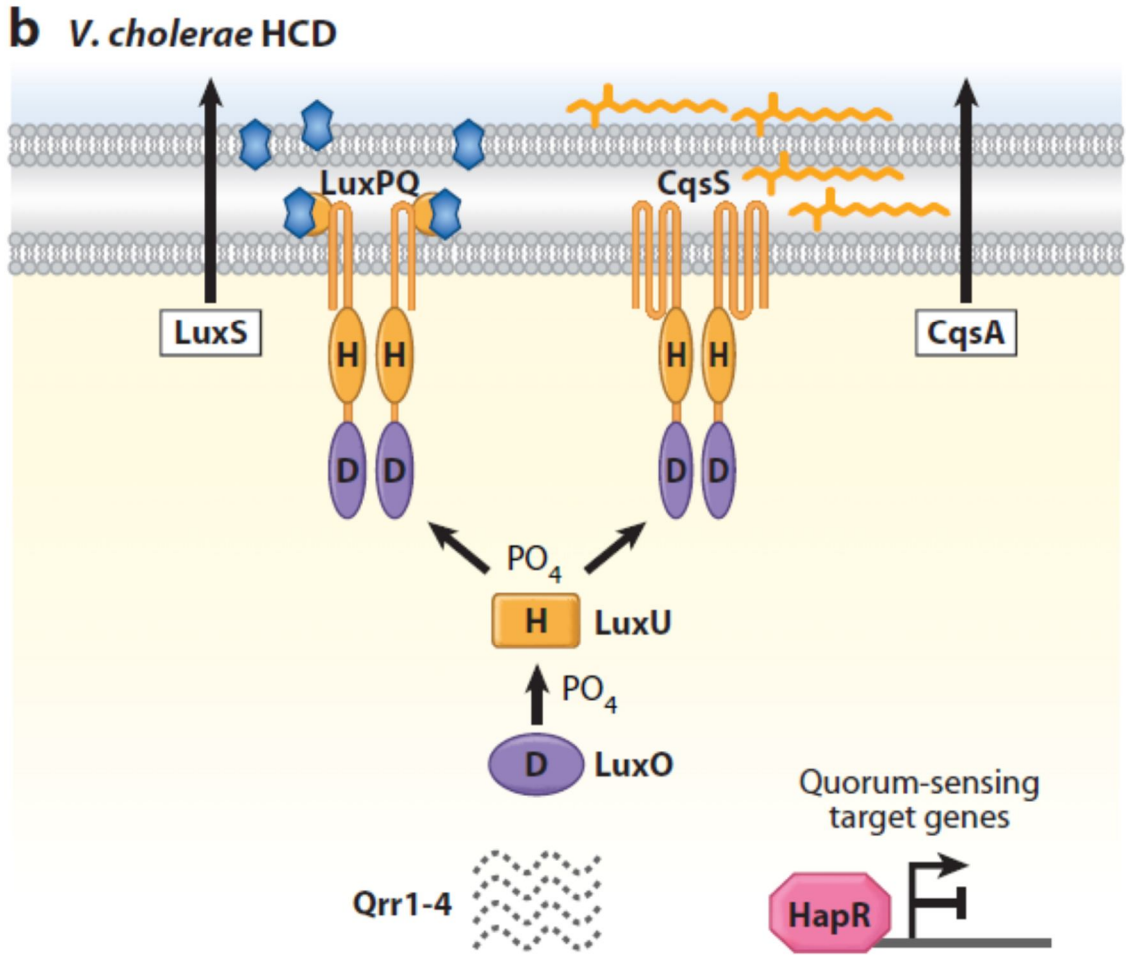


Figure 1.6: Cholera Quorum Sensing at High Cell Density

In the human body, cholera infections occur when infected water is ingested. In this medium, the bacteria can be present in low densities; once enough cycles of reproduction have taken place and the density has reached a limit, the bacteria release from the host, triggering diarrhea and severe water loss. Therefore, a control of this pathway would be desirable as a treatment of cholera infections. Using covalent modification of the enzyme would provide a potentially permanent solution since the change in the protein function could be irreversible.^[15] Prevention of the formation of biofilms in the host gastrointestinal tract can be used to prevent the symptoms of cholera. By precluding biofilm formation, the toxin release that results from cholera virulence in the host intestines can also be avoided. The release of toxins induces diarrhea in infected hosts and can lead to dehydration. The aforementioned treatment is one that seems to be a promising option if quorum sensing can be controlled.

Bibliography

- [1] Miller, M.B.; Bassler, B.L. (2001). "Quorum sensing in bacteria". *Annu. Rev. Microbiol.* 55: 165–99.
- [2] Henke, J. M. and B. L. Bassler (2004). "Three Parallel Quorum-Sensing Systems Regulate Gene Expression in *Vibrio harveyi*." *J. Bacteriol.* 186(20): 6902-6914.
- [3] Schauder, S., Bonnie L. Bassler, Michael G. Surette, and Kevan Shokat. "The LuxS family of bacterial autoinducers: biosynthesis of a novel quorum-sensing signal molecule." *Molecular Microbiology* 41.2 (2001): 463-76. .
- [4] Rajamani, S., Jinge Zhu, Dehua Pei, and Richard Sayre. "A LuxP-FRET-Based Reporter for the Detection and Quantification of AI-2 Bacterial Quorum-Sensing Signal Compounds." *Biochemistry* 46 (2007): 3990-997.
- [5] Hilgers, M. T. and M. L. Ludwig (2001). "Crystal structure of the quorum-sensing protein LuxS reveals a catalytic metal site." *Proceedings of the National Academy of Sciences* 98(20): 11169-11174.
- [6] Pei, D. and J. Zhu (2004). "Mechanism of action of S-ribosylhomocysteinase (LuxS)." *Current Opinion in Chemical Biology* 8(5): 492-497.
- [7] Zhu, J., Dizin, Eric, Hu, Xubo, Wavreille, Anne-Sophie, Park, Junguk , and Pei, Dehua. "S-Ribosylhomocysteinase (LuxS) Is a Mononuclear Iron Protein." *Biochemistry* 42 (2003): 4717-4726.
- [8] Wang, F., Min Zhang, Yong-hua Hu, Wei-wei Zhang, and Li Sun. "Regulation of the *Edwardsiella tarda* Hemolysin Gene and luxS by EthR." *Journal of Microbiology and Biotechnology* 19.8 (2009): 765-73.
- [9] Shen, G., Rakhi Rajan, Jinge Zhu, Charles E. Bell, and Dehua Pei. "Design and Synthesis of Substrate and Intermediate Analogue Inhibitors of S-Ribosylhomocysteinase." *Journal of Medicinal Chemistry* 49 (2006): 3003-011.
- [10] Howell BA, Chauhan A. "Interaction of cationic drugs with liposomes." *Langmuir.* 25(20):12056-64.
- [11] Borchardt, R. T., Edward H. Kerns, Michael J. Hageman, Dhiren R. Thakker, and James L. Stevens. *Optimizing the "Drug-Like" Properties of Leads in Drug Discovery (Biotechnology: Pharmaceutical Aspects)*. New York: Springer, 2006. 221-242.

- [12] Higgins, D. A., M. E. Pomianek, et al. (2007). "The major *Vibrio cholerae* autoinducer and its role in virulence factor production." *Nature* 450(7171): 883-886.
- [13] Bassler, B. L., and Brian K. Hammer. "Quorum Sensing Controls Biofilm Formation in *Vibrio Cholerae*." *Molecular Microbiology* 50.1 (2003): 101-14.
- [14] Ng, W.-L. and B. L. Bassler (2009). "Bacterial Quorum-Sensing Network Architectures." *Annual Review of Genetics* 43(1): 197-222.
- [15] Hinman, A., Huai-hu Chuang, Diana M. Bautista, and David Julius. "TRP Channel Activation by Reversible Covalent Modification." *Proceedings of the National Academy of the Sciences* 103.51 (2006): 19564-9568.

2 Introduction to Cholera

2.1 Background

Cholera is the disease caused by Gram-negative bacteria of the genus *Vibrio*. There are currently approximately 200 different serotypes of *Vibrio cholerae*.^[1] Cholera generally affects large groups of people via epidemics, which consists of a widespread infection in a particular region. Pandemics are also possible, and are defined as epidemics which expand over an extended period of time, usually for years or decades. In terms of the recorded history of cholera, there have been seven pandemics, all of which originated in Asia and spread to other continents.^[2] Most cholera bacteria are sensitive to acidic environments and do not survive the highly acidic gastric secretions.^[3] In the small intestine, any surviving cholera bacteria can reproduce and produce the cholera toxin (CT). This toxin induces water and electrolytes to enter the intestines and subsequently be excreted in the form of diarrhea.^[4]

2.2 Symptoms

Prior to the onset of primary symptoms, patients experience moist lips, mouth, and tongue, along with normal skin elasticity. During this early stage, patients typically lose less than five percent of their body weight in hydration. There are varying degrees of dehydration possible with cholera. Common symptoms include diarrhea, vomiting, muscle cramps and spasms, weak pulse, alterations in voice, thirst, shock, and muscle weakness.^[5]

2.3 Molecular Mechanisms of Infection

In order for *Vibrio cholerae* to form biofilms in the host organism, several colonization factors need to be transcribed from key virulence genes. The primary factors necessary to initiate aggregation of cholera cells are toxin-coregulated pili (TCP), accessory colonization factors (ACFs), mannose-fuses-resistant hemagglutinin, TolC, regulatory proteins, outer membrane porins, biotin and purine biosynthetic genes, iron-regulated OMP protein IrgA, O-antigen of the lipopolysaccharide, and the core regions of lipopolysaccharide.^[6] TCP is generally the critical factor necessary for colonization; this is confirmed by the fact that it is necessary for cholera colonies to thrive in both human and animal models. TCP is a polymer which acts as a receptor for CTX-alpha bacteriophage. This phage is vital to inducing virulence and can convert non-toxigenic strains into infectious versions through gene transduction. Though TCP is essential for biofilm formation, it does not play a straightforward role in the binding of cholera cells to the epithelial layers of the intestinal wall. Rather, these proteins are necessary for proper initiation of bacterial-bacterial self-interactions. These microcolonies then accumulate on the epithelial wall to form the biofilms which eventually secrete the toxins causing diarrhea. The proteins necessary for adhesion to the intestinal wall have not yet been identified.^[7]

2.4 Treatment Options

2.4.1 Oral Rehydration Therapy

The first treatment approach generally considered is known as oral rehydration therapy. Treatment typically varies based on the severity of dehydration being experienced by patients. Patients are generally divided into three groups based on levels of dehydration: no dehydration, limited degree of dehydration, and acute dehydration.

For patients with minimal or no dehydration, the most important objective is to prevent future dehydration by increasing intake of fluids as a preemptive measure. Commonly used fluids which are appropriate in these situations are rice water, weak tea, and salt/sugar solution. The administration of these fluids is age-dependent. For children under two, the recommended volume is 50-100 mL per loose stool, whereas the advised volume is 100-200 mL for children between the ages of 2-10 years. Larger amounts are advised for adolescents and adults. The fluid should be taken slowly; a few teaspoons should be given every 10 to 15 minutes.

For patients with a limited degree of dehydration, the preferred method is to make use of oral rehydration salt (ORS) solution in two phases, according to the World Health Organization. As seen in the case with minimal to no dehydration, the treatment varies based on the age of the patient. For adults and adolescents, the volume of fluids and electrolytes lost in stool should be replaced as quickly as possible. For younger children (generally under 10 years old), the dose for fluid replacement is body weight-dependent. ORS solution should be administered in a dose of 75 mL/kg over a course of 4 to 6 hours.^[8]

For younger children, use of bottles to contain ORS solution is not recommended; this is done in order to prevent potential contamination of the ORS solution by previously contaminated bottles. After a period of 4-6 hours, children should be reassessed for their level of dehydration. Oral rehydration therapy should be continued even after normal levels of hydration have been attained. ORS solution should be administered in volumes equal to stool loss until diarrhea ceases as a form of maintenance therapy. For the most part, limited dehydration can be treated in the home or community setting. If the condition worsens to severe dehydration, it is recommended to move into a clinical or hospital setting.^[9]

For patients with severe dehydration, hospital treatment is required and intravenous rehydration is necessary. For infants under the age of twelve months, 30 mL/kg of solution should be administered within the first hour. This should be repeated once if the radial pulse is weak or not detectable. Following these initial doses, 70 mL/kg should be administered in 5 hours. For children ranging in age from 12 months to 5 years, the rate of administration is increased. The first 30 mL/kg is given within half an hour; again, this should be repeated given a weak or non-detectable radial pulse. The following 70 mL/kg dose should be given within two and a half hours. Children should be reassessed every 1-2 hours. Children should be provided with a 5 mL/kg per hour dose of oral rehydration salt solution as soon as they are able to drink; this period usually ranges from 3-4 hours for infants and 1-2 hours for children. Infants should be reassessed after 6 hours and children after 3 hours.^[10]

2.4.2 Antibiotics

This oral rehydration therapy is given in conjunction with antibiotics. The main purpose of this is to reduce the bacterial load in patients so that the duration/volume of purging is decreased. The usual prescription is tetracycline, which has several beneficial effects. The most important benefit is that it reduces the duration of diarrhea by approximately 50%; the resulting diarrhea episodes average about 2 days. The reduction in diarrhea volume after initiating the tetracycline is about 60%. The antibiotic regimen also reduces vibrio excretion to an average of 24 hours and a maximum of 48 hours. The usual dosage for adults is 500 mg given every 6 hours for 48 to 72 hours; for less severe cases, 250 mg can be given every 6 hours for 72 hours. For children, the recommended dose is a maximum of 50 mg/kg per day, divided evenly over four doses; these doses should be continued for 48 to 72 hours, similarly to the timeframe for adults.^[11]

Doxycycline, a member of the tetracycline family of medications, generally has a longer-lasting effect; adults can be given a single dose of 300 mg, and children below 15 years of age can be given 4 to 6 mg/kg. If patients have an allergic reaction to tetracycline, furazolidone can be given in a dose of 100 mg every 6 hours for adults and 5 mg/kg per day in four doses for children, given over a course of 72 hours. Erythromycin can be given in a dose of 250 mg every 6 hours for adults and 30 mg/kg per day in four doses for children, given over a course of 72 hours. Trimethoprim-sulfamethoxazole can be given in a dose of 8 mg trimethoprim and 40 mg sulfamethoxazole per kg body weight per day in 2 doses, given over a course of 72 hours.^[12]

Antibiotics can also be given prophylactically to family members of infected patients. The most common and effective treatments in these cases, as seen with primary infections, are tetracycline and doxycycline. The general procedure to be followed is to administer prophylactically to anyone family member who has had direct contact with the patient. This creates a problem due to the fact that infected family members represent only a small proportion of the potential infections within the community. The issues with prophylactic antibiotics are primarily related to cost-effectiveness; it is difficult to determine which people are prone to having the highest risk of secondary infection, and thus, over-dispensation of medications is possible. This possible excessive medication can help to eliminate less virile strains of cholera, reducing the rate of future infections. More virulent strains, however, are likely to survive this evolutionary pressure and cause increased severity in future infections. Therefore, from a monetary and feasibility perspective, prophylactic antibiotics are generally not recommended on a large scale.^[13]

2.4.3 Antidiarrheal Agents

Another approach utilized in clinical treatment of cholera symptoms is an antidiarrheal and antisecretory agent regimen. This method is more of a palliative care measure than a direct cure. Antidiarrheals aim to reduce the volume of water lost by the body, therefore decreasing the need for oral rehydration. Previously attempted therapies include kaolin, pectin, bismuth sub-salicylate, and activated charcoal; these treatments, however, have minimal effectiveness, and may actually have detrimental effects on the activity of tetracycline. Activated charcoal has shown some degree of binding to cholera toxin, which can help to alleviate the level of elimination in the host. Other options include drugs that reduce the absorption of the intestinal epithelial wall; this decreases the uptake of the cholera toxin.

Antisecretory agents aim to reduce secretion from the intestinal mucus layer. This would have the same effects of reducing the length and severity of the clearing by the infected host. Multiple drugs have been tested to determine the extent of their antisecretory properties. Chlorpromazine has been proven to have antisecretory effects in animal models; it also has substantially lessened the fecal volume in patients when concurrently given with oral rehydration therapy. In cases where chlorpromazine was given with intravenous fluids and antibiotics, differences in purging were negligible in the average patient. In severely infected younger children, chlorpromazine given with the typical treatment regimen did have positive effects in terms of diarrhea reduction.

Berberine is commonly used as an antidiarrheal agent and has antisecretory effects in animal models. In clinical trials, this alkaloid has had mixed results. Two

different studies showed either no benefits or marginal reduction in elimination volume in patients. In addition, no negative side effects were determined; this suggests that addition of berberine to treatment regimens would have few, if any, adverse effects. Another study was completed using patients with *E. coli*-induced diarrhea; in this case, berberine had a significant reduction in stool volumes. This may indicate that use in cholera patients is still possible and that different dosage routines must be tested in order to determine the optimal dose. Other tested alternatives for antisecretory drugs include nicotinic acid, chloroquine, somatostatin, aspirin, and methacin; nicotinic acid showed only slight benefits, while the rest had no positive clinical results.^[14] Overall, no universally effective antisecretory agent has been discovered as of yet.

Bibliography

- [1] Koelle, K., M. Pascual, et al. (2006). "Serotype cycles in cholera dynamics." *Proceedings of the Royal Society B: Biological Sciences* 273(1603): 2879-2886.
- [2] Artenstein, A. W. (2009). *Vaccines: A Biography*, Springer.
- [3] Constantin de Magny, G., R. Murtugudde, et al. (2008). "Environmental signatures associated with cholera epidemics." *Proceedings of the National Academy of Sciences* 105(46): 17676-17681.
- [4] Chaudhuri, K. and S. N. Chatterjee (2009). *Cholera Toxins*, Springer.
- [5] Wachsmuth, K., P. A. Blake, et al. (1994). *Vibrio cholerae and cholera: molecular to global perspectives*, ASM Press.
- [6] Faruque, S. M. and G. B. Nair (2008). *Vibrio cholerae: genomics and molecular biology*, Caister Academic Press.
- [7] Ramamurthy, T. and S. K. Bhattacharya (2010). *Cholera: Molecular and Epidemiological Aspects*, Springer Verlag.
- [8] Guerrant, R. L., T. Van Gilder, et al. (2001). "Practice Guidelines for the Management of Infectious Diarrhea." *Clinical Infectious Diseases* 32(3): 331-351.
- [9] Farthing, M., Lindberg G., et al. (2008). "Acute diarrhea." *World Gastroenterology Organization practice guideline*. 1-29.
- [10] Coleman, W. and H. Babcock (2008). *Cholera, Facts on File*.
- [11] Nelson, E. J., D. S. Nelson, et al. (2011). "Antibiotics for Both Moderate and Severe Cholera." *New England Journal of Medicine* 364(1): 5-7.
- [12] Thiagarajah, J. R. and A. S. Verkman (2005). "New drug targets for cholera therapy." *Trends in Pharmacological Sciences* 26(4): 172-174.
- [13] Reidl, J. and K. E. Klose (2002). "Vibrio cholerae and cholera: out of the water and into the host." *FEMS Microbiology Reviews* 26(2): 125-139.
- [14] Barua, D. and W. B. Greenough (1992). *Cholera*, Plenum Medical Book Co.

3 Experimental Rationale

The initial project was aimed to develop molecules that could covalently inhibit the CqsS sensor in order to keep it in its predominantly active state. By doing this, the receptor would keep the quorum sensing pathway activated and indicate the presence of a high density of cells. By keeping the pathway active, the adhesion of *Vibrio cholerae* cells to the intestines could be inhibited, thus precluding infection-related symptoms.

Molecules were synthesized based on the native structure of CAI-1, shown in Figure 3.1:

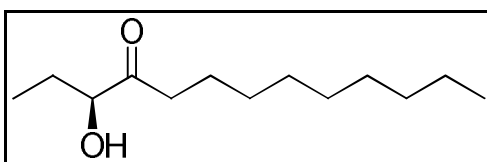


Figure 3.1: Structure of Native CAI-1 Molecule

All of the synthesized analogs conserve the polar head group containing a secondary hydroxyl group and a carbonyl group in the appropriate locations (the carbonyl is located on the alpha-carbon relative to the alcohol). This head group is analogous to the head group of the native CAI-1 molecule. Rather than using the ketone present in CAI-1, all analogs were esters. Previous work done with CAI-1 analogs has demonstrated that ester analogs of CAI-1 give the same level of activity as the native molecule.^[1] The alkyl chain was synthesized using an ester formation procedure. The alkyl chain was coupled using a terminal alcohol. This made the addition of an alkyl chain easier to facilitate due to the electrophilic nature of the carbonyl carbon and the nucleophilic nature of the hydroxyl oxygen.

[1] Brook, Karolina (2010). Small Molecule Modulation of *Vibrio cholerae* Virulence Through Quorum Sensing. Princeton University.

The mechanism, which uses 4-dimethylaminopyridine (DMAP) as a catalyst, is shown in

Figure 3.2:

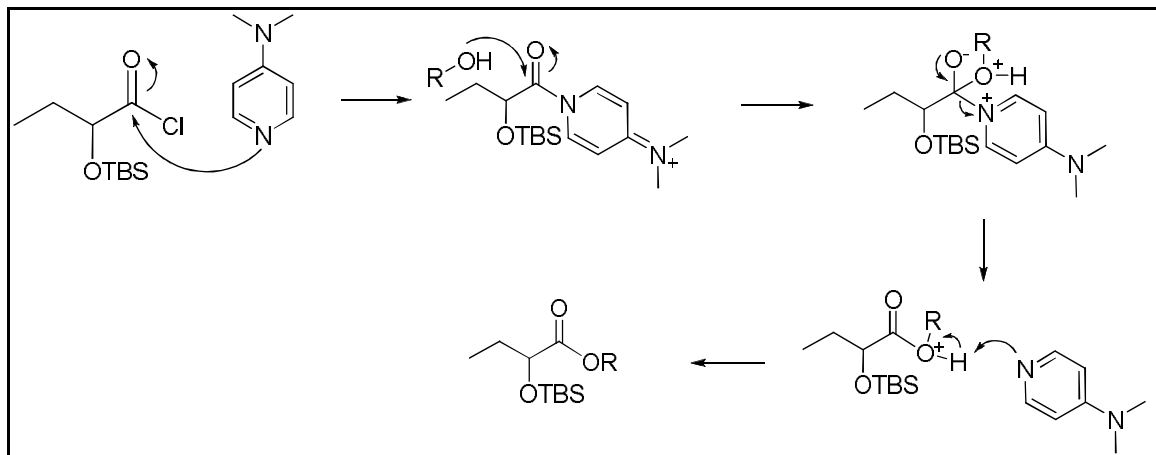


Figure 3.2: General Esterification Mechanism Catalyzed by DMAP

The formation of the carbon-oxygen bond is easily facilitated by addition of roughly one equivalent of the desired alcohol, whereas the formation of a new carbon-carbon bond at that location would have been more difficult. For example, Grignard reagents could be employed to synthesize ketone analogs instead of the intended esters. However, Grignard reagents can yield side reactions due to their high level of basicity.^[2] In addition, Grignard reagents have also been known to react with solvents in some cases.^[3] This would make handling and syntheses more difficult than with the intended ester formation route. Therefore, ester analogs were chosen to increase ease of synthesis and handling of reagents.

[2] Kürti, L. and B. Czako (2005). Strategic applications of named reactions in organic synthesis: background and detailed mechanisms, Elsevier Academic Press.

[3] Silverman, G. S. and P. E. Rakita (1996). Handbook of Grignard reagents, Marcel Dekker.

In order to facilitate covalent modification of the cysteine residue in the active site, the synthesized CAI-1 analogs possess alkyl chains with groups susceptible to bimolecular nucleophilic substitution.

The general mechanism for this covalent modification is detailed in Figure 3.3:

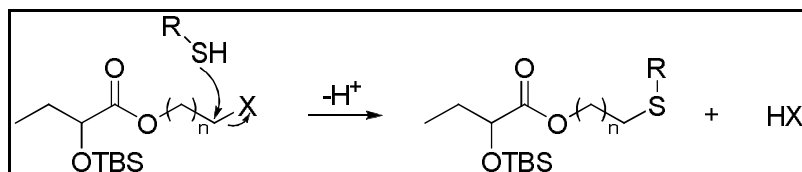


Figure 3.3: Covalent Modification of Cysteine Residue in CqsS

Here, R-SH represents the thiol group which comprises the cysteine side chain. In the CAI-1 analog, the leaving group at the terminus of the alkyl chain is denoted by X.

Another goal was to synthesize molecules which could be used to elucidate the structure of the CqsS receptor. By modifying the alkyl chain of the CAI-1 molecule to be unsaturated, the chain could be constrained in certain configurations. It is unknown whether the molecule remains in the straight-chain conformation or undergoes an intramolecular folding. This concept is shown in Figure 3.4:

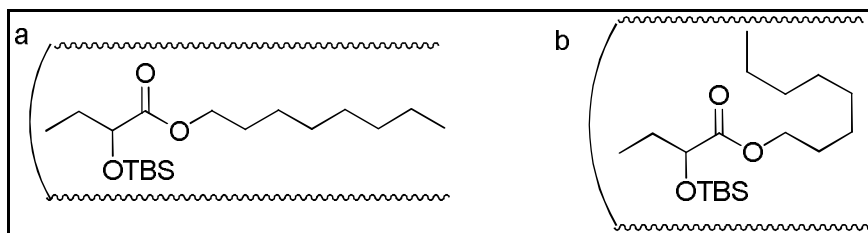


Figure 3.4: (a) Straight Chain in CqsS (b) Folded Chain in CqsS

By using triple bonds, as well as *E*- and *Z*-double bonds, molecules can be synthesized and tested for levels of CqsS agonist activity. Alkyl chains with triple bonds limit

intramolecular folding; the use of a Z-alkene in the alkyl chain also increases the volume of the molecule and could illustrate the overall volume of the binding pocket of CqsS. Rather than using the solution-phase chemistry outlined for the covalent modification molecules, a solid support method, the benefits of which are explained in Chapter 4, would be employed to synthesize the target molecules in this case. If higher activity is observed for molecules which limit rotation of the alkyl chain, this may mean that the molecule activates the receptor while in an unfolded state. This may indicate that the active site is a narrow, long pocket. If higher activity is observed for molecules which are not restricted to a straight chain conformation, this may indicate that the active site is shorter and wider. This project could provide valuable insight about the *in vivo* binding of CAI-1 in the CqsS receptor.

4 CqsS Receptor Structure Elucidation

4.1 Solid Phase Synthesis

Chemical syntheses are generally categorized into two groups. Those which occur in a single phase are homogenous, whereas those which occur at the boundary of two phases are classified as heterogeneous. Within the class of heterogeneous reactions, solid phase reactions make use of a solid support in order to bind a given starting material.^[1] A series of reactions can then be performed on the bound molecule until the final product is formed. This target molecule can then be cleaved from the solid support to yield the desired final product.

A variety of solid supports are available for reactions done in the solid phase. The most common type of support includes hydrophobic polystyrene resin beads.^[2] Molecules which are bound to resins are generally characterized by infrared spectroscopy rather than NMR due to the difficulty associated with preparation of NMR samples of resin-protected materials. Solid phase synthesis generally requires fewer chromatographic steps than solution phase synthesis since the solid desired product is easily separable from the reaction mixture.^[3]

The Wang resin was selected as a solid support because it is stable and the final cleavage of the target molecule is easily accomplished by a reaction with trifluoroacetic acid (TFA).^[4]

[1] Seneci, P. (2000). Solid phase synthesis and combinatorial technologies, John Wiley & Sons.

[2] Grabley, S. and R. Thiericke (1999). Drug discovery from nature, Springer.

[3] Dörwald, F. Z. (2002). Organic synthesis on solid phase: supports, linkers, reactions, Wiley-VCH.

[4] Wipf, P. (2005). Handbook of Reagents for Organic Synthesis: Reagents for high-throughput solid-phase and solution-phase organic synthesis, Wiley.

4.2 Syntheses

The following reaction was used to form the needed alkyne molecules (2-, 3-, 4-, and 5-octyn-1-ol):

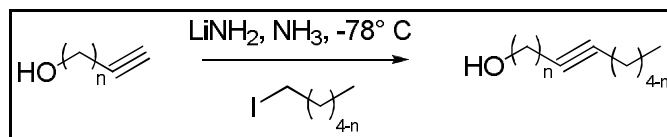


Figure 4.1: Synthesis of Alkyne Molecules (n=1, 2, 3, or 4)

This synthesis successfully gave the four desired octyn-1-ol molecules. These molecules can potentially be subjected to reductions or coupled to form the desired analogs.

4.2.1 Issues with Z-Alkene Formation

In order to form the Z-alkene isomers, the alkyne molecules were subjected to a general olefination procedure, using Lindlar catalyst and quinoline under a bulb of hydrogen (1 atm). The first attempted synthesis was for the formation of 2-Z-octen-1-ol from the 2-alkyne molecule. The reaction is shown in Figure 4.2:

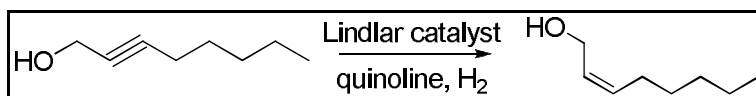


Figure 4.2: 2-Z Isomer Formation from 2-Alkyne

This reaction was run for 2 hours and purified via chromatography. Both proton and carbon NMR indicated a mixture of products. In the carbon NMR spectrum, the 2-Z isomer olefinic carbon atoms appear at shifts near 128 ppm and 133 ppm. For this reaction, there appear to be two doublets in this region, indicating a mixture of products. One possible scenario considered was acetylation, given the use of ethyl acetate as an

eluent in the purification. The reaction between the 2-Z isomer formed in the reaction and ethyl acetate would form an ester, as shown in Figure 4.3:

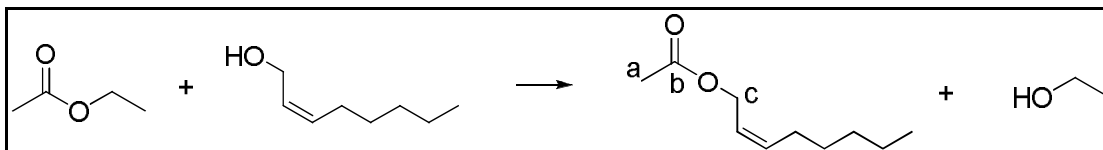


Figure 4.3: Potential Acetylation of 2-Z-Alkene

The characteristic peak for this ester would be the carbonyl carbon (position b) in the molecule, which would appear at a shift of approximately 170 ppm. This key peak was not observed. Additional evidence that the ester molecule was not in the mixture is the lack of a signal from protons (at position a), which would appear as a singlet integrating to approximately 3.00 protons at a shift of 2.1 ppm. The alpha-ester carbon (position c) should appear near 60 ppm, upshifted from the corresponding alpha-hydroxyl carbon (~58 ppm) in the free 2-Z alcohol; this peak at 60 ppm was not observed either.

Another possibility would be an alkene shift. In this isomerization, the double bond could potentially shift toward the oxygen to form a vinyl alcohol. This vinyl alcohol would quickly tautomerize to form an aldehyde, as detailed in Figure 4.4:

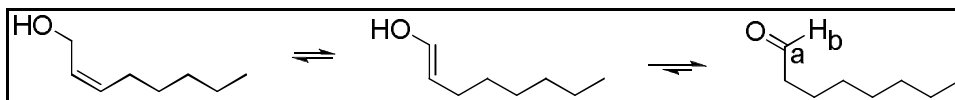


Figure 4.4: Potential Alkene Shift followed by Tautomerization

In the resulting aldehyde, the carbonyl carbon (position a) would appear near 170 ppm. Again, this key peak was not observed, indicating that this product was not present. This

is further confirmed by the lack of signal from the aldehyde proton (position b) at a shift between 9-10 ppm.

Another possibility considered was the formation of *E*- and *Z*-isomer products. The olefinic carbon atoms appear at slightly different shifts for the *E*- and *Z*-isomers. For the pure 2-*E* isomer, the olefinic carbons appear at 133.78 and 128.87 ppm. The overlap of the reaction mixture spectrum with that of pure 2-*E* isomer indicated that the two larger peaks in this region were for the 2-*E* olefinic carbon atoms. Therefore, the major product in this reaction was the 2-*E* isomer. In proton NMR, this was confirmed. The alpha-hydroxyl methylene protons of pure 2-*E*-octen-1-ol appear at a shift of 4.07 ppm, whereas they appear at 4.20 ppm for 2-*Z*-octen-1-ol. The proton NMR of this reaction shows a 4.18:1 ratio of these protons, indicating that the mixture is roughly twenty percent desired product. In addition, the olefinic protons appear as a multiplet at approximately 4.6 ppm. In the reaction mixture, there appeared to be two overlapping multiplets, corresponding to the *E*- and *Z* isomers. The overlap for the 2 hour reaction and pure, commercially available 2-*E*-octen-1-ol is shown in Figure 4.5:

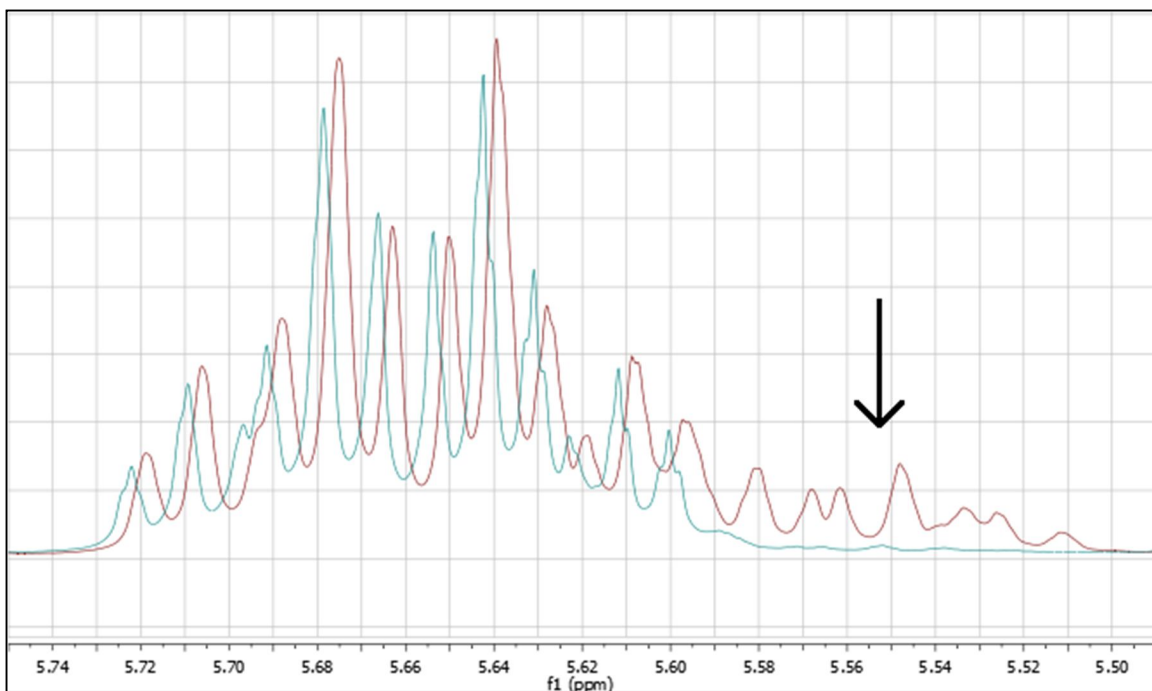


Figure 4.5: Overlap of 2 Hour Reaction Mixture and Pure 2-*E*-octen-1-ol

The reaction mixture has a signal from 5.5-5.73 ppm and pure 2-*E*-octen-1-ol has a signal from 5.6-5.73 ppm. There is a clear overlap between the mixture and the pure 2-*E* isomer, indicating the presence of 2-*E*-alkene in the mixture. There is also a small multiplet slightly upfield of the 2-*E* peaks; this multiplet, under the arrow in Figure 4.5, corresponds to the 2-*Z* olefinic protons. These multiplets are difficult to use to quantify the ratio of *E*- to *Z*-isomer because the overlap makes it difficult to accurately integrate the *E*-olefinic protons and the *Z*-olefinic protons separately. Therefore, the alpha-hydroxyl methylene protons are used to quantify the ratio of *E*- to *Z*-isomer.

The mixture of isomers is difficult to purify due to the structural similarities of the *E*- and *Z*-isomers, which co-elute during silica gel chromatography. As shown above, the 2 hour reaction time formed both the *E*- and *Z*-isomers and may not have been the proper reaction length. In order to find an optimal reaction time, a series of time-controlled

reactions was completed. The goal of these reactions was to find the reaction time which resulted in complete consumption of the starting alkyne and only formation of the *Z*-isomer. Complete consumption of the alkyne starting material can be confirmed by disappearance of the alkyne carbon peaks, which appear as two peaks between 78-90 ppm. The reduction was repeated, and aliquots were taken after 30 minutes, 1 hour, and 1.5 hours. All aliquots indicated the presence of *E*-isomer, as indicated by doublets in the olefinic carbon range (128-133 ppm), two peaks for the alpha-hydroxyl methylene protons (near 4 ppm), and two overlapping multiplets for the olefinic protons (near 4.6 ppm).

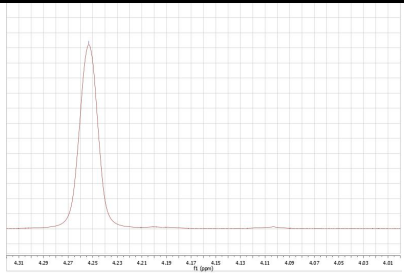
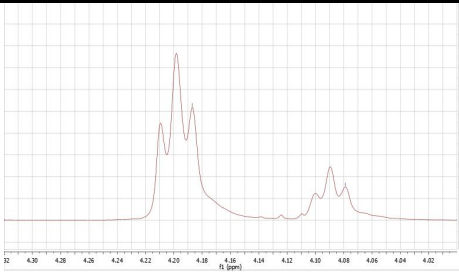
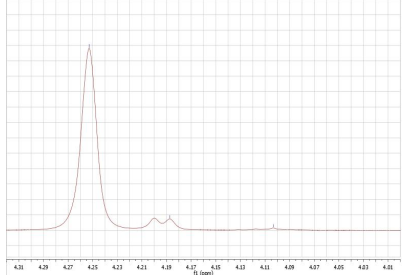
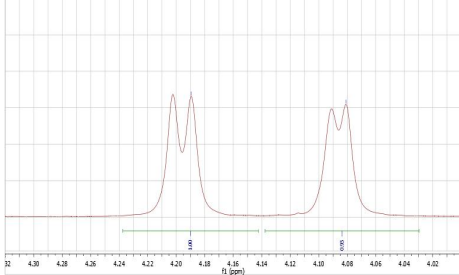
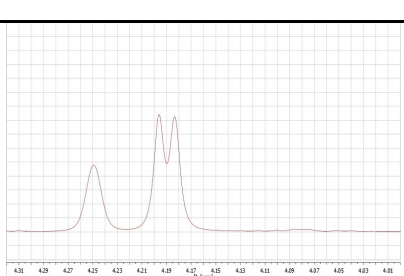
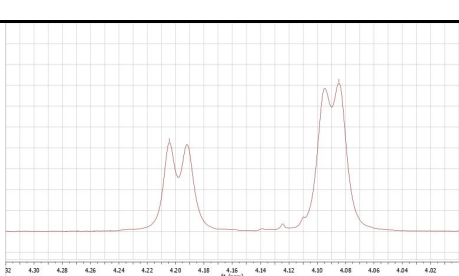
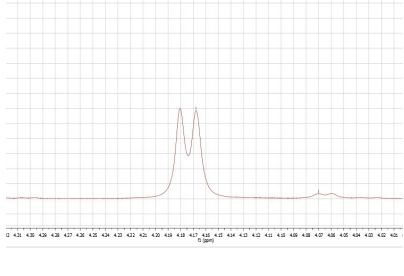
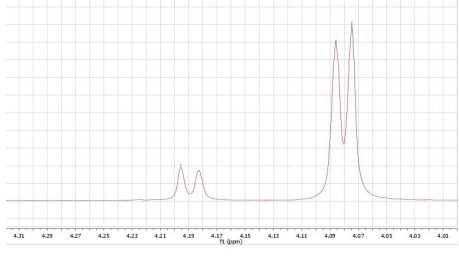
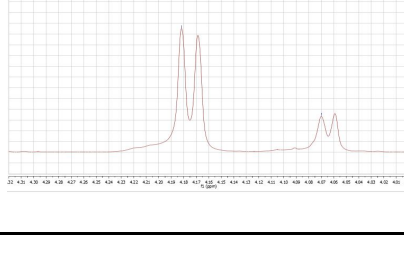
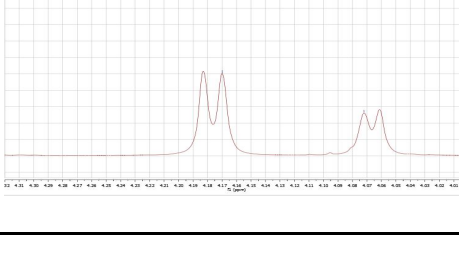
This experiment was repeated, and aliquots were taken at 2 minutes, 5 minutes, 15 minutes, and 30 minutes. The 2 minute aliquot indicated no reduction, as shown by the lack of olefinic carbon atoms in carbon NMR and no appearance of olefinic protons in proton NMR. In the 5 minute aliquot, there was minimal formation of the *E*- and *Z*-isomers, as shown by the presence of 3 distinct peaks (at 4.25 ppm for the alkyne, 4.17 ppm for the *Z*-isomer, and 4.07 ppm for the *E*-isomer) for the alpha-hydroxyl methylene protons. In the 15 minute aliquot, the alkyne starting material was present, along with both isomers, again indicated by 3 signals in the 4.2 ppm range. In the 30 minute reaction, there were no peaks in the 78-90 ppm range for the alkyne carbons, indicating complete consumption of starting material. However, there is a mixture of *E*- and *Z*-isomer present. The reaction was then repeated for 20 and 25 minutes in order to obtain data about the extent of reduction between 15 and 30 minutes. In both cases, the alkyne was completely consumed, but there was minimal *E*-isomer present. Unfortunately, none

of the reaction times tested appeared to be successful in complete consumption of starting alkyne and exclusive formation of *Z*-isomer. Table 4.1 shows the quantification of each potential component (starting alkyne, *Z*-isomer, *E*-isomer) in the reaction mixture, as well as the alpha-hydroxyl methylene peaks for each time point. This is calculated using the integration for the alpha-hydroxyl methylene protons in the 4.2 ppm range. For the time points in which alkyne is present, the alkyne peak integration is set to 1.00 protons; in the time points where only *E*- and *Z*-isomers are present, the *Z*-isomer is set to 1.00 protons. The percent of *Z*-isomer as a fraction of the total mixture is also included.

Table 4.1: Reduction Reaction Mixtures for Various Time Points

Time	Alkyne	<i>Z</i> -Isomer	<i>E</i> -Isomer	<i>Z</i> -Isomer (%)
2 min	1.00	0.00	0.00	0
5 min	1.00	0.09	0.01	8.2
15 min	1.00	2.32	0.07	68.4
20 min	0.00	1.00	0.07	93.5
25 min	0.00	1.00	0.29	77.5
30 min	0.00	1.00	0.32	75.6
1 hour	0.00	1.00	0.95	51.3
1.5 hours	0.00	1.00	1.72	36.8
2 hours	0.00	1.00	5.18	16.5
1 hour (0°C)	0.00	1.00	0.56	64.1

Table 4.2: Alpha-Hydroxyl Methylene Peaks for Time Series Reactions

Time		Time	
2 min		30 min	
5 min		1 hour	
15 min		1.5 hours	
20 min		2 hours	
25 min		1 hour (0° C)	

Note: Peaks may appear as a triplet rather than the expected doublet due to proton exchange with the terminal hydroxyl group.

The formation of the *E*-isomer from this reaction is somewhat difficult to explain. Lindlar catalyst is a palladium which has been poisoned by lead and contains calcium carbonate as a support. Generally, catalysts are poisoned in order to reduce their reactivity. Palladium is known to have a high ability to adsorb hydrogen atoms once exposed to a hydrogen gas atmosphere. These adsorbed hydrogen atoms become interspersed within the lattice of palladium in the catalyst. During the course of hydrogenation reactions, the consistency of the catalyst shifts dramatically; the catalyst is a hard material initially but begins to transition into an agglomeration as the reaction proceeds. In this beta-hydride phase, the lattice structure of the palladium crystals increases in size by about six percent.^[5] This phase is the active formation of the catalyst and allows hydrogen to be transferred to the alkyne. Changes in the reactivity of Lindlar catalyst can occur due to formation of palladium oxides or oxy-chlorides due to reactions with atmospheric moisture. There can also be changes in the oxidation state of palladium in the catalyst as a result of reactions with air.^[6] These changes can alter the levels of reactivity of the catalyst, as well as the promotion rates of reduction.

It is difficult to determine how this formation of *E*-isomer occurs in the presence of Lindlar catalyst. The mechanism for the formation of the *Z*-isomer is shown in Figure 4.6:

[5] Ulan, J. G., W. F. Maier, et al. (1987). "Rational design of a heterogeneous palladium catalyst for the selective hydrogenation of alkynes." *The Journal of Organic Chemistry* 52(14): 3132-3142.

[6] Albers, P., J. Pietsch, et al. (2001). "Poisoning and deactivation of palladium catalysts." *Journal of Molecular Catalysis A: Chemical* 173(1-2): 275-286.

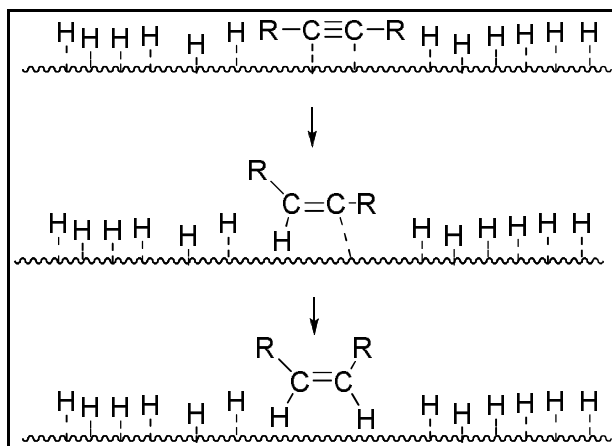


Figure 4.6: Alkyne Reduction to form Z-Isomer

From this figure, it seems that the presence of the catalyst support makes it difficult for the *E*-isomer to form. For the *E*-isomer to form, the R groups in the molecule would have to be on opposite sides of the unsaturated bond. Steric effects would make this difficult due to the presence of the catalytic framework on one side of the molecule.

Studies have shown that there can be significant variations within the composition of palladium-based catalysts. In experiments using palladium catalysts to reduce lead ions, different catalysts with different lead contents were found to have significant differences in the phase lattice sizes, some of which were nearly three times as large as others. As mentioned previously, the phase size of the catalyst is a critical parameter in reactivity. In addition to lattice size, the level of dispersion of the starting material can vary. In some cases, the level of dispersion of the substrate was a factor of three higher than in other cases. These variations between catalysts, along with potential oxidation by exposure to air, could explain the irregular results observed in the attempted reduction reactions.^[7]

[7] Noack, K., H. Zbinden, et al. (1990). "Identification of the state of palladium in various hydrogenation catalysts by XPS." *Catalysis Letters* 4(2): 145-155.

Though it is uncommon, different levels of *Z*-selectivity have been observed with Lindlar catalysts. On the palladium surface, motifs known as steps and terraces may be present. A terrace is a relatively flat, extended portion of the surface as shown above in Figure 4.6. A step, on the other hand, is a portion of the surface which has multiple levels. In this case, the steric hindrance from the structural framework of the catalyst is less prominent and may provide a surface for isomerization to occur, as shown in Figure 4.7:

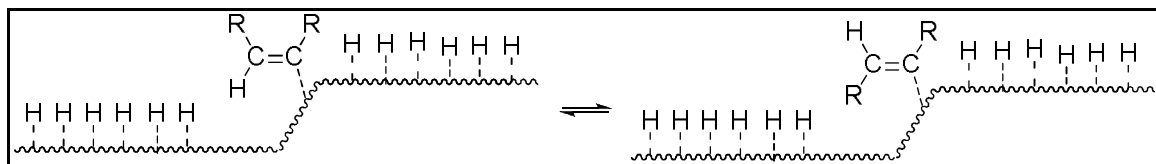


Figure 4.7: Step Motif on Surface of Lindlar Catalyst

In studies analyzing the selectivity of catalytic hydrogenation of 2-hexyne, it has been found that the maximum *Z*-isomer selectivity observed was 87%. 2-hexyne, like the 2-octyn-1-ol starting material of this reduction, is an asymmetric internal alkyne and can undergo *Z*-*E* isomerization, as well as bond shifts. In the reductions of 2-hexyne, a variety of products were formed, including 2-*Z*-hexene, 2-*E*-hexene, *n*-hexane, 1- and 3-hexenes, and *n*-hexane. These results may shed light on the perplexing formation of *E*-isomer in the reduction of the 2-alkyne to the intended 2-*Z*-isomer. The presence of steps in the catalyst surface may explain the formation of the *E*-isomer. The terrace form appears to be the most selective for formation of *Z*-alkenes. It is difficult to standardize the surface of the catalyst into the terrace form due to the changes in the palladium bulk structure from reactions with air and lattice size increases. One proposed solution to this

issue is the formation of alloys to lock the palladium structure into a given conformation. For example, contamination with rhodium, which has a higher lattice energy value than palladium, may allow the bulk structure of palladium catalysts to be stabilized in the desired terrace form.^[8]

In the time series study, it can be seen that at no time point is there pure *Z*-isomer in the reaction mixture. There is also no time point where the alkyne is completely consumed and exclusively *Z*-isomer is present. The *Z*-isomer is difficult to separate from the unreacted alkyne, again due to structural similarities which lead to co-elution in chromatography. There is a potential method for performing this separation using a silver-impregnated silica gel column. In order to do this, silver nitrate can be added to the silica gel prior to the chromatographic step. Because the double bond in the *Z*-isomer is less sterically hindered than in the *E*-isomer, silver coordinates more with the *Z*-isomer. Therefore, the retention time for the *Z*-isomer is greater than that of the *E*-isomer. However, the separation would still be fairly difficult because the difference in elution rates probably would not be significant. In addition, preparation of silver-impregnated silica gel is somewhat difficult. There are issues with the removal of excess silver nitrate, as well as a limited life-time for silver-impregnated TLC plates.^[9]

[8] Stachurski, J. and J. M. Thomas (1988). "Structural aspects of the lindlar catalyst for selective hydrogenation." *Catalysis Letters* 1(1): 67-72.

[9] Li, T. S., J. T. Li, et al. (1995). "Modified and convenient preparation of silica impregnated with silver nitrate and its application to the separation of steroids and triterpenes." *J. Chromatogr., A* 715(2): 372-375.

Therefore, an alternative method is needed to synthesize the Z-isomer. The method used is detailed in Figure 4.8:

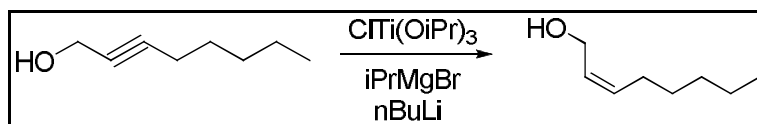


Figure 4.8: Alternate Synthesis for 2-Z Isomer

This reaction was performed in diethyl ether at -78°C and allowed to warm to room temperature. Following purification, the yield was 78%. This method may be employed in the future to synthesize the necessary Z-isomers from the appropriate alkynes.

4.2.2 Issues with *E*-Alkene Formation

In order to form the 3-*E*-alkene from the 3-alkyne, the alkyne was reacted with solid sodium in ammonia at -78°C; the reaction was allowed to slowly cool to room temperature overnight. The first reaction used 2.5 equivalents of sodium, and yielded a mixture of unreacted starting material, as indicated by the alkyne carbon atoms in the 78-90 ppm range, and the 3-*E*-isomer, as indicated by the presence of olefinic protons in the 5.6 ppm range and olefinic carbons in the 128-133 ppm range. According to carbon NMR, the reaction mixture contained only unreacted starting material and desired product; there were a total of 16 peaks, 8 for the unreacted 3-alkyne and 8 for the *E*-isomer. In order to push the reaction to completion, the reaction was repeated with 5 equivalents of sodium. Again, the reaction did not proceed to completion and unreacted starting material was still present. Using 10 equivalents of sodium, there was still a mixture of unreacted starting material and product.

Looking at the alpha-hydroxyl methylene protons in the 3.6-3.7 ppm range, the peak for the alkyne appears at 3.68 ppm, while these protons appear at 3.62 ppm for the *E*-isomer. The ratio of these peaks can be used to determine the degree of completion of the reaction. Table 4.3 details the integrations for these peaks for the three different sodium equivalents. The percent of alkyne as a fraction of the total mixture is also included.

Table 4.3: Reduction Reaction Mixtures for Various Sodium Equivalents

Equivalents of Sodium	Alkyne	<i>E</i> -Alkene	% <i>E</i> -Alkene
2.5	0.84	0.92	52.3
5.0	1.30	1.94	59.9
10.0	0.43	1.93	81.8

The fractional percentage of alkyne is seen to decrease with increasing equivalents of sodium. This fraction was plotted against equivalents of sodium, as shown in Chart 4.1:

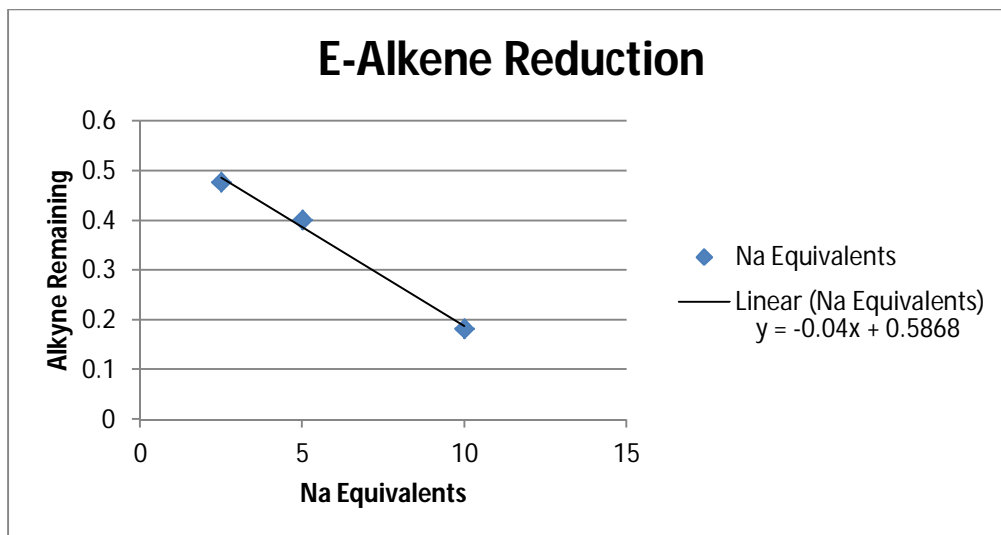


Chart 4.1: Alkyne Fraction as a Function of Sodium Equivalents

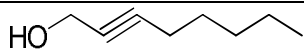
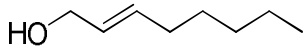
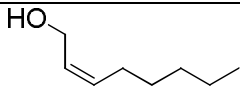
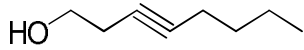
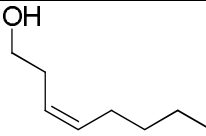
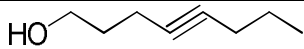
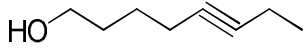
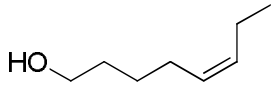
A linear regression was fitted to this plot, and this equation was used to approximate the number of equivalents necessary to completely consume the alkyne starting material. This would occur when the trend line crosses the independent variable axis. Using the linear regression equation, this number of equivalents needed to have no alkyne remaining after the reaction is 14.67 equivalents. In order to test this, the reduction reaction was repeated, using 15 equivalents of sodium. This reaction also indicated the

presence of unreacted starting material along with the desired *E*-alkene product. This may indicate that the reaction time is not long enough to allow for completion. Future reactions could be run for a longer period of time before allowing the mixture to warm to room temperature.

4.3 Results

Table 4.4 shows the molecules available at the moment to couple with the CAI-1 polar head group to form analogs.

Table 4.4: Alkyne and Alkene Chains Available for Coupling

Molecule	Structure
5-1	
5-2	
5-3	
5-4	
5-5	
5-6	
5-7	
5-8	

4.4 Conclusion

The synthesis of the alkyne molecules was generally successful. The initial attempts for the synthesis of *E*- and *Z*-alkenes were unsuccessful but provided valuable information about how to approach these syntheses in the future. The Wang resin protection approach was found to be difficult to standardize due to inconsistencies with the Wang resin itself. Therefore, it is recommended that other synthetic approaches be attempted. Once a replicable method for coupling of the polar head group to the alkyl chain is determined, the synthesized alkynes and alkenes can be used to form the analogs.

4.5 Future Directions

The other molecules needed are the 3-*E*-alkene, 4-*E*-alkene, 4-*Z*-alkene, and the 5-*E*-alkene. Once these molecules are synthesized, they can be coupled with the polar head group to form the desired series of analogs. In order to synthesize the needed *E*-alkenes, the following alternative method may be used, as shown in Figure 4.9:

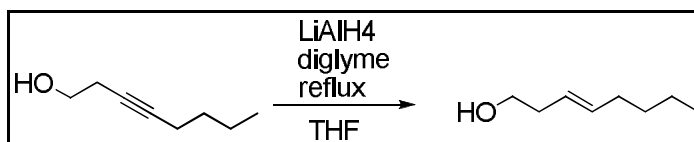


Figure 4.9: Alternative Synthesis for 3-*E*-Alkene

The 4-*Z*-alkene could be synthesized from the 4-alkyne using the method used to synthesize the 2-*Z*-alkene.

In order to synthesize the desired molecules, the use of the Wang resin protected head group was initially intended. This, however, presented issues in terms of stability and uniformity of commercially available Wang resin. Transesterification may be a

solution to these problems. After the coupling reaction, no further chemistry is needed to form the desired product. Therefore, the transesterification can be performed on the unprotected polar head group, as shown in Figure 4.10:

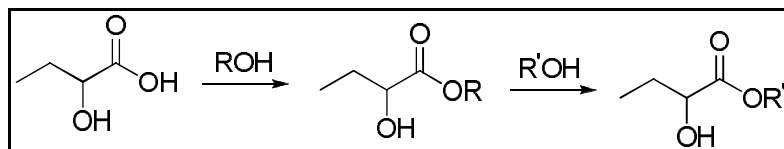


Figure 4.10: Transesterification Sequence

5 Covalent Modification of *Vibrio cholerae* CqsS

5.1 Use of TBS Protection Groups

In order to prevent any reactions from occurring at the secondary alcohol in the head group, the tert-butyldimethylsilyl (TBS) protection group was selected. The oxygen atom in the secondary alcohol can perform a nucleophilic attack on the silicon atom in the TBS molecule. This reaction forms a silyl ether molecule, which is stable in a variety of conditions. The mechanism for this formation is illustrated in Figure 5.1:

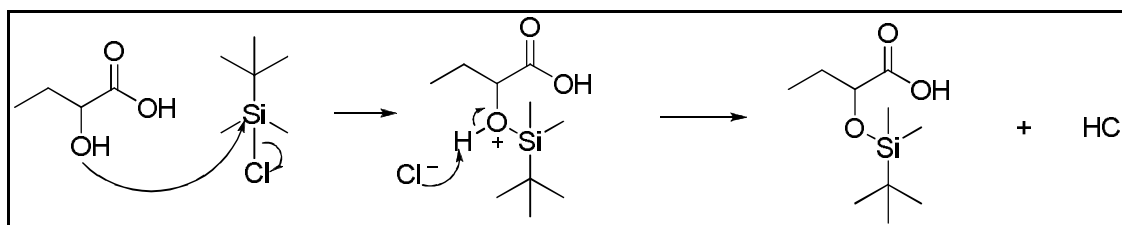


Figure 5.1: Silylation Mechanism

TBS ethers are relatively unreactive in chromatographic conditions, through a range of temperatures, and in the presence of Grignard reagents, metal sulfones, n-alkyllithiums, and enolates.^[1] Though tert-butyllithium can deprotonate the silicon methyl groups, this was not a major concern since highly basic conditions were not required in the synthesis schemes utilized in this project. TBS ethers are stable in mild bases, but labile in mildly acidic conditions; they are also stable in the presence of metal hydrides. The TBS group is also readily identifiable by NMR. The two silyl methyl groups appear as a singlet at approximately 0.2 ppm in proton NMR, and the tert-butyl methyl protons appear as a prominent singlet at a shift of approximately 0.9 ppm.

[1] Kociński, P. J. (2005). Protecting groups, Georg Thieme Verlag.

There are also a variety of conditions that can be used to complete deprotection of a silyl ether molecule. These include Lewis acids, fluorides, and mixtures of hydrofluoric acids and amines. The approach selected for final deprotection included the use of tertbutylammonium fluoride (TBAF) as the fluoride cleaving agent. This deprotection proceeds according to the mechanism shown in Figure 5.2:

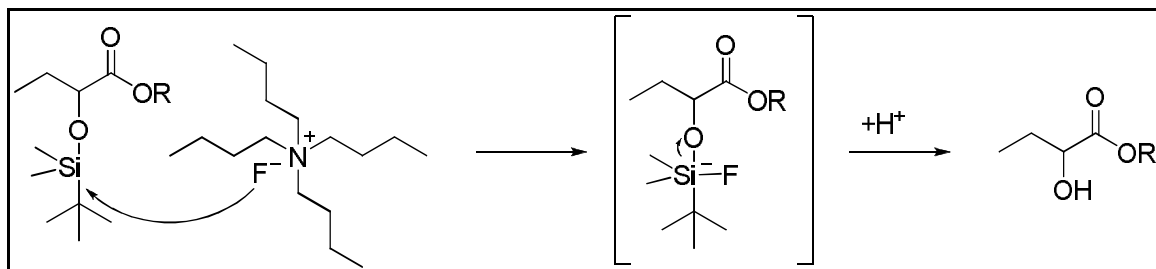


Figure 5.2: Silyl Deprotection Mechanism Using TBAF

5.2 Issues with Bis-silylation

The first step in the synthesis scheme is to protect the secondary alcohol in the polar head group with the TBS group while leaving the free, mono-silylated carboxylic acid available for reactions, according to the sequence shown in Figure 5.3:

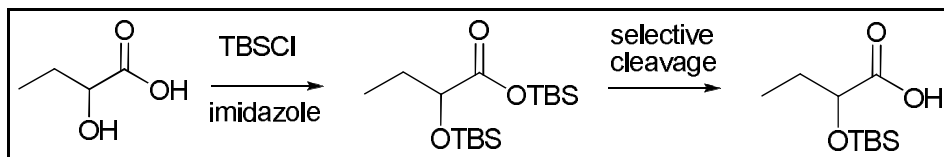


Figure 5.3: General Procedure for Synthesis of Free, Mono-Silylated Carboxylic Acid
 Generally, TBS chloride and imidazole were reacted with 2-hydroxybutyric acid overnight in DMF. This reaction was followed by a reaction using potassium hydroxide to selectively cleave the carboxyl TBS group, yielding mono-silylated 2-(*tert*-butyldimethylsilyloxy)butanoic acid. The goal of forming the mono-silylated carboxylic acid was to provide a pure compound which could then be carried on to form an acid

chloride using oxalyl chloride. The use of a pure compound to form acid chloride was pursued because it would allow for a higher degree of purity for further reactions, thereby reducing the need for future chromatographic procedures. The series of reactions intended to produce the mono-silylated carboxylic acid, however, presented issues because there was incomplete cleavage of the carboxylic acid silyl ether, yielding a mixture of products. This mixture included the bis-silylated molecule as well as the desired mono-silylated, free carboxylic acid shown above.

Various conditions were tested in attempts to selectively form the mono-silylated secondary alcohol. For the first set of cleavage conditions, 10 mL of 1 N potassium hydroxide were added to the bis-silylated product, followed by addition of 1 N HCl until pH was below 2. The resulting solution was purified via aqueous workup. The second set of reaction conditions included the addition to 10 mL of 1 N KOH, followed by addition of 1 N HCl until pH was below 6; the resulting solution was also purified via workup to obtain the desired product.

Analysis of the proton NMR of this product had much higher integrations than expected for the characteristic peaks for the TBS group. The tert-butyl methyl groups, expected to integrate to 9 protons, integrate to 25.49 protons; the silyl methyl groups, expected to integrate to 6 protons, integrate to 11.36 protons. These higher-than-expected integrations indicate the potential presence of tert-butyldimethylsilyl hydroxide (TBSOH) along with the desired product.

In order to separate TBSOH from the mono-silylated product, an aqueous separation was performed. 50 mL of KOH were added to the mixture. The mono-silylated free carboxylic acid would preferentially be deprotonated over TBSOH and brought into the aqueous layer, leaving TBSOH in the organic layer. This organic layer was collected in a clean flask and concentrated. Diethyl ether was added to the aqueous layer, which contained the mono-silylated carboxylate; this mixture was acidified using approximately 50 mL of 1 N HCl in order to bring the desired product into the organic layer.

This organic layer was collected and concentrated; NMR revealed minimal product. NMR was taken of the previously collected fraction, which was thought to contain TBSOH. The proton NMR of this fraction indicated the presence of a mixture of mono-silylated carboxylic acid along with bis-silylated molecules. The tert-butyl methyl groups integrated to 12.81 protons and the silyl methyl groups integrated to 6.11 protons, higher than expected. Figure 5.4a shows the potential mixture of products:

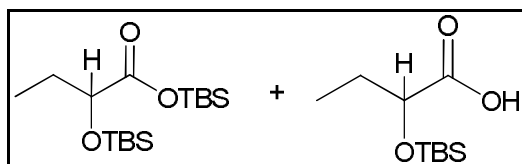


Figure 5.4a: Mixture of Bis-Silylated and Mono-Silylated Molecules

In addition to the aforementioned high integrations, the methine proton, labeled in Figure 5.4a, did not appear as expected. The methine proton has a proton NMR shift of approximately 5.05 ppm and should appear as a triplet. In the mixture, however, the

proton appears as a multiplet and integrates to 1.30, indicating the shown mixture of products.

In order to form mono-silylated molecules, additional cleavage conditions were tested. For example, rather than adding KOH after the overnight TBS coupling, a 15 mL mixture of 1:1 ethyl acetate: toluene was added. This was followed by the addition of methanol, the solution was cooled to 0°C, and potassium carbonate was added. This solution was acidified by 10% citric acid to pH 4, followed by an aqueous separation. The carbon NMR of this product indicated four distinct peaks in the 70-75 ppm, corresponding to the alpha-carbonyl carbon (bearing the methine proton shown above). The presence of these multiple peaks indicates that there are four unidentical, but structurally related molecules present in the reaction mixture. These four products appear to be in the ratio of 2:2:1:1, as indicated in Figure 5.4b, which shows the peaks for the methine proton highlighted in Figure 5.4a.

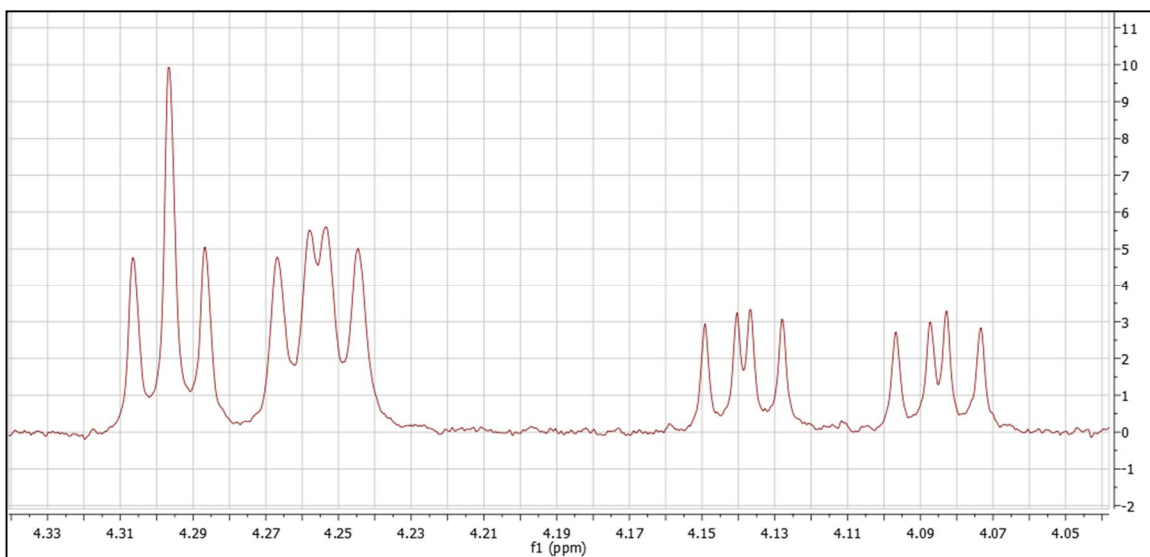


Figure 5.4b: NMR Peaks for Methine Protons in 4.2 ppm Range

Figure 5.4c highlights the NMR peaks for the carbon atoms bearing this methine proton. These peaks appear in the 70-75 ppm range.

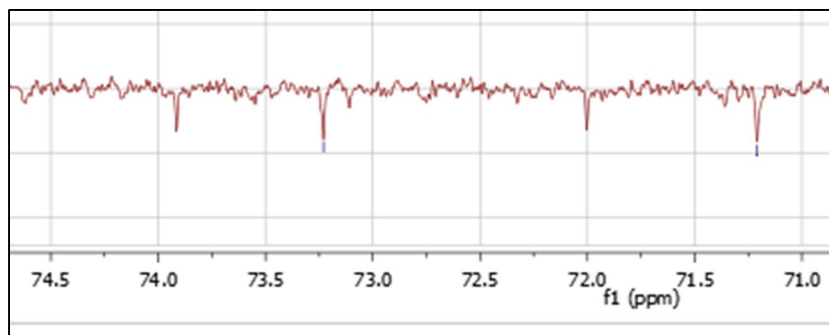


Figure 5.4c: NMR Peaks for Carbons Bearing Methine Proton

The presence of four different molecules is reiterated by the four peaks in the region of 25 ppm, which corresponds to the secondary carbon adjacent to the methine proton labeled in Figure 5.4. This mixture of four molecules is consistent with a double cleavage of both TBS groups from the bis-silylated molecule, no cleavage of the TBS groups, cleavage of only the carboxyl TBS group, and cleavage of only the secondary alcohol TBS group. The presumed mixture of products is shown in Figure 5.5:

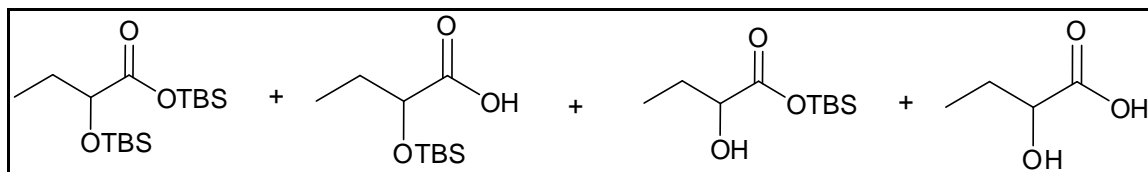


Figure 5.5: Mixture of Products from Selective Deprotection Reaction

Based on thin layer chromatography analysis, it would be difficult to separate these molecules due to their co-elution. Using 60% ethyl acetate in hexanes, there appeared to be one large spot on the silica plate.

In order to avoid this purification, an alternate synthesis was attempted. In this sequence, ethanol was reacted with 2-hydroxybutyric acid to form an unprotected ethyl ester. This ethyl ester was then subjected to the protection reaction (overnight stirring with TBSCl and imidazole). The goal of this series of reactions was to ensure that the only possible addition of the TBS group would be to the secondary alcohol. The ethyl ester reduces the reactivity of the ester oxygen, facilitating selective protection of the secondary hydroxyl group. This mono-silylated ethyl ester is then subjected to a saponification to yield the desired mono-silylated carboxylic acid, as shown in Figure 5.6:

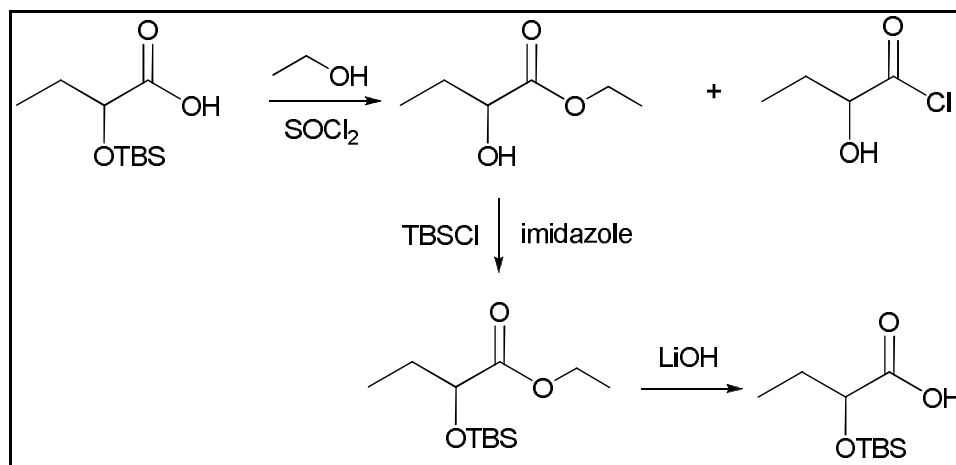


Figure 5.6: Alternative Synthesis Scheme for Free, Mono-Silylated Carboxylic Acid

Using this approach, the esterification appeared to contain a mixture of the desired ethyl ester, along with the acid chloride (shown in the first step of the sequence above). According to software predictions for the shift of the carbonyl carbon, it is difficult to distinguish the carbonyl carbons of the ethyl ester and the acid chloride; in both molecules, this carbon appears at approximately 175 ppm. Therefore, the presence of two different peaks for the secondary carbon was used to establish the presence of the two

molecules. In the ethyl ester, the carbon bearing the secondary alcohol appears at a shift of 71.57 ppm; for the acid chloride, this secondary carbon appears at a shift of 94.6 ppm in the carbon NMR. This is sensible since the electronegativity of the chloride atom withdraws electron density from the carbonyl carbon, increasing the partial positive charge developing at that position. This partial charge, along with the inductive effects of the chloride atom, helps to deshield the secondary carbon, causing it to shift downfield.

This crude mixture was carried forward and subjected to the TBS protection procedure, followed by the lithium hydroxide saponification. The mixture was carried forward because the acid chloride could also undergo nucleophilic substitution at the carbonyl carbon by the hydroxide ions available from dissociated LiOH; this would ultimately yield the desired TBS protected free carboxylic acid.

This first saponification reaction was run and according to proton NMR, there was still unreacted ethyl ester present based on the protons in the 4.2 ppm region. In the ethyl ester, the methyl protons appear as a triplet at 1.25 ppm, whereas the methylene protons appear as a quartet near 4.2 ppm; these protons are shown in Figure 5.7:

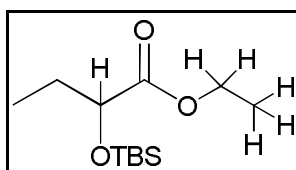


Figure 5.7: Ethyl Ester, with Characteristic Protons

The two methylene protons overlap with the methine proton indicated above. In the TBS protected free carboxylic acid, only the methine proton should appear in the region of 4.2 ppm and integrate to a value of approximately one. In the proton NMR of the products of

the saponification reaction, the protons in this region have a higher-than-expected integration of 4.37.

This mixture was again subjected to cleavage with a 1 N solution of LiOH. TLC was performed on the previously synthesized ethyl ester to determine the position of elution on a silica plate; the ethyl ester spot had an R_f value of 0.8. The reaction was then monitored at intervals of 1 hour; completion would be indicated by the disappearance of the starting material spot. Once the starting material spot was no longer visible by TLC, the reaction was stopped. NMR of the reaction products indicated four distinct products. In the proton NMR region of 4.1-4.3 ppm, there are four distinct multiplets, in the ratio of about 3:3:1:1; this means there are four distinct methine protons.

This is confirmed by the carbon NMR spectra. In the region near 70 ppm, where the carbon bearing the secondary hydroxyl group is located, there are also four peaks. These four peaks seem to indicate two major products and two minor products. Therefore, both the proton and carbon NMR confirm the presence of four products. The presumed products are shown in Figure 5.8:

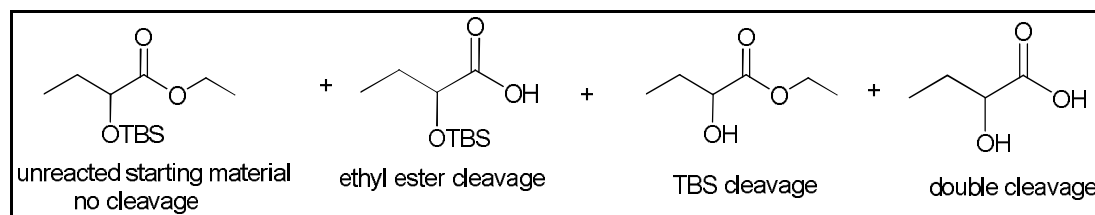


Figure 5.8: Mixture of Attempted Selective Ethyl Ester Deprotection

These products are consistent with the potential reactions which could have occurred over the course of the saponification. The four products are a result: 1) the intended saponification, 2) no reaction (yielding unreacted TBS protected ethyl ester), 3) the TBS

cleavage yielding an unprotected ethyl ester, and 4) double cleavage yielding 2-hydroxybutyric acid.

This series of reactions highlights the difficulties associated with forming a mono-silylated, free carboxylic acid. The initial approach using a simple base-catalyzed cleavage yielded a mixture of products which would be difficult to purify. The use of multiple conditions did not solve this issue. The use of a transesterification to form an ethyl ester, followed by TBS protection, also yielded issues during saponification. Just as the selective cleavage of a silyl ester was difficult to achieve, the cleavage of the ethyl ester was difficult to complete with high selectivity.

In order to continue forward with the synthesis of CAI-1 analogs, the bis-silylated material previously mentioned was carried forward. This compound was subjected to an overnight reaction with thionyl chloride at reflux (60°C) in order to drive the formation of the acid chloride forward. This reaction proceeds via the mechanism detailed in Figure 5.9:

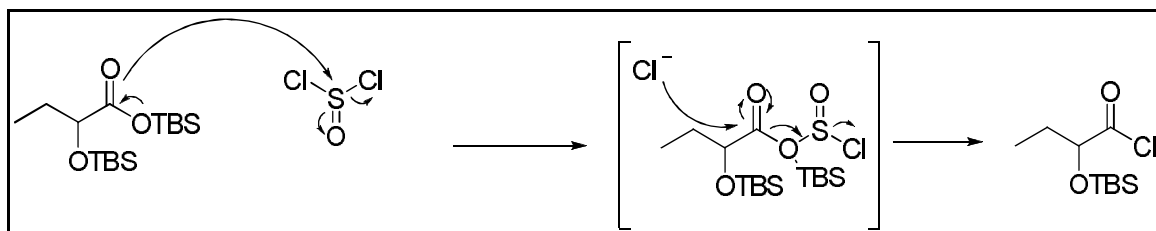


Figure 5.9: Mechanism for Acid Chloride Formation

The crude mixture of this reaction was carried forward and reacted with various alcohols to continue the CAI-1 analog intermediates. For the purpose of future reactions, the yield of the TBS protection protocol was assumed to be form 100% bis-silylated product. The

reactions were carried forward with this mixture because the targeted secondary hydroxyl group was still protected by the TBS group and the formation of the acid chloride from both the free acid and the TBS ester was still possible.

5.3 Syntheses

Note: Cleavage of TBS group would be done via a reaction with TBAF, as detailed in Chapter 3.

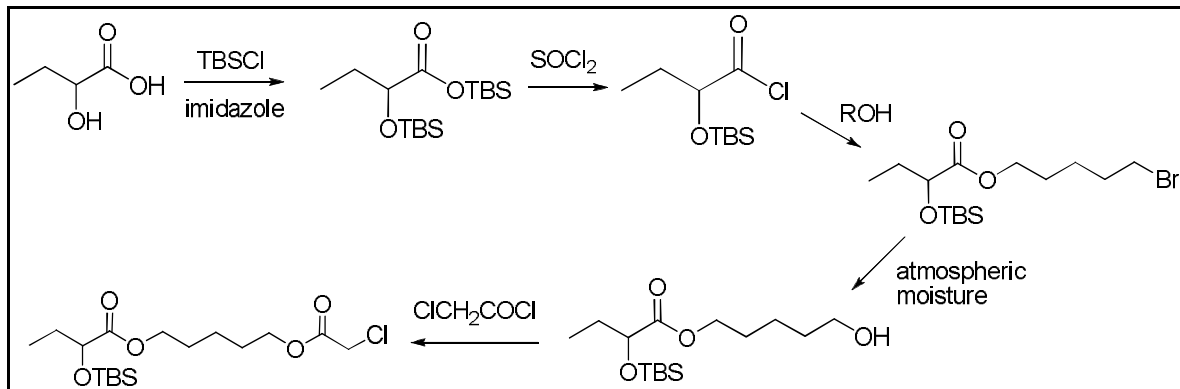


Figure 5.10: Attempted Synthesis Sequence for Alpha-Chloro Ester Analogs

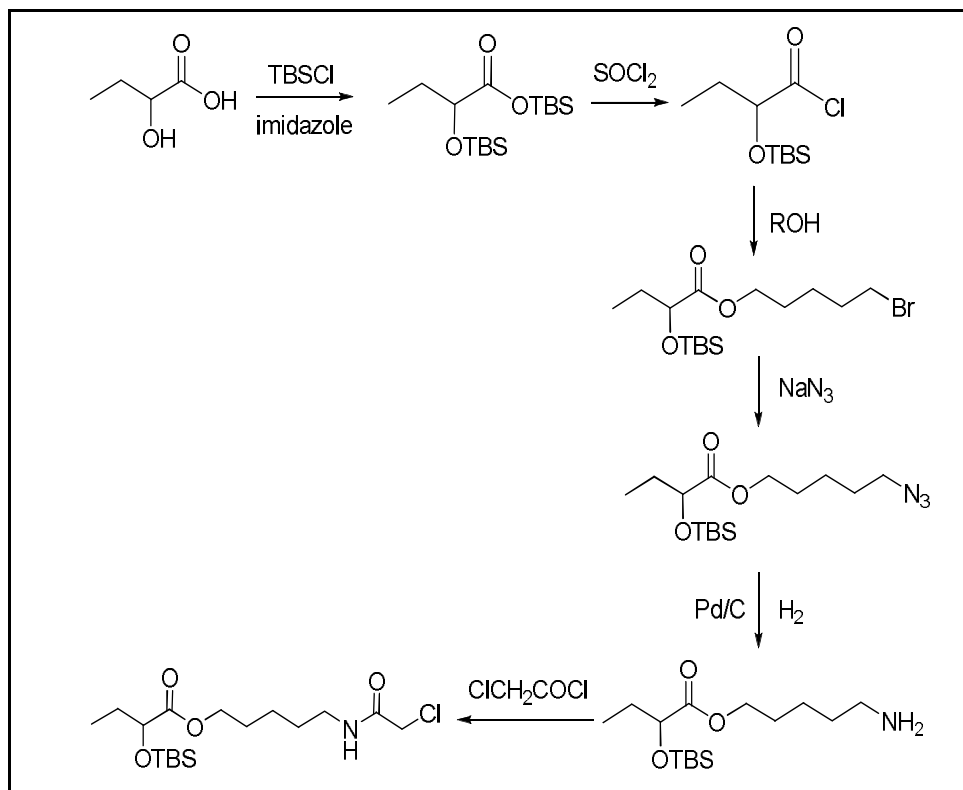


Figure 5.11: Synthesis Sequence for Alpha-Chloro Amide Analogs

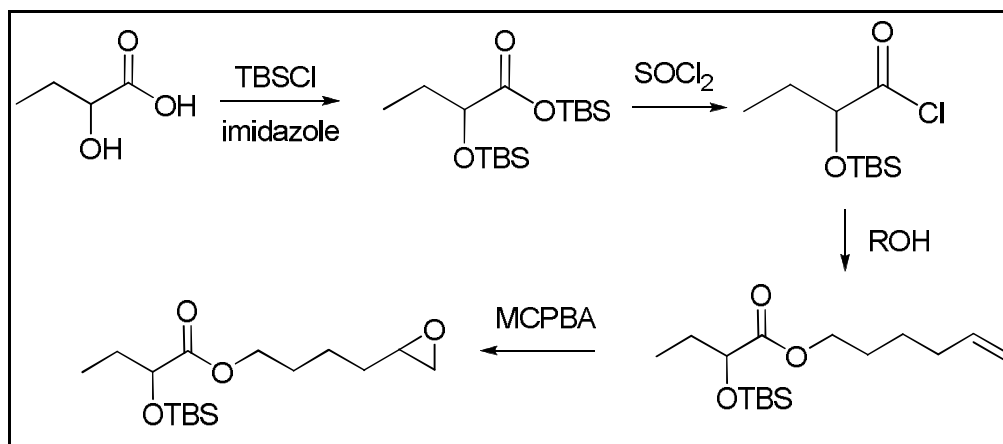


Figure 5.12: Synthesis Sequence for Terminal Epoxide Analogs

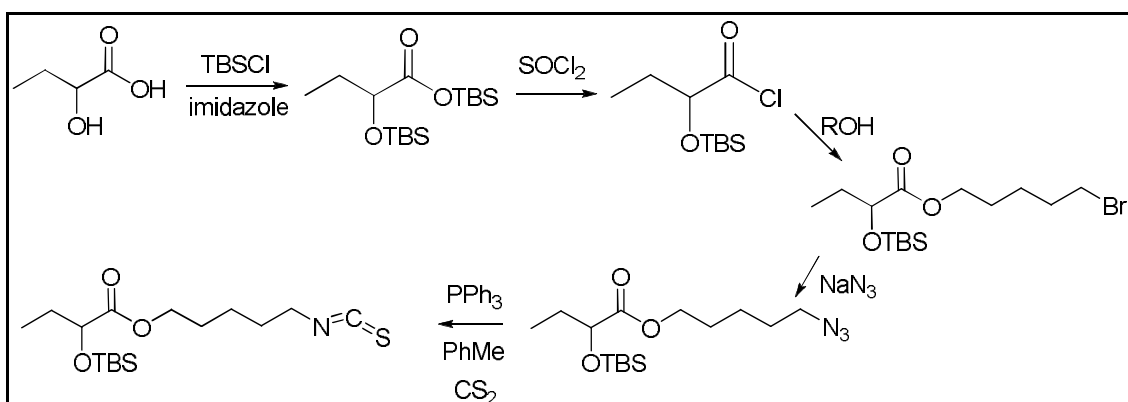


Figure 5.13: Synthesis Sequence for Terminal Isothiocyanate Analogs

5.3.1 Synthesis of Terminal Alpha-Chloro Amide Analogs

In order to begin the syntheses sequences, the acid chloride was formed from the bis-silylated compound, as detailed in the previous section. After formation of the acid chloride, an ester was formed via addition of 5-bromo-1-pentanol. The product was repurified by TLC and column chromatography. This material was then reacted with sodium azide in order to replace the terminal bromide with an azide functional group via a simple bimolecular substitution reaction.

The NMR of this reaction indicated that the reaction had not proceeded and completely unreacted starting material was present. In the proton NMR, the two silyl methyl groups integrate for a total of 6.94 protons, slightly higher than the expected 6.00 protons. According to software predictions, the alpha-bromine methylene protons should appear as a triplet near 3.6 ppm. In the region of 4.2 ppm, the methine proton of the head group (located on the secondary carbon bearing the silyl ether) overlaps with the two alpha-ester methylene protons on the alkyl chain. The expected ratio of these protons to the alpha-bromine methylene protons is expected to be 3:2. The observed ratio is 3.11:2.00. This seems to confirm the presence of the desired terminal bromide.

Additional confirmation is provided by the carbon NMR. In the carbon NMR spectra of this material, the silyl dimethyl group carbons of the TBS group appear at a shift of -5.13 ppm. The carbonyl carbon of the head group appears at 175.52 ppm, as expected. The TBS tert-butyl carbon atoms are difficult to distinguish because they overlap with the carbons of the alkane chain. Nine carbon atoms are expected to appear in the 20-35 ppm range; the NMR, however, indicates eight carbon atoms in this region, which is inconsistent with this count. Only one carbon (the alpha-ester carbon in the alkyl chain) is expected to be in the 60-70 ppm range. NMR of this compound has two peaks in this region.

HRMS (high resolution mass spectroscopy) further indicated that this molecule had a potential formula of $C_{17}H_{36}O_4Si$ and mass of 332.238 g/mol, significantly lower than the 394.15 g expected for the terminal bromide. The difference in mass is 61.912 g;

the total mass and formula is consistent with a terminal hydroxyl instead of the terminal bromide expected from the failed azide displacement reaction. This seems to confirm the loss of a bromine atom (mass loss of 78.92 g), followed by the addition of a hydroxyl group (mass gain of 17.00 g). This would yield a net loss of 61.92 g, consistent with the observed mass difference.

The presence of the terminal alcohol instead of the terminal bromide would be difficult to discern by proton NMR because the triplet indicative of the methylene protons on the carbon located alpha to the terminal bromide have a shift of about 3.51 ppm. This shift is similar to that of the methylene protons on the carbon located alpha to the terminal alcohol (3.50 ppm). It is, however, confirmed by re-analysis of the carbon NMR. The carbon bearing the terminal hydroxyl group appears in the 65 ppm area; in the terminal bromide, the alpha-bromine carbon appears at approximately 33 ppm. There is one peak less than expected in the 20-35 ppm range and one more peak than expected in the 60-70 ppm range. This, along with the HRMS data, confirms that this molecule is the terminal hydroxyl rather than the terminal bromide.

There could be two potential explanations for the formation of this molecule. It could be that the acid chloride was hydrolyzed, and the resulting free carboxylic acid was deprotonated and substituted the terminal bromide. Another possible mechanism by which this could have formed was if hydration of the terminal bromide occurred. This mechanism would be consistent with the formation of a TBS protected ester with a terminal hydroxyl. This mechanism is detailed in Figure 5.14:

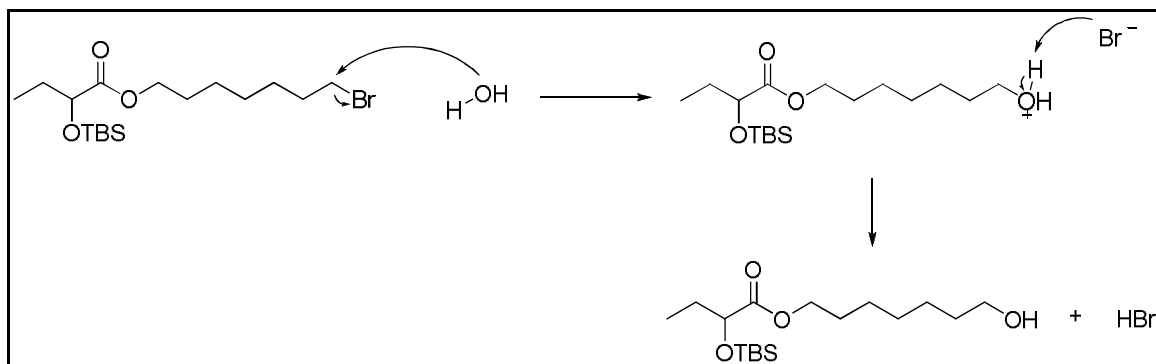


Figure 5.14: Potential Mechanism for Terminal Hydroxyl Formation

These two mechanisms could account for the formation of the terminal hydroxyl molecule. Careful *red*-analysis of the carbon NMR of the ester formation reaction, which was thought to have produced the terminal bromide, indicated that the terminal bromide had not formed to begin with. Again, two peaks are present in the 60-70 ppm region, consistent with the terminal hydroxyl but one more than expected with the terminal bromide. Eight peaks are present in the 20-35 ppm range, consistent with the terminal hydroxyl but one less than expected with the terminal bromide.

The intended reaction path for the terminal bromide was to form a terminal azide, which would then be reduced to form a terminal amine molecule. This would then be reacted with chloroacetyl chloride to form the alpha-chloro amide molecule. In order to arrive at a molecule with similar functionality to this one using the on-hand terminal hydroxyl molecule, chloroacetyl chloride was added directly to form an alpha-carbonyl halogen. This yielded an alpha-chloro ester analog of the intended alpha-chloro amide. This reaction is shown in Figure 5.15, alongside the intended reaction to form the alpha-chloro amide analog, and highlights the structural similarities between the two target molecules.

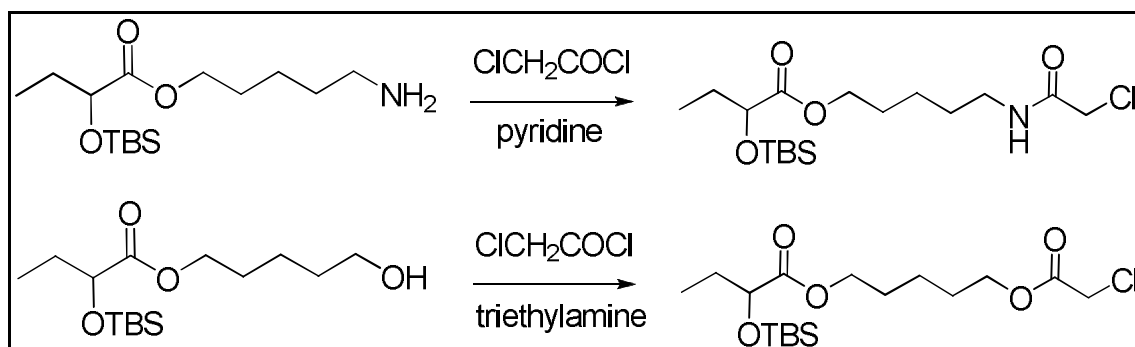


Figure 5.15: Formation of Alpha-Chloro Analogs

The alpha-chloro ester product was purified by TLC and column chromatography and NMR was taken. This NMR indicated that the reaction did not proceed and that the terminal group was a hydroxyl group. A potential cause of this could be that the thirty minute reaction time was not sufficient to allow the reaction to proceed. Generally, hydroxyl groups have two free electron pairs, giving them high electron density; this gives them a highly nucleophilic character. The carbonyl carbon in chloroacetyl chloride should be highly electrophilic. The partial positive charge on the carbon atom would be exacerbated by the inductive effects of the two electronegative chlorine atoms in the molecule. This should yield a rather rapid substitution, but instead, no reaction was observed.

This may be due to some degree of intramolecular folding. The alkyl tail of the molecule consists of single carbon-carbon bonds, which can allow for rotation. It could be possible that rotation is occurring around one of these bonds, allowing for the molecule to take a conformation which allows an intramolecular hydrogen bond, as shown in Figure 5.16:

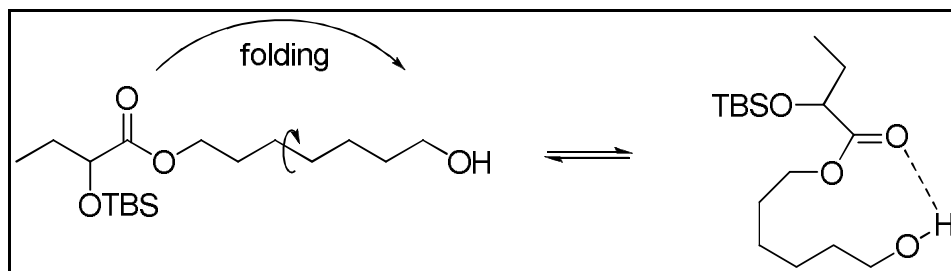


Figure 5.16: Potential Folding of Terminal Hydroxyl Molecule

In this conformation, a hydrogen bond forms between the hydrogen of the terminal hydroxyl group and the carbonyl oxygen of the ester. This would stabilize the molecule; for this molecule to react with chloroacetyl chloride, the energy gained by the hydrogen bond would have to be offset by the energy benefit from stabilizing the partial positive charge on the carbonyl carbon of the chloroacetyl chloride molecules. One possible explanation is that the solution was not basic enough to favor formation of the deprotonated hydroxyl. Since the hydrogen atom of the terminal hydroxyl is engaged in a favorable hydrogen bond, a higher concentration of base may be needed to effectively cause deprotonation. Though 1.5 equivalents of base were used, using a larger excess in the future may yield a higher rate of nucleophilic addition. Another concern which is made clear by this illustration relates to steric hindrance. In the hypothesized molecular structure, it may be difficult for the molecule to approach the chloroacetyl chloride molecule and nucleophilically substitute at the carbonyl carbon. This would also account for a slow reaction rate, and explain why the reaction did not proceed in thirty minutes. Future reactions could proceed for a longer period of time with a higher concentration of base; another potential solution is to heat the reaction slightly to allow it to run at a higher temperature, since reaction rates are directly proportional to temperature.

The aforementioned series of reactions was repeated in order to synthesize to synthesize the desired terminal bromides. 5-bromo-1-pentanol was added to the acid chloride and stirred overnight. Column chromatography was performed to remove any unreacted 5-bromo-1-pentanol. Analysis of the carbon NMR of this material confirmed the presence of the desired terminal bromide. The nine expected peaks in the 20-35 ppm range were all present, as well as only one peak (corresponding to the alpha-ester carbon in the alkyl chain) in the 60-70 ppm range. In the proton NMR, the silyl methyl groups integrate to 6.11, and the TBS tert-butyl methyl groups integrate to 9.09 protons. These values are consistent with expectation and indicate that the terminal bromine is still TBS-protected.

This molecule was then reacted with sodium azide to form a terminal azide molecule via a displacement of the bromine ion. In order to confirm the presence of this molecule, the proton NMR spectra of the terminal bromide and the newly formed terminal azide were overlaid. The alpha-bromo methylene protons appear at a shift of 3.41 ppm, whereas the alpha-azide methylene protons appear at 3.27 ppm. This shift indicates that the terminal bromide was fully consumed in the reaction. The presence of the azide was also confirmed by HRMS, which indicated a molecular mass of 329.213 g, consistent with the calculated 329.21 g.

After a flash column, the purified terminal azide was reduced to a terminal amine. The first set of reaction conditions made use of zinc powder and FeCl_3 as reducing agents. After the overnight reaction, HRMS was performed and indicated no reaction had occurred. The expected peak of 303.2 grams/mol for the terminal amine did not appear.

The reduction reaction was then performed using different conditions; palladium on carbon was used under hydrogen. After 2 hours, a small aliquot of solution was taken. HRMS indicated a large peak for a molecule with a mass of 303.22 grams/mol, consistent with the terminal amine mass.

This was then reacted with chloroacetyl chloride and triethylamine to form the final alpha-chloro amide molecule. A column was run to purify this molecule, but the elution fractions indicated no product. The characteristic TBS peaks mentioned previously, along with the alkyl carbons, were not present. The crude NMR of the products of the reaction indicated that the reaction had not occurred. Had the reaction occurred, the alpha-chloro methylene protons would appear as a distinct singlet integrating to 2.00 protons at approximately 4.2 ppm. This peak was not observed, and therefore, the reaction had not occurred. To recover the free amine from the column, a wash of 100 mL of ethyl acetate with 1% triethylamine was run on the column; this was followed by a wash using 100 mL dichloromethane and 5% methanol. Neither wash contained the free amine. The unreacted free amine, which had been run on a silica column, had most likely been adsorbed to the column after being protonated. The protonation of the free amine could have proceeded via the following mechanism, shown in Figure 5.17, in the presence of water (from atmospheric moisture):

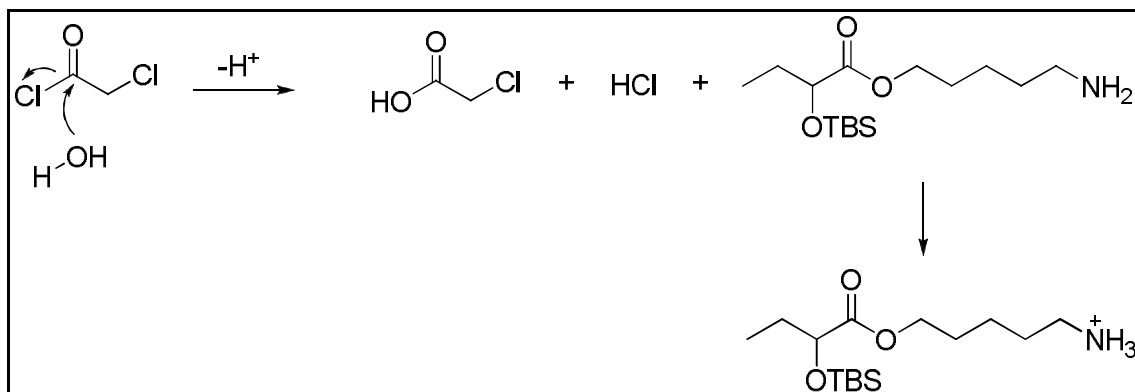


Figure 5.17: Protonation of Terminal Amine Molecule

In the reaction between chloroacetyl chloride and water, the products provide two sources of H⁺ (hydrochloric acid and a carboxylic acid) to acidify the terminal amine, which readily accepts protons with its lone pair of electrons on the nitrogen atom. The resulting protonated amine would readily adsorb to silica gel and be difficult to desorb. One of the potential reasons that the formation of the alpha-chloro amide did not occur may again be the formation of an intramolecular hydrogen bond, as previously explained.

5.3.2 Potential Alternate Synthesis of Terminal Bromide Molecules

An alternate synthesis was attempted to form the terminal bromide molecule. The previous sequence included coupling a bromoalcohol with the acid chloride followed by an azide displacement. In the new sequence, the azide displacement was performed directly on the bromoalcohol to give an alkyl chain with a hydroxyl at one terminus and azide functionality at the other. This alcohol was then coupled with the acid chloride to give the TBS protected terminal azide molecule, which could then be carried forward. The goal of this sequence is to make use of a convergent synthesis rather than a linear

synthesis to increase yields. The sequences for these two parallel syntheses are detailed in Figure 5.18:

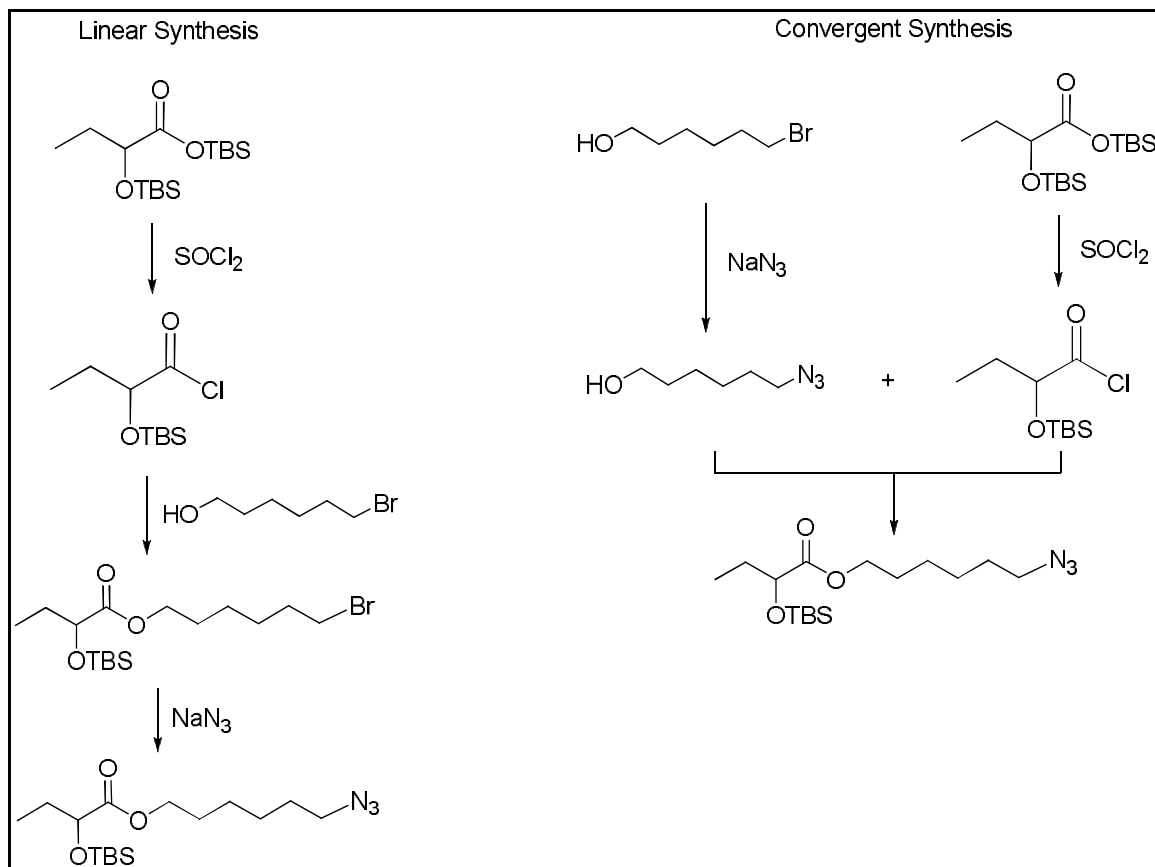


Figure 5.18: Alternate Synthesis Sequence for Terminal Bromide Analogs

The synthesis of the azidoalcohol had a very high yield of 96.1%. The successful synthesis of this molecule was confirmed by NMR. The alpha-azide methylene protons appear at a shift of 3.27 ppm, compared to a shift of 3.4 ppm for the alpha-bromo methylene protons. Additionally, the presence of a peak at 51.50 ppm is consistent with the alpha-azide carbon atom. This molecule was then coupled to the acid chloride to form the terminal azide. For the uncoupled azidoalcohol, the alpha-hydroxyl carbon peak

appears at approximately 63 ppm. Coupling was confirmed by the presence of a peak at 65.52 ppm in the carbon NMR corresponding to the alpha-ester carbon.

Though esterification did occur, this reaction presented other issues. It appeared that the TBS protecting group was not present in this molecule. In the proton NMR, the six protons for the two silyl methyl groups do not appear at a shift near 0.2 ppm. The peak at 0.9 ppm integrates to 4.59 protons, which is significantly lower than the expected twelve protons (which includes the nine protons of the tert-butyl methyl groups of the TBS group and the methyl group of the head group). In the carbon NMR, the peaks for the two silyl methyl groups do not appear at -2.3 ppm as expected. In the region of 20-30 ppm, there are four peaks rather than the expected seven peaks. Additionally, the three tert-butyl methyl group carbons are expected to appear in this region but are not present. According to NMR, the products of this reaction appeared to be the two molecules shown in Figure 5.19:

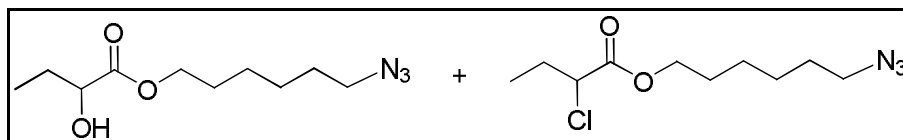


Figure 5.19: Mixture of Products from Convergent Synthesis Approach

In the unprotected terminal azide above, the secondary carbon bearing the hydroxyl group is expected to appear at approximately 72 ppm. This is confirmed by the peak at 71.42 ppm. The secondary chloride molecule above, which may have formed as a side product of the thionyl chloride reflux reaction used to form the acid chloride, should have

a peak at approximately 59 ppm for the carbon bearing the chloride atom. This appears at a peak of 60.52 ppm, confirming the presence of this molecule.

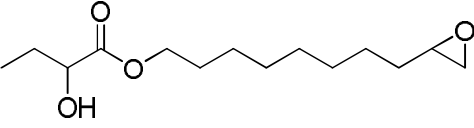
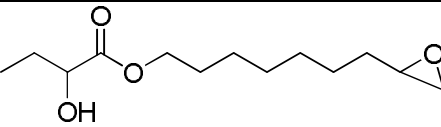
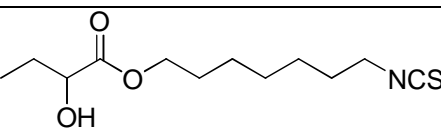
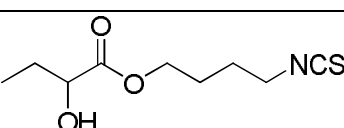
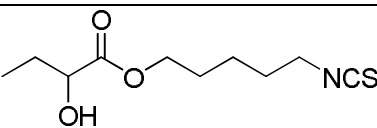
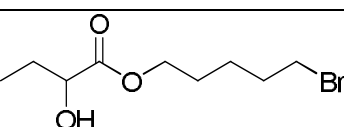
Additional evidence for the presence of these two molecules is provided by proton NMR. The methine proton at the secondary carbon bearing the hydroxyl can be differentiated from the methine proton in the chlorinated molecule; they appear at 4.16 and 4.3 ppm, respectively. The ratio of these peaks is 3.05:0.23, indicating that the mixture contained a low proportion of the secondary chlorine molecule.

A column was performed on this mixture to isolate 0.025 g of the unprotected, secondary hydroxyl molecule. The yield of this product was 31.3% and this material was resubjected to TBS protection. The yield of the silylation was 68.9%. Therefore, the overall yield of this convergent synthesis was 20.7%. For the linear synthesis, the overall yield was 52.4%, significantly higher than that of the convergent approach. This is unexpected because the convergent synthesis was anticipated to have a higher yield than the linear approach. However, issues with desilylation required an additional reaction to reprotect the material with a TBS group, which lowered the overall yield. It could be possible that repeating this convergent synthesis would have a higher yield in the future.

5.4 Results

The molecules shown in Table 5.1 were synthesized and tested via bioassay in order to determine levels of CqsS activation.

Table 5.1: Synthesized Molecules for Covalent Modification

Molecule	Structure
5-1	
5-2	
5-3	
5-4	
5-5	
5-6	

5.4.1 Bioassay Results

Depending on cell density, the plasma membrane sensor can act as a phosphatase (removing phosphate groups from the first substrates in the pathway) or a kinase (phosphorylating substrates). At low cell density, shown in Figure 1, the quorum sensing figure, the activation of the CqsS sensor allows it to act as kinase and activate the pathway, ultimately resulting in the upregulation of HapR gene transcription. At high cell density, the sensor acts to dephosphorylate and prevent gene expression, leading to reduced biofilm formation and virulence. Any phosphatase activity causes the induction level to drop below the full kinase potential. This causes the curve to have a lower maximum induction than the native molecule. The analogs found to be active in the first bioassay were retested for a larger range of concentrations. The bioassay results are shown in Figure 5.20:

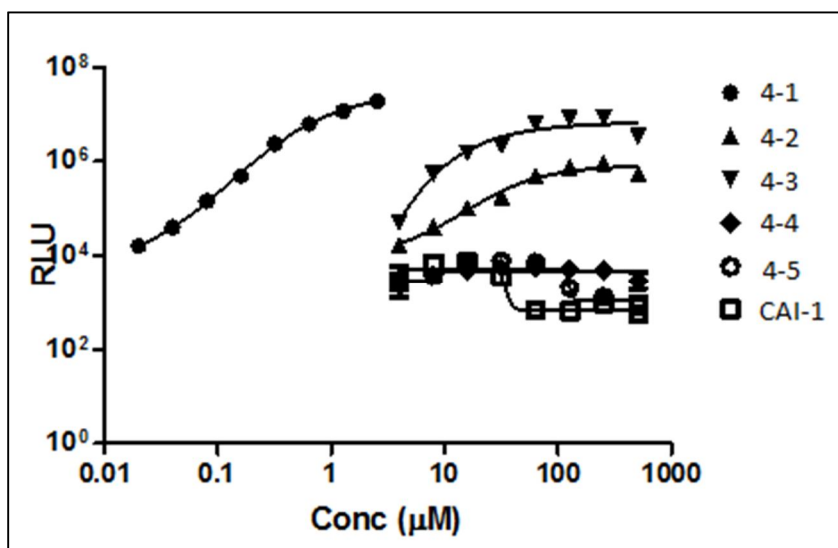


Figure 5.20a: Bioassay Results for Synthesized CAI-1 Analogs

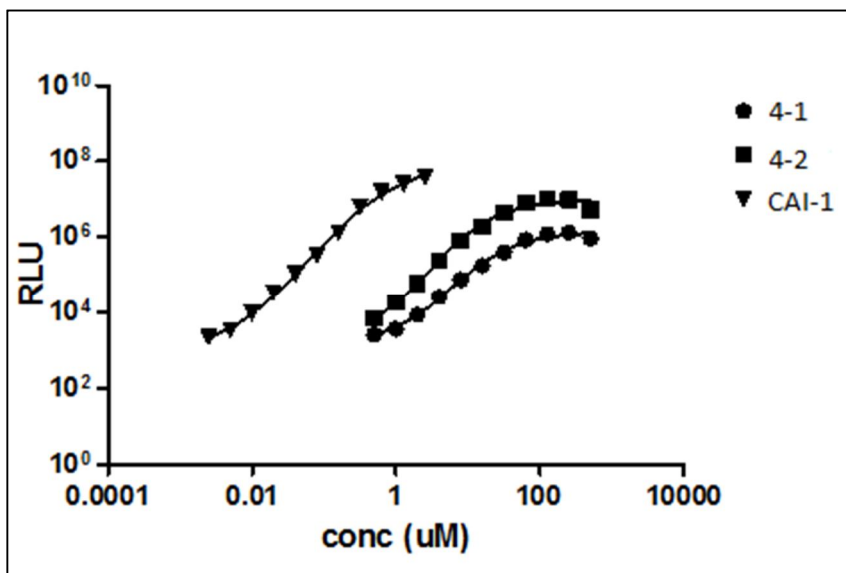


Figure 5.20b: Bioassay Results for Active CAI-1 Analogs

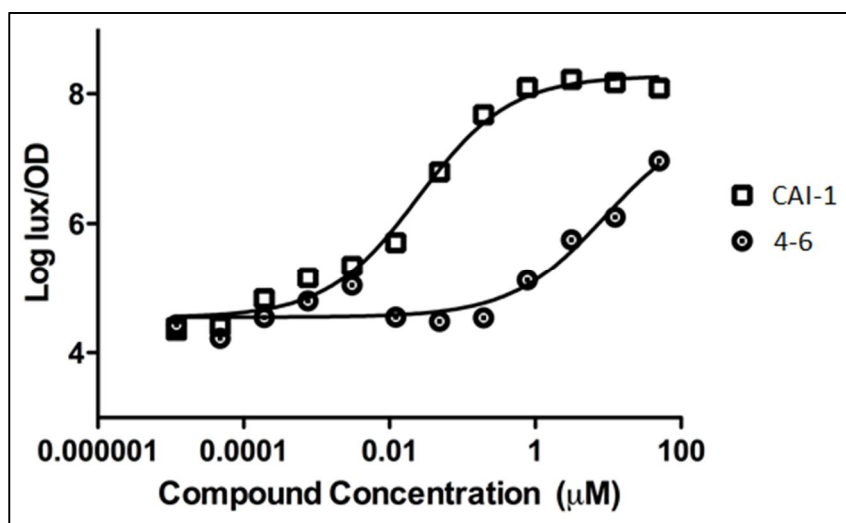


Figure 5.20c: Bioassay Results for Terminal Bromide Analog

The figure above indicates the results for bioassays done to test the binding affinity and levels of activity of the analogs in reference to the native autoinducer. The tests were run in *E.coli* cells which expressed the CqsS receptor in their membrane. In these cells, the autoinducer synthase was eliminated and instead, the receptor was coupled with the LuxCDABE gene. This allowed bioluminescence to be the product of

the phosphorylation cascade instead of virulence or biofilm formation. This light formation was measured and was assumed to be a function of activity of the tested molecules.

The two main measures of interest are the percent induction and EC_{50} levels. Percent induction is an indicator of activity levels. The maximum luminescence for the native molecule is set as the baseline (100% activity). For the other molecules, the maximum can be viewed as a fraction of the reference level set by CAI-1. Shifting the curve upwards indicates a greater activity level, and shifts downward mean a lower percent induction for a given molecule. EC_{50} is an indicator of affinity levels. This measure is the value of concentration for which the luminescence is half of its highest level. Shifting to the right denotes a lower binding affinity, while shifting to the left indicates a lower necessary concentration needed to allow for half the maximum activity.

For the epoxide analogs, both showed a higher EC_{50} level than the native molecule. The concentration required for half activity is approximately the same for both analogs, but nearly double that of CAI-1. The maximum percent induction for 5-2 was above eighty percent, whereas the maximum activity for the longer chain 5-1 was noticeably lower. This can most likely be attributed to the length of the alkyl chain. In 5-2, the length from the carbonyl carbon to the site of addition by the cysteine sulfur is eleven atoms as opposed to twelve in 5-1. The native form of the inducer has ten atoms, making 5-1 closer in overall structure to the original molecule. This allows for better agonist activity in the active site of the receptor.

For the cross-linkers (isothiocyanate terminal groups), the activity curves are flat, indicating no activity, and therefore, the EC₅₀ level and percent induction are not relevant. The activity curve denotes that there is no agonistic effect. This may indicate that there is no addition of the cysteine sulfur to the carbon in the isothiocyanate group. It may also suggest that there is no binding in the active site. Again, the retest with 5-1 and 5-2 shows a similar binding curve to CAI-1 and a much higher percent induction than the cross-linkers. This data signals that the cross-linkers are not as effective as the epoxides in an agonist role, and the epoxides may be better candidates for future study. For molecule 5-6, the approximate EC₅₀ value is 9 uM, which is approximately three orders of magnitude higher than that of CAI-1. It is important to note that 5-6 has a length of eight molecules from the carbonyl carbon to the site of potential nucleophilic substitution. It could be possible that a ten atom chain length with a terminal bromide would have higher activity, and should be a target for future synthesis and testing.

5.4.2 Drug-like Properties of Synthesized Molecules

One of the goals of this project was to synthesize molecules which could be administered orally. For this to be feasible, the molecules must have properties which prevent rapid biological elimination. Certain physicochemical properties of molecules make them inherently less favorable as drugs. For example, more polar molecules generally metabolized more rapidly than less polar ones. Lipophilic molecules, along with structures which have fewer opportunities to form hydrogen bonds, generally have longer lifetimes. These molecules are less likely to be oxidized by cytochrome P450, a

biological enzyme responsible for metabolism of pharmaceutical compounds in the body.^[2]

The most important properties generally considered when evaluating the drug-like properties of a molecule are clogP, the number of hydrogen bond donors (HBD), the number of hydrogen bond acceptors (HBA), the molecular weight (MW, in grams/mol), and the polar surface area (PSA, in Å³). These properties for the synthesized molecules are summarized in the Table 5.2:

Table 5.2: Chemical Properties of Synthesized Molecules

Molecule	clogP	HBD	HBA	MW (grams/mol)
5-1	3.06	1	3	258.35
5-2	2.53	1	3	244.33
5-3	3.45	1	3	259.37
5-4	1.86	1	3	217.29
5-5	2.39	1	3	231.31
5-6	2.29	1	2	253.13

The PSA for the epoxides is approximately 59.06 Å³, for the isothiocyanates is 46.53 Å³, and for the bromide is 46.53 Å³, as predicted by software.

The “Rule of Five,” a general guideline used to analyze the drug-like properties of drugs. This evaluation is based on an analysis of the properties of molecules which have

[2] Lipinski, C. A., F. Lombardo, et al. (1997). "Experimental and computational approaches to estimate solubility and permeability in drug discovery and development settings." *Advanced Drug Delivery Reviews* 23(1-3): 3-25.

high activity in high-throughput screenings. This guideline states that molecules generally are more favorable as drugs if they have a clogP value below 5, have less than 5 hydrogen bond donors, less than 5 hydrogen bond acceptors, and molecular weights below 500 grams/mol. Another favorable property is having a polar surface area less than 140 \AA^3 . According to these parameters, these synthesized molecules all have favorable physicochemical properties and may have favorable profiles in the body.

5.5 Conclusion

From the obtained data, it seems that molecules 5-1, 5-2, and 5-6 may have potential in future testing. Though there is activation of the CqsS sensor, this does not necessarily indicate that covalent modification is taking place. In order to test for covalent modification, mass spectrometry would have to be performed on the CqsS receptor after adding an active analog. The target of the covalent modification was a cysteine residue in the active site of the receptor. If covalent modification has occurred, the fragment containing this residue would have a larger mass than if it were unmodified. If the difference in mass corresponds to the mass of the CAI-1 analog, this may indicate that covalent modification has taken place.

The terminal bromide, molecule 5-6, shows some level of activity, despite having a shorter chain length than native CAI-1. A series of terminal bromides of varying chain lengths should be synthesized in order to fully test the activity of this type of molecule.

5.6 Future Directions

The next major direction for this project is to continue synthesis of molecules that range from 9-11 atoms from the carbonyl carbon of the polar head group to the site of nucleophilic substitution to submit for testing. In general, any terminal functional group that can stabilize a net negative charge upon displacement can potentially be applied as the terminal group of the analogs. Weak bases are usually good leaving groups in this substitution reaction. This general approach seems like a logical one to follow because it would work well as a typical bimolecular substitution *in vitro*. However, when looking at the mechanism *in vivo*, a potential problem arises. In the case of leaving groups which are halogens, the displacement of the halide ion may cause extraction of a hydrogen ion from the cysteine-analog intermediate and form a halogen acid. This strong acid would easily dissociate and acidify the receptor active site, which would cause the hydrogen bonds necessary to maintain active site shape to be disturbed. The same problem would arise from use of the terminal bromine analog. The displaced bromine ion could act as a base and extract a proton, yielding an acidification of the active site environment. Using a chain length of 9-11 atoms and using the alpha-carbonyl chlorine and bromine combinations, these molecules would constitute six targets out of the library to be made.

It is important to note that one set of intermediates made in the synthesis sequence are molecules of interest themselves. The terminal bromide series is another set of molecules of interest. These molecules are capable of undergoing nucleophilic substitution and it is possible the displacement of the bromine could result in covalent modification of the key cysteine residue. One of the terminal bromide molecules was

submitted for bioassay; other terminal bromides with varying alkyl chain lengths were synthesized but were lost in a laboratory fire. These molecules should be resynthesized and evaluated in the future.

In the library of molecules to be made, any electrophilic group could possibly be placed at the substitution position. In addition to the epoxides, aziridine functional groups could potentially be used. These molecules are the nitrogen counterparts of the epoxides and would react in a similar manner. An electron withdrawing group on the nitrogen atom would be necessary for the aziridine compounds to be susceptible to attack. The reaction is shown in Figure 5.21 with a sulfonamide group:

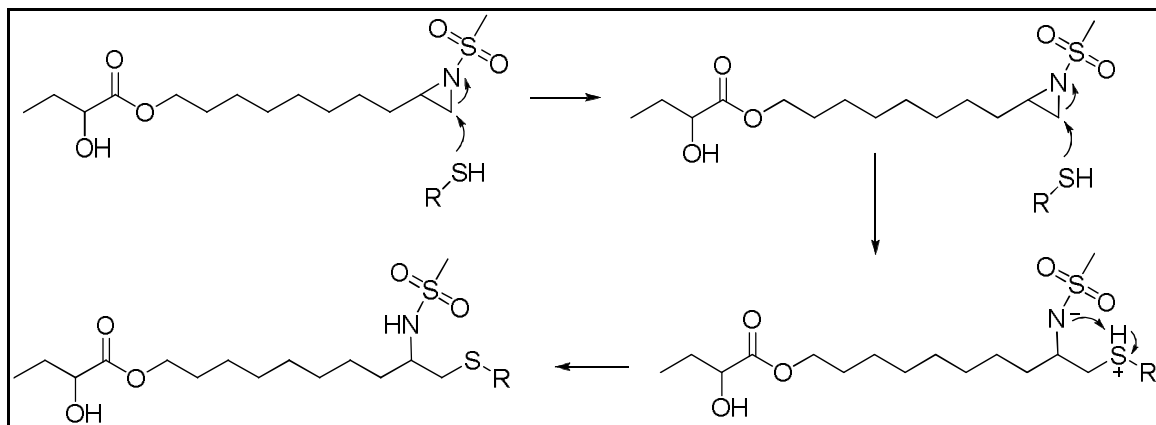


Figure 5.21: Covalent Modification with Terminal Aziridine Analogs

The addition of the cysteine residue sulfur would cause a favorable ring opening, relieving bond angle strain. In addition, the electronegative nitrogen atom can favorably stabilize the negative charge that arises from addition. It can then accept a proton from solution to form a stable modification. As with other intermediates, the reactivity might pose a problem *in vivo* because interactions with water might allow the ring to open by a substitution reaction. This would render the molecule inactive once it reaches the target site. However, this class of molecules may still have potential applications. By varying

the alkyl chain length again from 9-11 atoms, three analogs of this type can also potentially be synthesized.

Another viable possibility for an analog family would be the use of lactone groups at the terminus of the molecules. Rings of varying sizes (ranging from four- to six-membered lactones) could be used as potential candidates for the functional groups. Each of these different rings could be tested in conjunction with varying alkyl chain lengths as previously mentioned. The reaction would proceed as shown in Figure 5.22:

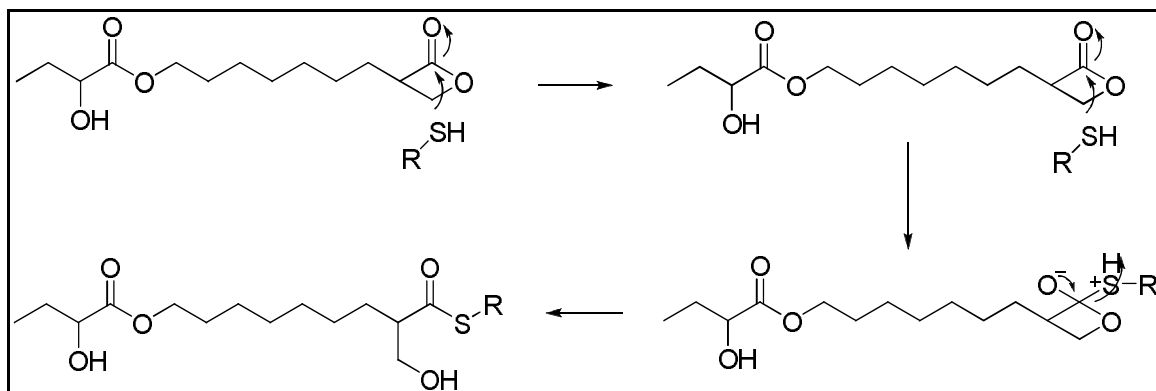


Figure 5.22: Covalent Modification with Terminal Lactone Analogs

In this reaction, the partial positive charge on the carbonyl carbon makes it susceptible for substitution by the nucleophilic sulfur. The opening of the ring and transfer of electrons onto the electronegative carbon oxygen also makes this mechanism favorable. It is important to note, however, that the size of the lactone ring will play a role because of steric interactions. If the ring is too large, it may be unfavorable for it to enter the active site of the CqsS sensor. It could also be that a large ring at one end of the molecule could cause the molecule to enter the active site in an orientation that slows or prevents the reaction from occurring. Another possible drawback of this analog candidate is the fact that water could potentially add as a nucleophile to the carbonyl carbon,

causing the ring to open. This side product would most likely be inactive and therefore ineffective in covalently modifying the key cysteine residue. The aforementioned molecules may be the subjects for future bioassays that will test their activity and binding affinity in the CqsS sensor.

6 Synthetic Procedures

General Conditions

All reactions were performed in oven-dried glassware connected to a double manifold under an inert nitrogen atmosphere, and using dry solvents and reagents unless otherwise noted. The inert gas was introduced at low pressure using a bubbler setup. All NMR spectra were recorded using a Varian Unity/INOVA (400 or 500 MHz) or a Bruker AVANCE (500MHz).

Reagents and Solvents

All chemicals were purchased from commercial vendors and used without further purification.

Solvent Removal

Removal of volatile solvents was accomplished using a Büchi 011 rotary evaporator under vacuum provided by a vacuum pump.

Purification

Silica chromatography was performed using silica gel 60Å porosity, 230x400 mesh (Sorbent Technologies). All analytical thin layer chromatography was performed using Silica C TLC Plates w/UV254, 200µm (SORBENT Technologies). Flash chromatography was performed using standard grade silica. Silica gel was loaded into glass columns in the least-polar elution used during the purification (this was usually hexanes). Visualization was performed by staining (with ceric ammonium molybdate and/or potassium permanganate) and/or by absorbance of UV light.

6.1 CqsS Receptor Structure Elucidation Procedures

2-octyn-1-ol. To 2-propyn-1-ol (1.0 g, 18.16 mmol, 1.0 equiv) in ~50 mL NH₃ (-78°C) was added LiNH₂ (1.752 g, 76.3 mmol, 4.2 equiv). This reaction was run for ~3 hours, followed by addition of 1-iodopentane (4.317 g, 21.8 mmol, 1.2 equiv). This reaction was run overnight and allowed to warm to room temperature, followed by an aqueous workup (diluted with 25 mL ether, quenched with NH₄Cl, and washed twice with 25 mL brine). After drying over Na₂SO₄, the solvents were removed *in vacuo*. A flash column was run in hexanes, 10% EtOAc in hexanes, 20% EtOAc in hexanes, and 40% EtOAc in hexanes. ¹H NMR (500 MHz, CDCl₃) δ 7.26 (s, 1H), 4.24 (s, 1H), 4.12 (s, 1H), 2.20 (s, 1H), 2.04 (s, 1H), 1.61 (s, 1H), 1.50 (s, 1H), 1.32 (s, 1H), 0.89 (s, 1H). ¹³C NMR (126 MHz, CDCl₃) δ 86.74, 78.30, 77.34, 77.09, 76.83, 60.50, 51.50, 31.10, 28.36, 22.26, 21.13, 18.76, 14.25, 14.03.

3-octyn-1-ol. To 3-butyne-1-ol (1.5 g, 21.5 mmol, 1.0 equiv) in ~50 mL NH₃ (-78°C) was added LiNH₂ (1.086 g, 47.3 mmol, 2.2 equiv). This reaction was run for ~3 hours, followed by addition of 1-iodobutane (4.748 g, 25.8 mmol, 1.2 equiv). This reaction was run overnight and allowed to warm to room temperature, followed by an aqueous workup (diluted with 25 mL ether, quenched with NH₄Cl, and washed twice with 25 mL brine). After drying over Na₂SO₄, the solvents were removed *in vacuo*. A flash column was run in hexanes, 10% EtOAc in hexanes, 20% EtOAc in hexanes, and 40% EtOAc in hexanes. ¹H NMR (501 MHz, CDCl₃) δ 7.26 (s, 1H), 3.66 (s, 1H), 2.43 (s, 1H), 2.16 (s, 1H), 1.45

(s, 1H), 1.39 (s, 1H), 0.90 (s, 1H). ^{13}C NMR (126 MHz, CDCl_3) δ 82.91, 77.41, 77.16, 76.91, 76.34, 61.49, 31.17, 23.29, 22.09, 18.54, 18.05, 15.49, 13.77.

4-octyn-1-ol. To 4-pentyn-1-ol (1.0 g, 11.89 mmol, 1.0 equiv) in ~50 mL NH_3 (-78°C) was added LiNH_2 (1.147 g, 49.9 mmol, 4.2 equiv). This reaction was run for ~3 hours, followed by addition of 1-iodopropane (2.425 g, 14.3 mmol, 1.2 equiv). This reaction was run overnight and allowed to warm to room temperature, followed by an aqueous workup (diluted with 25 mL ether, quenched with NH_4Cl , and washed twice with 25 mL brine). After drying over Na_2SO_4 , the solvents were removed *in vacuo*. A flash column was run in hexanes, 10% EtOAc in hexanes, 20% EtOAc in hexanes, and 40% EtOAc in hexanes. ^1H NMR (500 MHz, CDCl_3) δ 7.26 (s, 1H), 3.76 (s, 1H), 2.28 (s, 1H), 2.11 (s, 1H), 1.73 (s, 1H), 1.50 (s, 1H), 0.96 (s, 1H). ^{13}C NMR (126 MHz, CDCl_3) δ 81.13, 79.55, 77.41, 77.16, 76.91, 62.26, 31.72, 22.58, 20.85, 15.58, 13.63.

5-octyn-1-ol. To 5-hexyn-1-ol (1.0 g, 10.19 mmol, 1.0 equiv) in ~50 mL NH_3 (-78°C) was added LiNH_2 (0.749 g, 32.6 mmol, 3.2 equiv). This reaction was run for ~3 hours, followed by addition of iodoethane (1.907 g, 12.2 mmol, 1.2 equiv). This reaction was run overnight and allowed to warm to room temperature, followed by an aqueous workup (diluted with 25 mL ether, quenched with NH_4Cl , and washed twice with 25 mL brine). After drying over Na_2SO_4 , the solvents were removed *in vacuo*. A flash column was run in hexanes, 10% EtOAc in hexanes, 20% EtOAc in hexanes, and 40% EtOAc in hexanes. ^1H NMR (501 MHz, CDCl_3) δ 7.24 (s, 1H), 3.65 (s, 1H), 2.16 (s, 1H), 1.63 (s, 1H), 1.54 (s, 1H), 1.08 (s, 1H). ^{13}C NMR (126 MHz, CDCl_3) δ 82.23, 79.22, 77.41, 77.16, 76.91, 62.66, 62.62, 31.96, 31.94, 25.41, 18.61, 14.47, 12.51.

2-Z-octen-1-ol. To 2-octyn-1-ol (0.09 g, 0.71 mmol, 1 equiv) in hexanes (7.2 mL) was added quinoline (13.2 μ L, 0.111 mmol, 0.156 equiv) and Lindlar catalyst (0.264 g, 0.3697 g/mmol alkyne). A hydrogen balloon was used to provide hydrogen pressure. The solution was filtered through celite and a cotton plug through a pipette. Solvent was removed *in vacuo*. The peaks for each of the time points in the time series study are listed.

2 minutes: ^1H NMR (500 MHz, CDCl_3) δ 8.91 (s, 1H), 8.19 (s, 1H), 8.14 (s, 1H), 7.84 (s, 1H), 7.74 (s, 1H), 7.54 (s, 1H), 7.43 (s, 1H), 7.26 (s, 1H), 4.25 (s, 2H), 2.12 (d, $J = 68.1$ Hz, 3H), 1.83 (s, 1H), 1.49 (s, 2H), 1.35 (s, 1H), 0.92 (s, 3H), 0.06 (s, 1H). ^{13}C NMR (126 MHz, CDCl_3) δ 150.38, 136.45, 129.70, 129.33, 128.41, 127.91, 126.76, 121.22, 86.66, 78.43, 77.41, 77.16, 76.91, 51.45, 31.15, 28.41, 22.32, 18.82, 14.10.

5 minutes: ^1H NMR (500 MHz, CDCl_3) δ 8.92 (s, 1H), 8.16 (d, $J = 33.2$ Hz, 1H), 7.84 (s, 1H), 7.74 (s, 1H), 7.56 (s, 1H), 7.42 (s, 1H), 7.26 (s, 1H), 5.56 (s, 1H), 4.22 (d, $J = 32.8$ Hz, 2H), 2.20 (s, 2H), 2.05 (s, 1H), 1.50 (s, 2H), 1.32 (s, 4H), 0.90 (s, 3H). ^{13}C NMR (126 MHz, CDCl_3) δ 150.39, 136.44, 133.38, 129.70, 129.35, 128.41, 128.38, 127.91, 126.76, 121.22, 86.66, 78.44, 77.41, 77.16, 76.91, 58.69, 51.46, 31.52, 31.15, 29.39, 28.41, 27.50, 22.63, 22.33, 18.82, 14.17, 14.10.

15 minutes: ^1H NMR (500 MHz, CDCl_3) δ 8.90 (s, 1H), 8.18 (s, 1H), 7.83 (s, 1H), 7.73 (s, 1H), 7.55 (s, 1H), 7.40 (s, 1H), 7.26 (s, 1H), 5.57 (s, 1H), 4.22 (d, $J = 26.6$ Hz, 1H), 4.18 (s, 1H), 2.17 (s, 1H), 2.06 (s, 1H), 1.67 (s, 1H), 1.49 (s, 1H), 1.30 (s, 7H), 0.88 (s, 3H). ^{13}C NMR (126 MHz, CDCl_3) δ 150.40, 148.17, 136.39, 133.28, 129.67, 129.37,

128.44, 128.40, 127.90, 126.73, 121.21, 86.55, 78.50, 77.41, 77.16, 76.91, 58.65, 51.38, 31.52, 31.15, 29.38, 28.42, 27.50, 22.63, 22.32, 18.82, 14.17, 14.09.

20 minutes: ^1H NMR (500 MHz, CDCl_3) δ 8.89 (s, 1H), 8.12 (d, $J = 20.4$ Hz, 1H), 7.80 (s, 1H), 7.71 (s, 1H), 7.54 (s, 1H), 7.38 (s, 1H), 7.24 (s, 1H), 5.67 – 5.43 (m, 1H), 4.17 (s, 1H), 2.04 (s, 1H), 1.29 (d, $J = 37.5$ Hz, 1H), 0.86 (s, 1H). ^{13}C NMR (126 MHz, CDCl_3) δ 150.57, 148.37, 136.36, 133.76, 133.39, 129.71, 129.56, 128.99, 128.52, 128.47, 127.99, 126.78, 121.30, 77.48, 77.23, 76.98, 58.74, 32.38, 31.60, 29.91, 29.47, 29.00, 27.58, 22.71, 14.25.

25 minutes: ^1H NMR (500 MHz, CDCl_3) δ 8.88 (s, 1H), 8.12 (d, $J = 33.0$ Hz, 1H), 7.79 (s, 1H), 7.68 (s, 1H), 7.51 (s, 1H), 7.36 (s, 1H), 7.24 (s, 1H), 5.54 (d, $J = 50.3$ Hz, 1H), 4.13 (d, $J = 56.0$ Hz, 1H), 3.62 (s, 1H), 2.37 (s, 1H), 2.00 (s, 1H), 1.61 – 1.48 (m, 1H), 1.26 (d, $J = 26.5$ Hz, 1H), 0.83 (s, 1H). ^{13}C NMR (126 MHz, CDCl_3) δ 203.34, 150.46, 148.25, 136.40, 134.36, 133.53, 133.12, 129.71, 129.44, 129.07, 128.66, 128.45, 127.96, 126.77, 121.26, 77.48, 77.23, 76.98, 63.86, 63.09, 62.15, 58.62, 44.08, 32.97, 32.52, 32.36, 31.98, 31.78, 31.57, 31.54, 29.87, 29.57, 29.44, 29.27, 29.18, 28.98, 27.55, 25.93, 22.83, 22.75, 22.68, 22.22, 14.28, 14.22.

30 minutes: ^1H NMR (500 MHz, CDCl_3) δ 9.78 (s, 1H), 8.91 (s, 1H), 8.14 (d, $J = 38.2$ Hz, 1H), 7.82 (s, 1H), 7.71 (s, 1H), 7.55 (s, 1H), 7.41 (s, 1H), 7.26 (s, 1H), 5.59 (d, $J = 58.8$ Hz, 1H), 4.13 (d, $J = 54.2$ Hz, 1H), 3.65 (s, 1H), 3.48 (s, 1H), 2.43 (s, 1H), 2.02 (s, 1H), 1.57 (s, 2H), 1.26 (s, 7H), 0.88 (s, 3H). ^{13}C NMR (126 MHz, CDCl_3) δ 203.28, 150.48, 148.28, 136.31, 134.49, 133.68, 133.32, 129.64, 129.47, 128.92, 128.45, 128.40, 127.92, 126.71, 125.80, 125.07, 121.22, 77.41, 77.16, 76.91, 66.01, 63.95, 63.17, 62.42,

62.11, 58.68, 44.05, 36.11, 34.77, 32.92, 32.48, 32.31, 31.94, 31.75, 31.72, 31.53, 31.50, 29.84, 29.52, 29.41, 29.40, 29.24, 29.15, 28.93, 27.51, 25.87, 25.38, 22.79, 22.72, 22.65, 22.34, 22.18, 15.40, 14.27, 14.25, 14.20, 14.18, 14.08.

1 hour: ^1H NMR (500 MHz, CDCl_3) δ 7.24 (s, 1H), 5.59 (s, 1H), 5.50 (s, 1H), 4.17 (s, 1H), 4.07 (s, 1H), 3.63 (s, 1H), 2.40 – 2.35 (m, 1H), 2.02 (s, 1H), 1.55 (s, 1H), 1.27 (d, $J = 20.5$ Hz, 1H), 0.85 (s, 1H). ^{13}C NMR (126 MHz, CDCl_3) δ 150.54, 148.34, 136.37, 133.65, 133.27, 129.70, 129.53, 129.04, 128.59, 128.46, 127.98, 126.77, 121.28, 77.48, 77.23, 76.98, 63.95, 63.17, 58.69, 44.11, 32.99, 32.37, 32.00, 31.80, 31.59, 31.56, 29.89, 29.59, 29.47, 29.46, 29.29, 29.21, 28.99, 27.57, 25.94, 22.85, 22.77, 22.71, 22.70, 22.24, 14.31, 14.24.

1.5 hours: ^1H NMR (500 MHz, CDCl_3) δ 9.76 (s, 1H), 8.93 (s, 1H), 8.11 (s, 1H), 7.83 (s, 1H), 7.72 (s, 1H), 7.58 (s, 1H), 7.26 (s, 1H), 5.66 (s, 1H), 5.57 (s, 1H), 4.20 (s, 1H), 4.08 (s, 1H), 3.64 (s, 1H), 2.40 (s, 1H), 2.03 (s, 1H), 1.67 (s, 2H), 1.30 (s, 6H), 0.87 (s, 3H). ^{13}C NMR (126 MHz, CDCl_3) δ 150.56, 136.26, 133.80, 133.45, 129.63, 129.56, 128.89, 128.41, 128.39, 127.94, 126.71, 121.24, 77.41, 77.16, 76.91, 64.02, 63.24, 58.74, 32.94, 32.33, 31.95, 31.54, 31.51, 29.53, 29.42, 28.94, 27.52, 25.87, 22.80, 22.67, 14.27, 14.20.

2 hours: ^1H NMR (500 MHz, CDCl_3) δ 8.89 (d, $J = 4.0$ Hz, 1H), 8.14 (dd, $J = 33.2, 8.4$ Hz, 1H), 7.82 (d, $J = 8.2$ Hz, 1H), 7.72 (t, $J = 7.7$ Hz, 1H), 7.55 (t, $J = 7.5$ Hz, 1H), 7.41 (dd, $J = 8.2, 4.2$ Hz, 1H), 7.26 (s, 1H), 5.34 (s, 2H), 3.61 (s, 2H), 2.04 (s, 4H), 1.56 (s, 2H), 1.41 (s, 2H), 1.24 (s, 1H), 0.95 (s, 3H). ^{13}C NMR (126 MHz, CDCl_3) δ 150.35, 136.42, 132.49, 132.08, 131.87, 129.70, 129.29, 129.14, 128.91, 128.86, 127.90, 126.75, 121.21, 77.41, 77.16, 76.91, 63.14, 62.90, 32.40, 32.35, 32.28, 31.70, 31.22, 29.81,

29.51, 29.39, 26.89, 26.06, 25.95, 25.85, 25.79, 25.69, 22.77, 20.62, 14.47, 14.24, 14.22, 14.06.

1 hour (0°C): ¹H NMR (500 MHz, CDCl₃) δ 7.24 (s, 1H), 5.59 (s, 1H), 5.50 (s, 1H), 4.17 (s, 1H), 4.07 (s, 1H), 3.63 (s, 1H), 2.40 – 2.35 (m, 1H), 2.02 (s, 1H), 1.55 (s, 1H), 1.27 (d, *J* = 20.5 Hz, 1H), 0.85 (s, 1H). ¹³C NMR (126 MHz, CDCl₃) δ 150.54, 148.34, 136.37, 133.65, 133.27, 129.70, 129.53, 129.04, 128.59, 128.46, 127.98, 126.77, 121.28, 77.48, 77.23, 76.98, 63.95, 63.17, 58.69, 44.11, 32.99, 32.37, 32.00, 31.80, 31.59, 31.56, 29.89, 29.59, 29.47, 29.46, 29.29, 29.21, 28.99, 27.57, 25.94, 22.85, 22.77, 22.71, 22.70, 22.24, 14.31, 14.24.

3-*E*-octen-1-ol. To ~20 mL NH₃ (at -78°C) was added 0.115 g Na^o (0.115 g, 5.0 mmol, 2.5 equiv), followed by 5 mL THF. In a separate flask, to 5 mL THF was added 3-octyn-1-ol (0.252 g, 2.0 mmol, 1.0 equiv); this solution was then added to the reaction flask. The reaction was run overnight and slowly warmed to room temperature. Solution was then washed twice with 25 mL of water, extracted twice with 25 mL hexanes, and washed twice with 25 mL brine. After drying over Na₂SO₄, the solvents were removed *in vacuo*. [This protocol was repeated with the same parameters but different amounts of Na^o, as follows: 0.23 g (10 mmol, 5.0 equiv), 0.46 g (20 mmol, 10 equiv), and 0.69 g (30 mmol, 15 equiv).] The peaks for the different equivalence of sodium are listed.

2.5 equivalents: ¹H NMR (500 MHz, CDCl₃) δ 7.26 (s, 1H), 5.56 (s, 1H), 5.39 (s, 1H), 3.65 (d, *J* = 30.7 Hz, 2H), 2.45 (s, 1H), 2.26 (s, 1H), 2.16 (s, 1H), 2.01 (s, 1H), 1.78 (s, 1H), 1.59 (s, 1H), 1.52 – 1.17 (m, 5H), 0.92 (s, 3H). ¹³C NMR (126 MHz, CDCl₃) δ

134.62, 125.78, 82.94, 77.41, 77.16, 76.91, 76.34, 62.13, 61.50, 36.12, 32.50, 31.74, 31.18, 23.32, 22.37, 22.10, 18.56, 14.10, 13.78.

5 equivalents: ^1H NMR (500 MHz, CDCl_3) δ 7.26 (s, 1H), 5.46 (d, $J = 92.1$ Hz, 2H), 3.67 (s, 1H), 3.62 (s, 2H), 2.42 (s, 1H), 2.28 (s, 2H), 2.19 (s, 1H), 2.03 (s, 2H), 1.80 (s, 1H), 1.59 (s, 2H), 1.52 – 1.11 (m, 9H), 0.89 (s, 5H). ^{13}C NMR (126 MHz, CDCl_3) δ 134.62, 125.78, 77.41, 77.16, 76.91, 62.12, 61.50, 36.12, 32.50, 31.74, 31.18, 23.31, 22.36, 22.10, 18.55, 14.10, 13.78.

10 equivalents: ^1H NMR (500 MHz, CDCl_3) δ 7.26 (s, 1H), 5.45 (d, $J = 93.1$ Hz, 2H), 3.68 (s, 1H), 3.62 (s, 2H), 2.41 (s, 1H), 2.27 (s, 2H), 2.17 (s, 1H), 2.00 (s, 2H), 1.65 (s, 1H), 1.37 (d, $J = 59.8$ Hz, 7H), 0.90 (s, 4H). ^{13}C NMR (126 MHz, CDCl_3) δ 134.61, 125.78, 77.41, 77.16, 76.91, 62.12, 61.49, 36.12, 32.50, 31.74, 31.18, 23.31, 22.36, 22.10, 18.55, 14.10, 13.77.

15 equivalents: ^1H NMR (500 MHz, CDCl_3) δ 7.26 (s, 1H), 5.54 (s, 1H), 5.37 (s, 1H), 3.68 (s, 2H), 3.62 (s, 2H), 2.42 (s, 2H), 2.27 (s, 2H), 2.17 (s, 2H), 2.01 (s, 2H), 1.78 (s, 1H), 1.60 (s, 2H), 1.52 – 1.18 (m, 11H), 0.90 (s, 7H). ^{13}C NMR (126 MHz, CDCl_3) δ 134.62, 125.78, 82.94, 77.41, 77.16, 76.91, 76.34, 62.13, 61.50, 36.12, 32.50, 31.74, 31.18, 23.31, 22.36, 22.10, 18.55, 14.10, 13.78.

Note: 2-Z-octen-1-ol was synthesized by Lark Perez.

6.2 Covalent Modification of *Vibrio cholerae* CqsS Procedures

2-(tert-butyldimethylsilyoxy)butanoic acid. To 2-hydroxybutyric acid (1 g, 7.9 mmol) in DMF (10 mL) was added imidazole (2.58 g, 37.92 mmol, 4.8 equivalents) and TBSCl (2.86 g, 18.96 mmol, 2.4 equiv). Solution was stirred overnight at room temperature. Afterwards, 15 mL EtOAc/toluene (1:1) was added. Solution was then washed with 25 mL aqueous solution of citric acid (10%), saturated aqueous NaHCO₃, H₂O, and brine. After drying over Na₂SO₄, the solvents were removed *in vacuo*. The residue was dissolved in 43 mL MeOH. The solution was cooled to 0°C and K₂CO₃ (2.73 g, 19.5 mmol, 2.5 equiv) and 13 mL H₂O were added. Solution was stirred at room temperature for 4 hours and the solvent was removed *in vacuo* afterwards. Yield = 0.71 g (41.1%)

5-azidopentan-1-ol. To 5-bromo-1-pentanol (1 mL, 1.482 g, 8.9 mmol) in DMSO (9 mL) was added NaN₃ (1.74 g, 26.7 mmol, 3.0 equiv) and Bu₄NI (0.33 g, 0.9 mmol, 0.1 equiv). Solution was stirred at room temperature for 48 hours. Mixture was diluted by adding 45 mL DMSO, then washed with H₂O (2x25 mL) and brine (2x25 mL). Solution was dried over Na₂SO₄ and solvent removed *in vacuo*. Yield = 0.082 g (6.95%). ¹H NMR (501 MHz, CDCl₃) δ 7.26 (s, 1H), 6.96 (s, 5H), 4.30 (s, 2H), 2.08 (s, 1H), 1.92 (s, 2H), 1.75 (s, 2H), 1.27 (t, *J* = 7.1 HZ, 1H), 1.01 (s, 6H). ¹³C NMR (126 MHz, CDCl₃) δ 180.03 (s), 160.36 (s), 160.03 (s), 77.67 (s), 77.41 (s), 77.16 (s), 61.44 (s), 27.56 (s).

2-(tert-butyldimethylsilyoxy)butanoic acid. To 2-hydroxybutyric acid in DMF was added imidazole and TBSCl. The mixture was stirred at room temperature for 72 hours. Reaction was quenched with 12 mL 0.5 N HCl and washed with ether (2x20 mL), water

(20 mL), and brine (20 mL). Solvent was removed *in vacuo*. Yield = 1.822 g (69.4%). Column was run on VT20 using hexanes, 10% EtOAc, 20%, and 30%. NMR was run on product target. ¹H NMR (500 MHz, CDCl₃) δ 7.26 (s, 1H), 4.15 (d, *J* = 63.6 Hz, 1H), 2.03 (s, 1H), 1.87 – 1.62 (m, 2H), 1.60 (s, 1H), 1.49 (d, *J* = 4.4 Hz, 1H), 1.24 (s, 10H), 0.87 (s, 18H), 0.17 (d, *J* = 86.8 Hz, 5H). ¹³C NMR (126 MHz, CDCl₃) δ 73.93 (s), 73.20 (s), 36.22 (s), 25.97 – 25.34 (m), 21.15 (s), 20.80 (s), 18.87 (s), 14.27 (d, *J* = 4.9 Hz), 11.56 (s), 9.66 (s), 8.93 (s), -3.52 (s), -4.00 – -5.27 (m), -5.36 (s).

2-(*tert*-butyldimethylsilyloxy)butanoyl chloride. SOCl₂ (1.33 mL, 18.06 mmol, 10.0 equiv) was added dropwise to VT20 (0.6 g, 1.806 mmol, 1.0 equiv) and allowed to reflux overnight (~15 hours) at 60°C. Excess SOCl₂ was removed *in vacuo* with heating. Yield = 0.192 g (44.9%). ¹H NMR (500 MHz, CDCl₃) δ 7.26 (s, 1H), 4.35 (s, 1H), 2.18 (s, 1H), 1.99 – 1.77 (m, 3H), 1.25 (s, 2H), 0.96 (d, *J* = 38.2 Hz, 17H), 0.36 (s, 1H), 0.08 (s, 9H). ¹³C NMR (126 MHz, CDCl₃) δ 176.60 (s), 77.41 (s), 77.16 (s), 76.91 (s), 29.85 (s), 27.77 (d, *J* = 12.2 Hz), 27.44 (s), 24.53 (s), 18.30 (s).

5-bromopentyl 2-(*tert*-butyldimethylsilyloxy)butanoate. To 2-(*tert*-butyldimethylsilyloxy)butanoyl chloride (0.192 g, 0.811 mmol, 1 equiv) in THF was added DMAP (0.11 g, 0.88 mmol, 1.1 equiv) and 5-bromo-1-pentanol (0.1 mL, 0.88 mmol, 1.1 equiv). The solution was stirred overnight at room temperature and purified by column chromatography run in hexanes, 10% EtOAc in hexanes, 20%, and 50%. 20% fractions which indicated product via NMR and TLC were combined. ¹H NMR (500 MHz, CDCl₃) δ 7.26 (s, 4H), 4.13 (s, 3H), 3.39 (s, 2H), 1.87 (s, 2H), 1.69 (s, 4H), 1.57

(s, 5H), 1.25 (s, 9H), 0.91 (s, 18H), 0.06 (s, 8H). ^{13}C NMR (126 MHz, CDCl_3) δ 77.26 (dd, $J = 31.9, 5.4$ Hz), 77.09 – 77.01 (m), 76.91 (s), 64.44 (s), 33.62 (s), 32.39 (s), 29.85 (s), 28.56 (s), 27.96 (s), 24.71 (s).

6-azidohexan-1-ol. To 6-bromo-1-hexanol (1 mL, 7.3 mmol, 1.0 equiv) in DMSO (7.3 mL) was added NaN_3 (1.42 g, 21.9 mmol, 3.0 equiv) and Bu_4NI (0.28 g, 0.7 mmol, 0.1 equiv). Solution was stirred at room temperature for 96 hours, diluted with 35 mL EtOAc, then washed with water (2x25 mL) and brine (2x25 mL). Organic layer was then dried over sodium sulfate and solvent was removed *in vacuo*. Yield = 1.01 g (96.6%). ^1H NMR (501 MHz, CDCl_3) δ 7.26 (s, 1H), 4.12 (s, 1H), 3.65 (s, 2H), 3.40 (s, 1H), 3.27 (s, 2H), 2.05 (s, 2H), 1.59 (s, 5H), 1.40 (s, 4H), 1.26 (s, 4H), 0.95 (s, 1H), 0.88 (s, 2H). ^{13}C NMR (126 MHz, CDCl_3) δ 77.41 (s), 77.16 (s), 76.91 (s), 70.91 (d, $J = 19.1$ Hz), 63.03 (d, $J = 19.8$ Hz), 60.57 (s), 51.50 (s), 32.68 (s), 31.74 (s), 28.94 (s), 26.66 (s), 25.47 (s), 22.81 (s).

Ethyl 2-hydroxybutanoate. To 2-hydroxybutyric acid (10 g, 79.4 mmol, 1 equiv.) was added ethanol (160 mL, 0.5 M). Solution was chilled in acetone/dry ice bath and thionyl chloride (6.4 mL, 87.2 mmol, 1.1 equiv.) was added dropwise. Solution was mixed for 96 hours. ^1H NMR (500 MHz, CDCl_3) δ 7.26 (s, 2H), 4.26 (s, 2H), 3.80 (s, 1H), 2.18 (s, 1H), 1.79 (d, $J = 74.2$ Hz, 2H), 1.31 (s, 3H), 0.97 (s, 3H). ^{13}C NMR (126 MHz, CDCl_3) δ 175.47 (s), 77.41 (s), 77.16 (s), 76.91 (s), 61.97 (s), 27.70 (s).

5-azidopentyl 2-(tert-butyldimethylsilyloxy)butanoate. To 5-bromopentyl 2-(tert-butyldimethylsilyloxy)butanoate (0.2g, 0.603 mmol, 1.0 equiv) in DMF (2 mL) was

added sodium azide (0.117 g, 1.809 mmol, 3.0 equiv). The mixture was sealed and heated to 60°C and stirred for 24 hours. The solution was then diluted with diethyl ether (10 mL), quenched with water (10 mL), extracted with diethyl ether (2x10 mL), and dried over sodium sulfate. The solvent was removed *in vacuo*. Column chromatography was performed using hexanes, 10%, 20% and 40% EtOAc in hexanes. Yield = 0.14 g (70.5%). ¹H NMR (501 MHz, CDCl₃) δ 7.26 (s, 1H), 4.12 (s, 3H), 3.27 (s, 2H), 2.17 (s, 1H), 1.65 (s, 7H), 1.46 (s, 3H), 1.24 (s, 2H), 0.90 (s, 12H), 0.05 (s, 6H). ¹³C NMR (126 MHz, CDCl₃) δ 174.03 (s), 73.44 (s), 64.43 (s), 51.35 (s), 31.10 (s), 28.47 (d, *J* = 664.2 HZ), 25.83 (s), 25.83 (s), 18.46 (s), 9.78 (s), -4.81 (s), -5.21 (s). [M+H] calculated for C₁₅H₃₁N₃O₃Si, 330.21 g, found 330.22079.

5-aminopentyl 2-(*tert*-butyldimethylsilyoxy)butanoate. To 5-azidopentyl 2-(*tert*-butyldimethylsilyoxy)butanoate (0.07 g, 0.212 mmol, 1 equiv.) in ethyl acetate (1.34 mL) was added 5% palladium on carbon (0.024 g). A hydrogen balloon was used to provide hydrogen pressure. The solution was filtered through celite and a cotton plug through a pipette. Solvent was removed *in vacuo*. Yield = 0.062 g (96.4%). ¹H NMR (501 MHz, CDCl₃) δ 7.26 (s, 6H), 4.12 (s, 3H), 2.69 (s, 1H), 1.70 (dddd, *J* = 27.8, 23.5, 13.4, 7.7 HZ, 4H), 1.57 (s, 11H), 1.53 – 1.34 (m, 5H), 1.26 (dd, *J* = 11.8, 4.6 HZ, 2H), 0.93 (d, *J* = 20.6 HZ, 7H), 0.07 (d, *J* = 12.5 HZ, 4H). ¹³C NMR (126 MHz, CDCl₃) δ 77.31 (s), 77.06 (s), 76.81 (s), 64.65 (s), 42.09 (s), 28.50 (d, *J* = 12.0 HZ).

Ethyl 2-(*tert*-butyldiphenylsilyoxy)butanoate. To ethyl 2-hydroxybutanoate (1 g, 7.5 mmol, 1 equiv.) in DMF (10 mL) was added imidazole (2.47 g, 36 mmol, 4.8 equiv.) and

tert-butyldiphenylsilyloxy chloride (4.68 mL, 18 mmol, 2.4 equiv.). Solution was stirred overnight at room temperature. Solution was then acidified to pH 6 with 1 N HCl, extracted with diethyl ether (2x20 mL), washed with water (20 mL), washed with brine (20 mL) and dried over sodium sulfate. Solvent was removed *in vacuo*. ¹H NMR (501 MHz, CDCl₃) δ 7.71 (s, 19H), 7.39 (s, 29H), 7.26 (s, 8H), 4.26 (s, 2H), 4.13 (s, 4H), 2.92 (d, *J* = 36.7 Hz, 2H), 2.17 (s, 4H), 2.05 (s, 5H), 1.59 (s, 15H), 1.30 (s, 3H), 1.26 (s, 5H), 1.07 (s, 42H), 0.96 (s, 3H). ¹³C NMR (126 MHz, CDCl₃) δ 135.26 (s), 77.41 (s), 77.16 (s), 76.91 (s), 61.81 (s), 60.58 (s), 27.60 (s), 19.15 (s).

5-(2-chloroacetamido)pentyl 2-(tert-butyldimethylsilyloxy)butanoate. To 5-aminopentyl 2-(tert-butyldimethylsilyloxy)butanoate (0.062 g, 0.204 mmol, 1 equiv.) in dichloromethane (5 mL) was added triethylamine (70 microliters, 0.5 mmol, 2.45 equiv.) and chloroacetyl chloride (16.2 microliters, 0.204 mmol, 1 equiv.) dropwise. The reaction was stirred for 24 hours and the resulting solution was loaded onto a flash column and run in hexanes, 10% EtOAc in hexanes, 20% EtOAc in hexanes, and 40% EtOAc in hexanes. ¹H NMR (501 MHz, CDCl₃) δ 7.26 (s, 10H), 4.12 (s, 10H), 3.72 (s, 1H), 3.48 (s, 1H), 3.35 (s, 1H), 2.89 (s, 1H), 2.05 (s, 13H), 1.64 (s, 29H), 1.26 (s, 21H), 0.92 (d, *J* = 20.5 Hz, 12H), 0.05 (s, 6H). ¹³C NMR (126 MHz, CDCl₃) δ 77.41 (s), 77.16 (s), 76.91 (s), 60.58 (s), 29.85 (s), 28.55 (s).

6-azidoheptyl 2-hydroxybutanoate. To 2-(tert-butyldimethylsilyloxy)butanoic acid (0.083 g, 0.035 mmol, 1.0 equiv.) in THF (700 microliters) was added VT28 (0.055 g, 0.39 mmol, 1.1 equiv.) and DMAP (0.047 g, 0.39 mmol, 1.1 equiv.). The solution was

stirred overnight at room temperature, and loaded directly onto a column. ^1H NMR (500 MHz, CDCl_3) δ 7.26 (s, 3H), 4.18 (d, $J = 20.7$ HZ, 3H), 3.28 (s, 2H), 1.84 (s, 2H), 1.68 (s, 4H), 1.61 (s, 6H), 1.40 (s, 4H), 1.25 (s, 1H), 0.97 (s, 5H). ^{13}C NMR (126 MHz, CDCl_3) δ 175.48 (s), 77.41 (s), 77.16 (s), 76.91 (s), 65.62 (s), 51.45 (s), 28.86 (s), 28.59 (s), 27.66 (s), 26.46 (s), 25.58 (s).

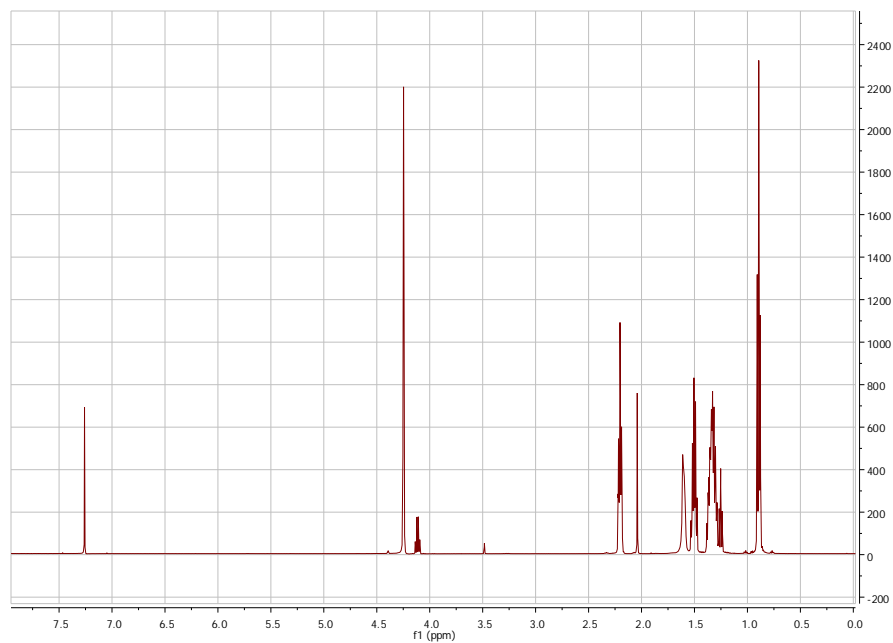
6-azidohexyl 2-(tert-butyldimethylsilyoxy)butanoate. To 6-azidohexyl 2-hydroxybutanoate (0.025 g, 0.109 mmol, 1.0 equiv.) in DMF (140 microliters) was added imidazole (0.035 g, 0.52 mmol, 4.8 equiv.) and TBSCl (0.04 g, 0.26 mmol, 2.4 equiv.). Solution was stirred overnight, quenched with 0.5 mL 1 N HCl, extracted with diethyl ether (2x10 mL), then washed with water (10 mL) and brine (10 mL). Solvent was removed *in vacuo*. ^1H NMR (500 MHz, CDCl_3) δ 7.26 (s, 1H), 5.29 (s, 1H), 4.19 (s, 3H), 3.27 (s, 2H), 2.04 (s, 1H), 1.82 (s, 1H), 1.69 (s, 5H), 1.60 (s, 3H), 1.40 (s, 4H), 1.24 (s, 6H), 0.92 (d, $J = 20.3$ HZ, 16H), 0.09 (s, 7H). ^{13}C NMR (126 MHz, CDCl_3) δ 175.46 (s), 77.41 (s), 77.16 (s), 76.91 (s), 70.86 (s), 65.67 – 65.28 (m), 60.56 (s), 51.43 (s), 32.06 (s), 29.83 (s), 29.50 (s), 28.84 (s), 28.54 (d, $J = 7.4$ HZ), 27.70 (d, $J = 15.5$ HZ), 27.42 (s), 26.44 (s), 25.53 (d, $J = 8.9$ HZ), 24.65 (d, $J = 3.5$ HZ), 18.11 (s).

Note: Molecules 4-1 through 4-5 were synthesized by Lark Perez.

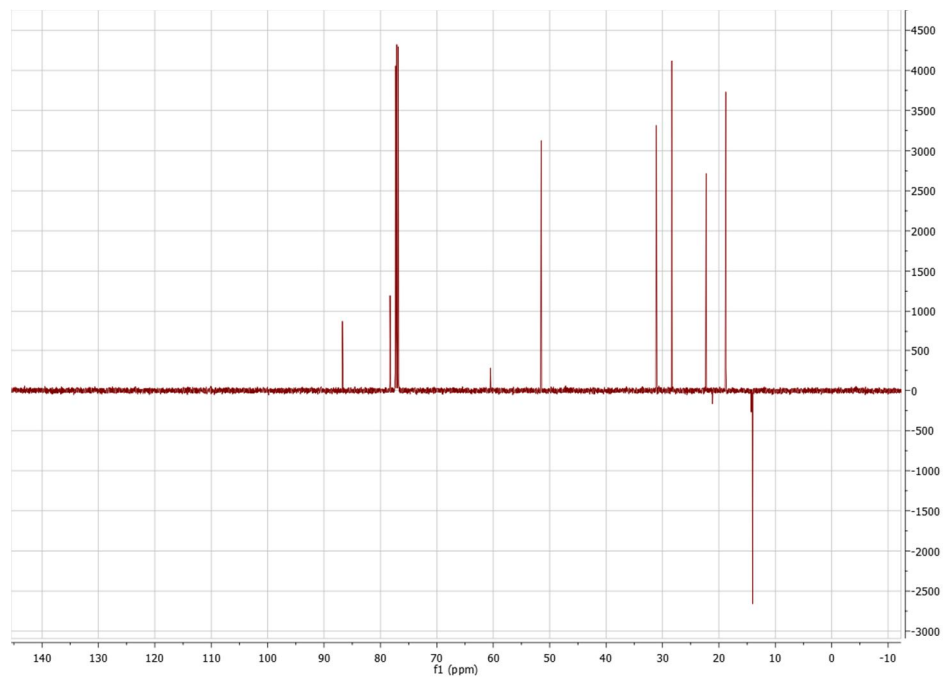
Appendices

Appendix A: CqsS Receptor Structure Elucidation Spectra

2-octyn-1-ol

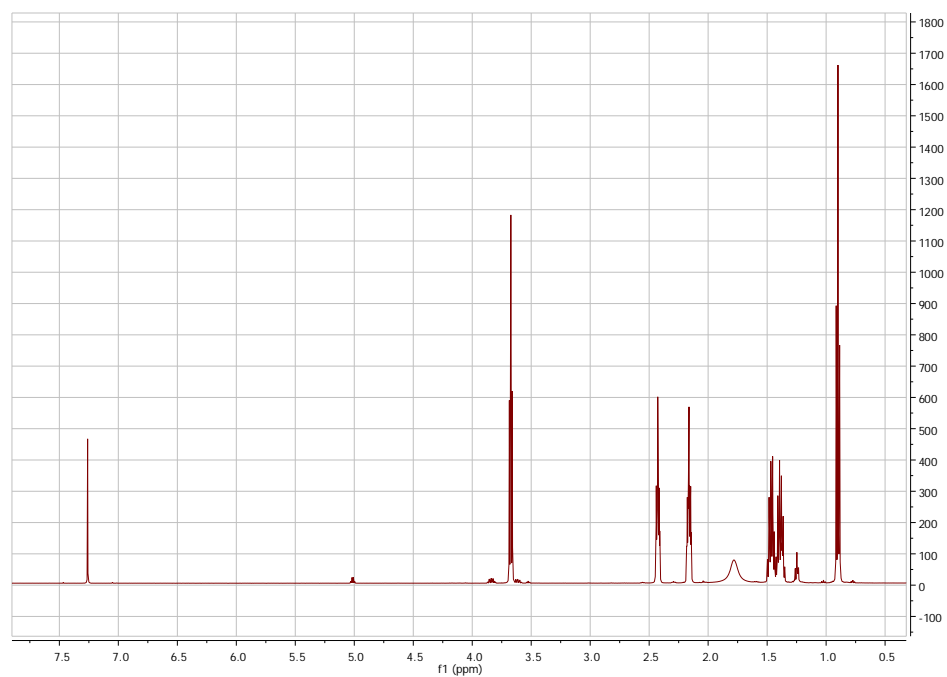


^1H NMR (500MHz, CDCl_3)

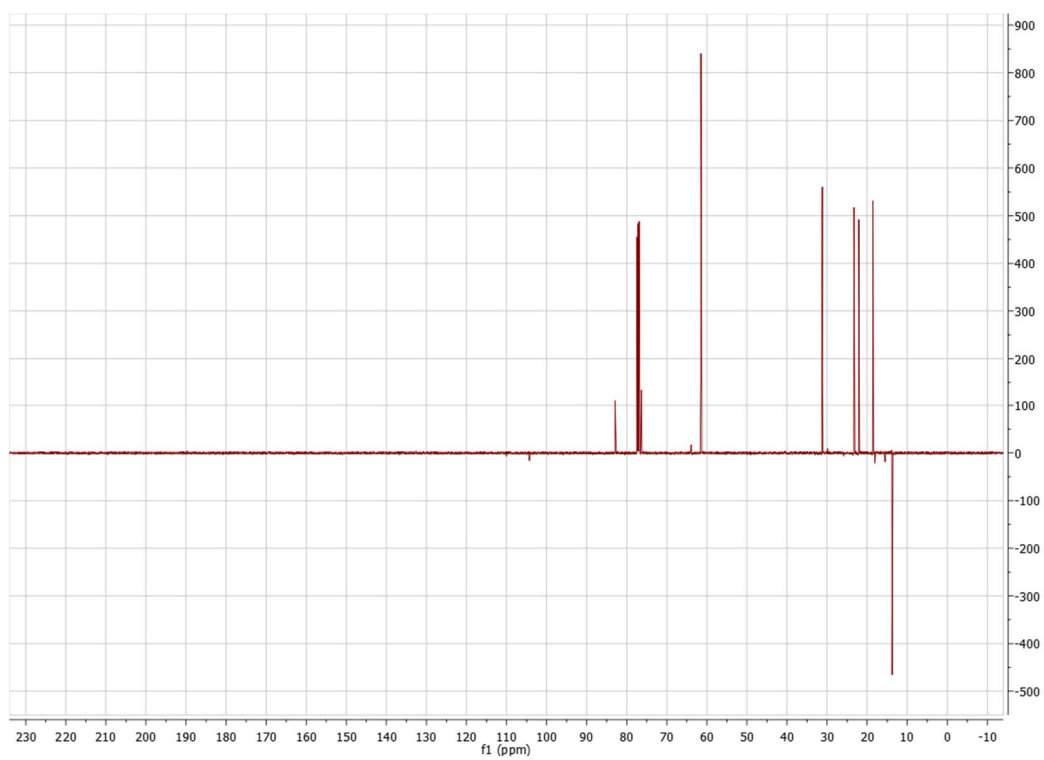


^{13}C NMR (125MHz, CDCl_3)

3-octyn-1-ol

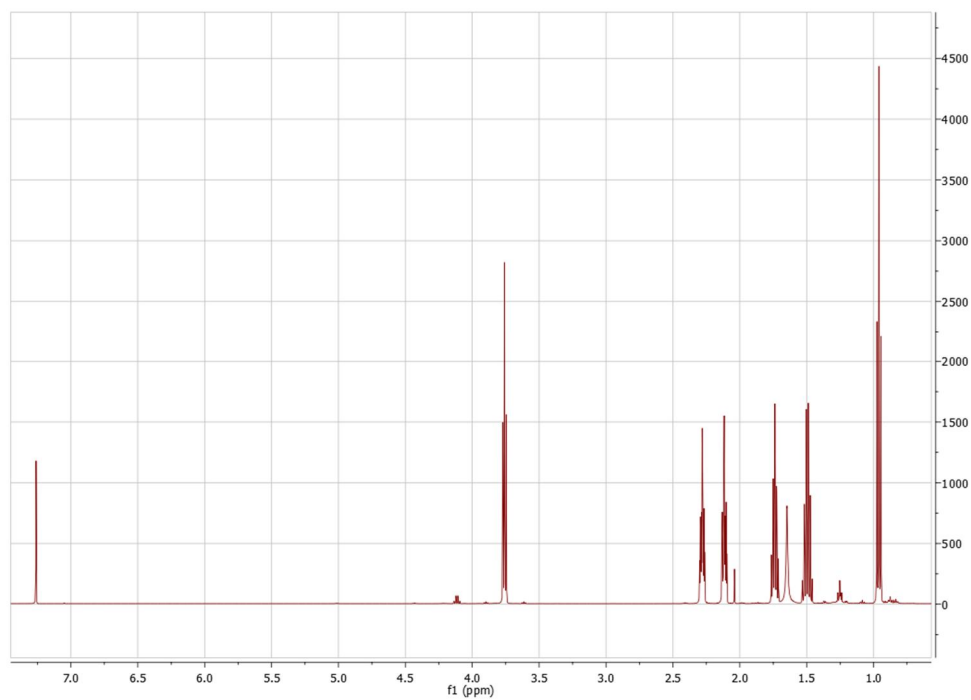


^1H NMR (500MHz, CDCl_3)

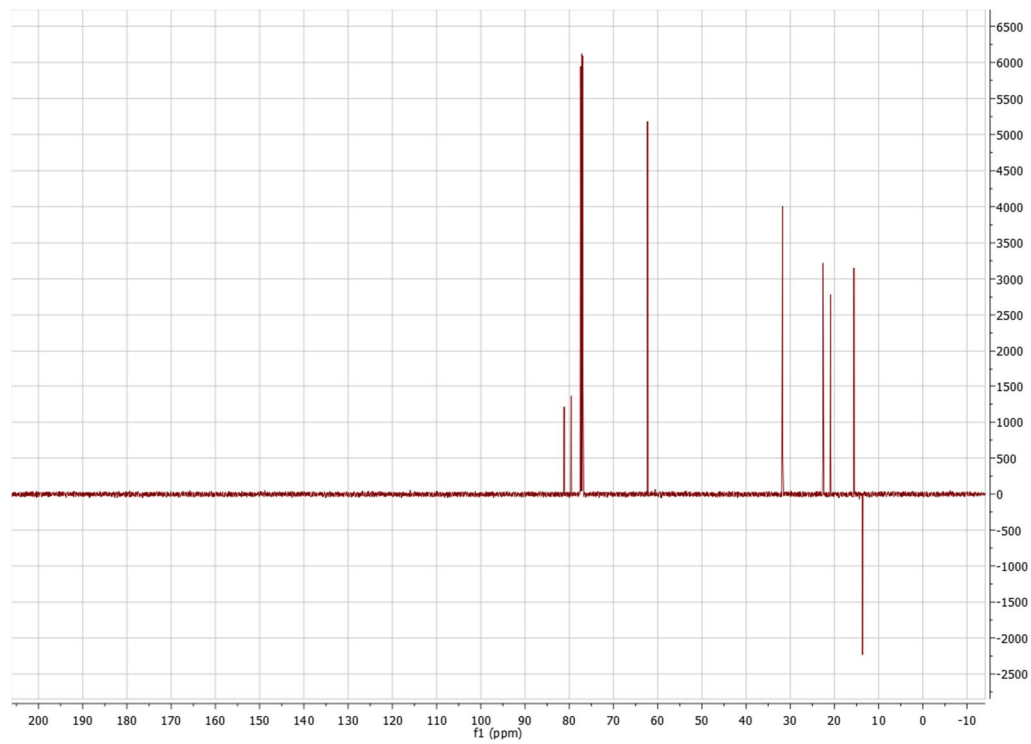


^{13}C NMR (125MHz, CDCl_3)

4-octyn-1-ol

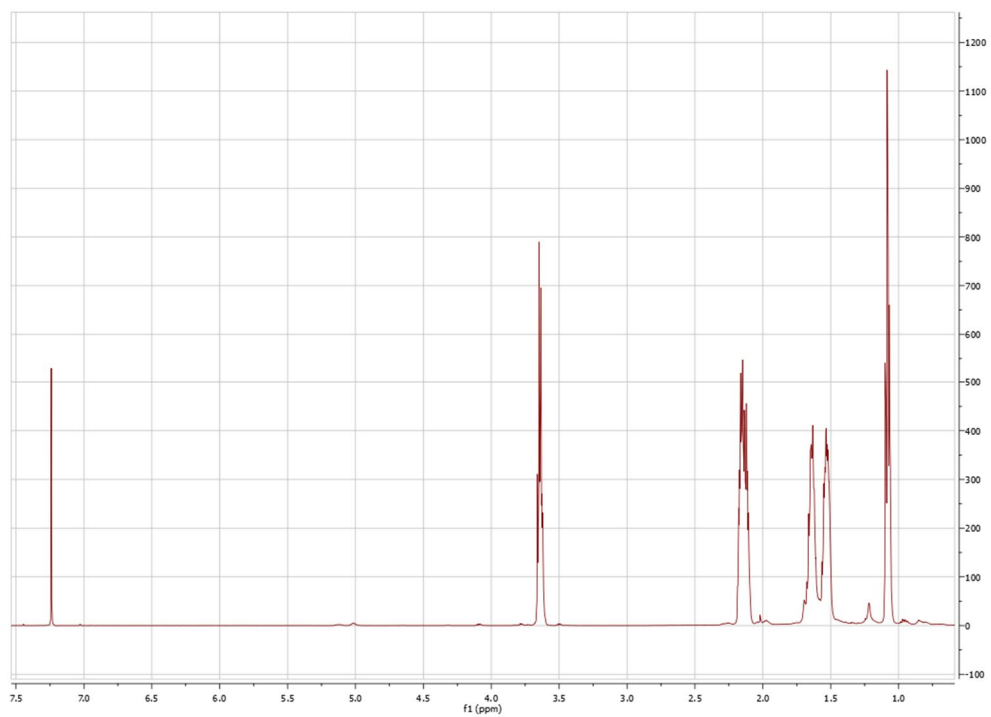


^1H NMR (500MHz, CDCl_3)

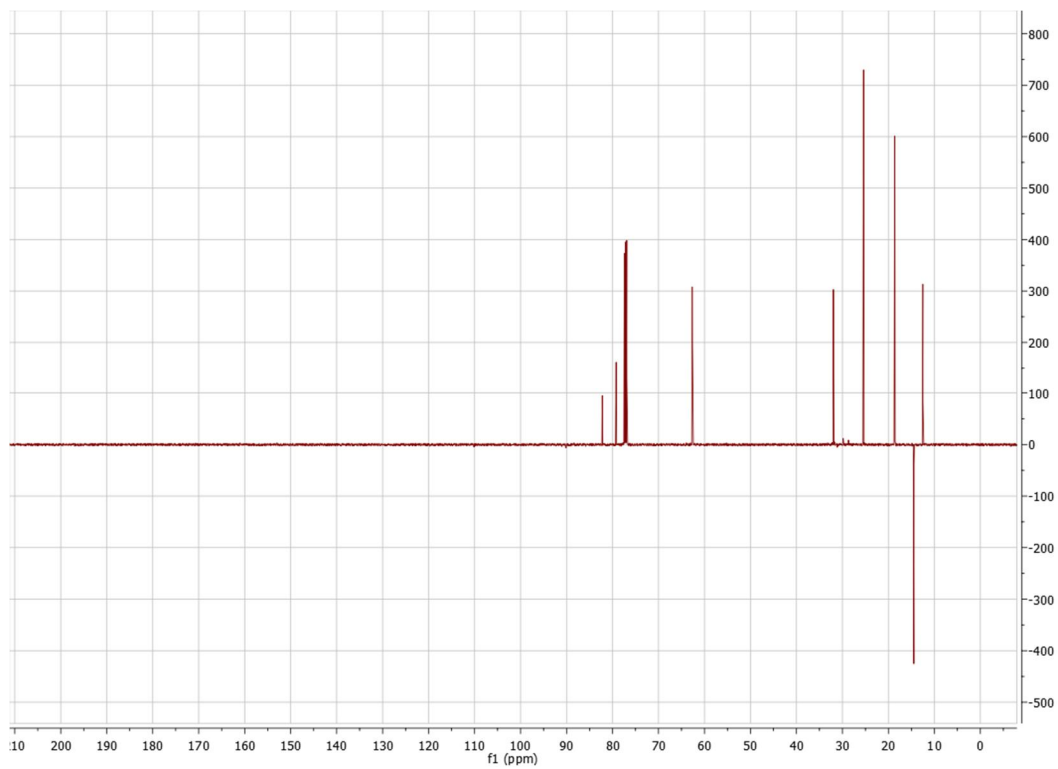


^{13}C NMR (125MHz, CDCl_3)

5-octyn-1-ol

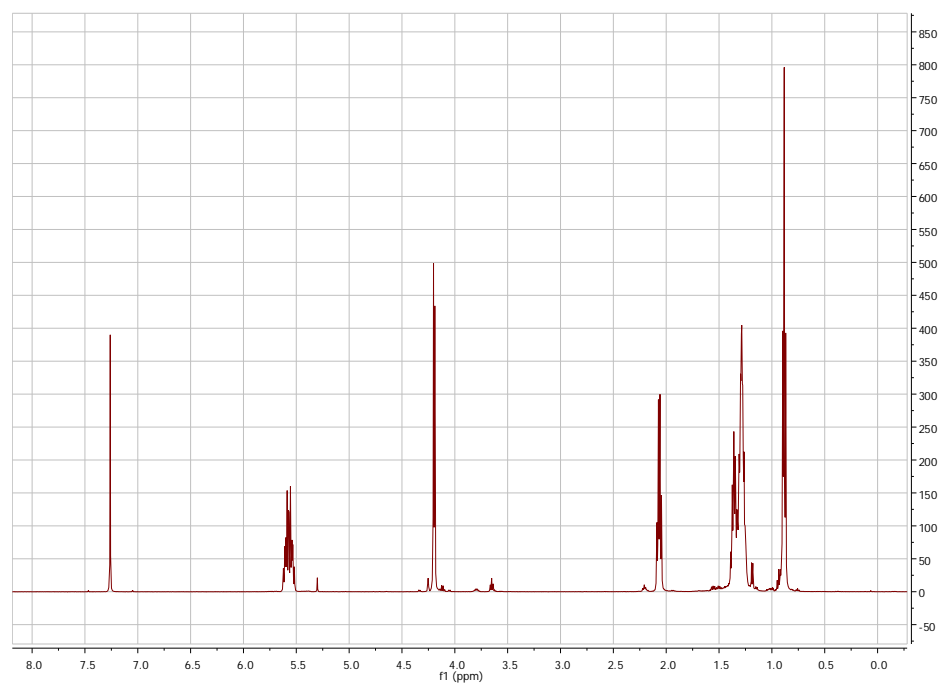


^1H NMR (500MHz, CDCl_3)

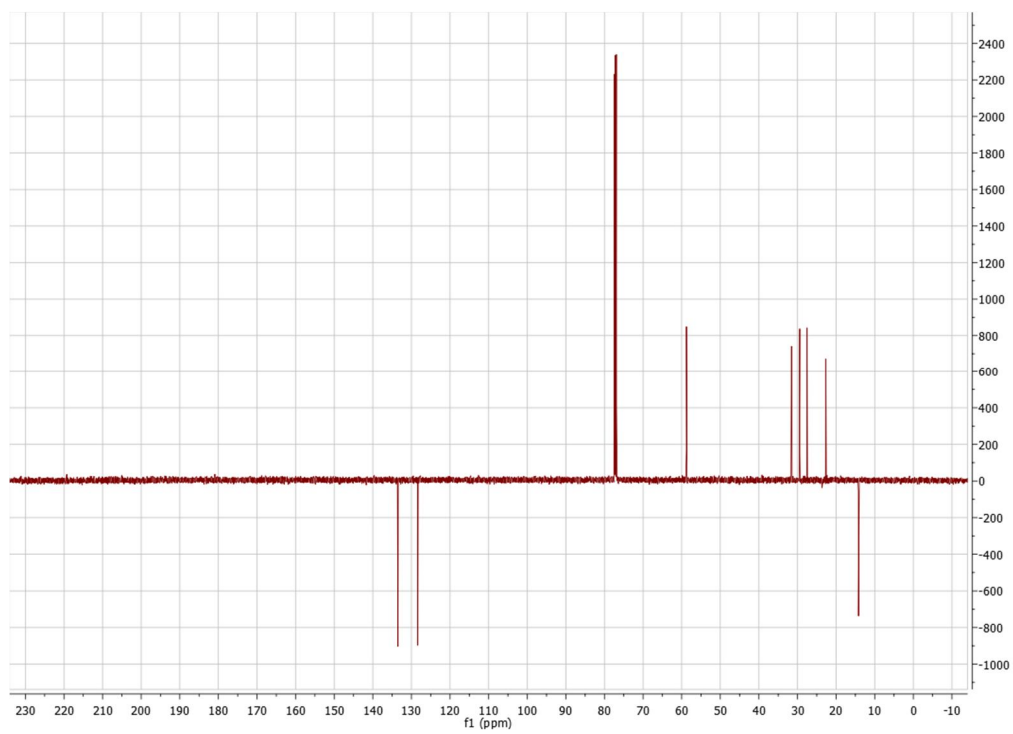


^{13}C NMR (125MHz, CDCl_3)

2-Z-octen-1-ol

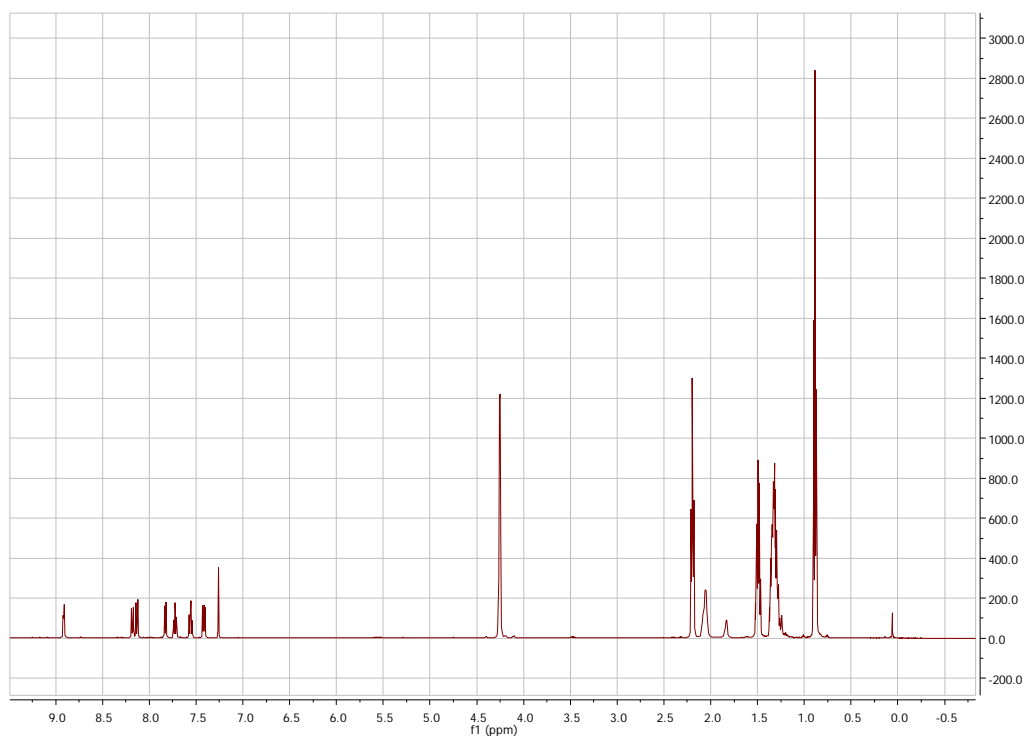


^1H NMR (500MHz, CDCl_3)

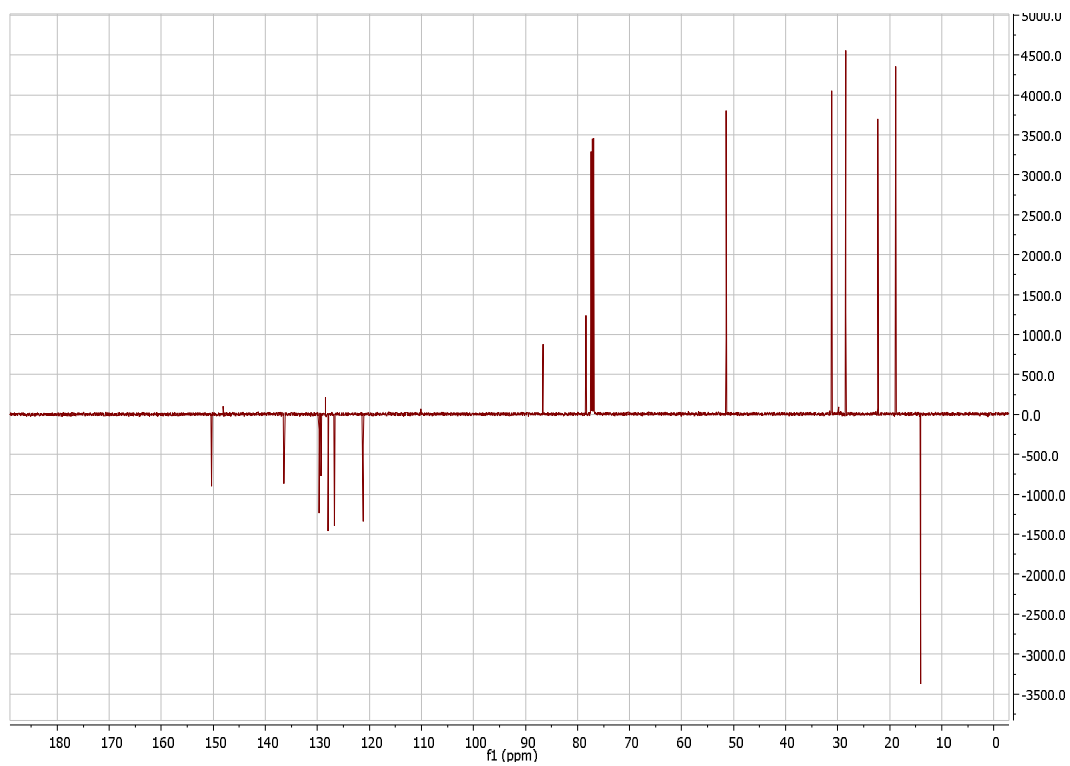


^{13}C NMR (125MHz, CDCl_3)

2-Z-octen-1-ol Synthesis (2 minutes)

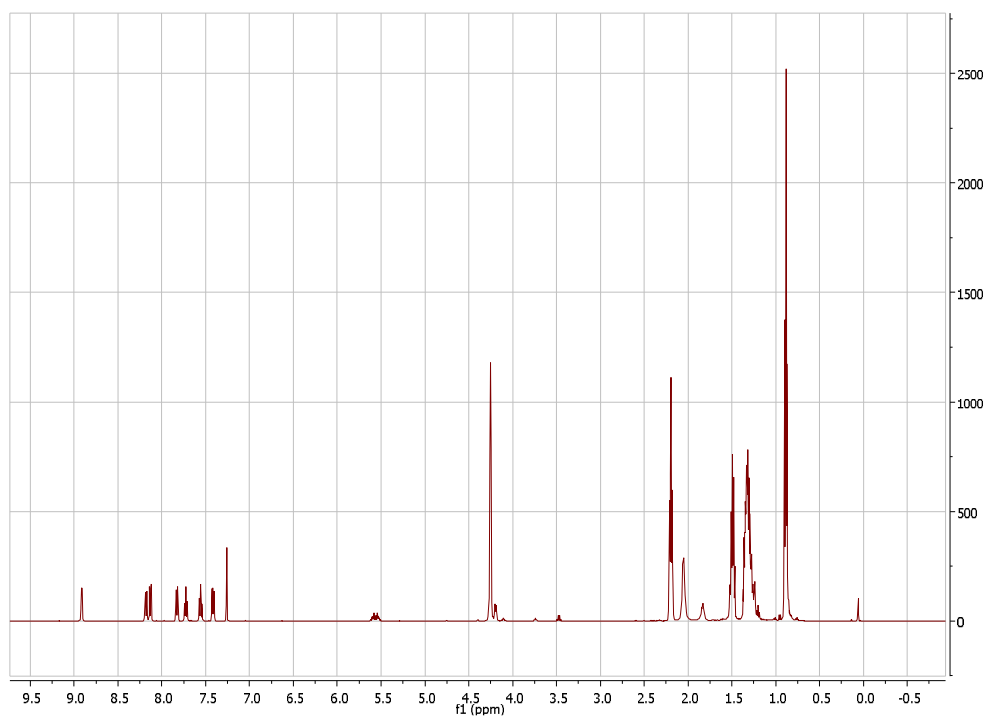


^1H NMR (500MHz, CDCl_3)

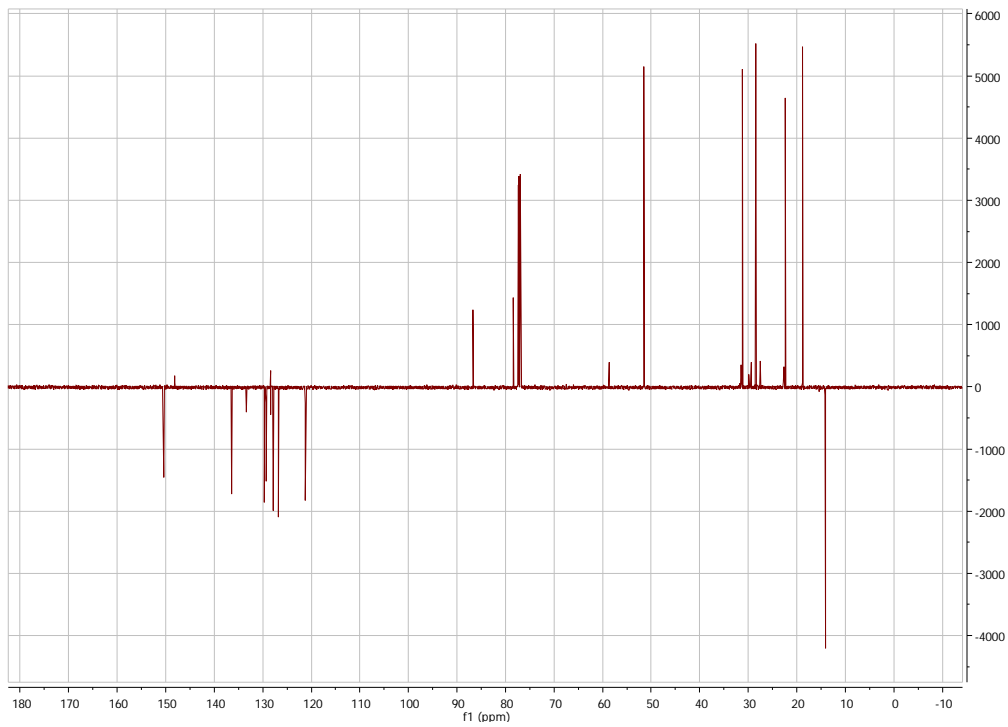


^{13}C NMR (125MHz, CDCl_3)

2-Z-octen-1-ol Synthesis (5 minutes)

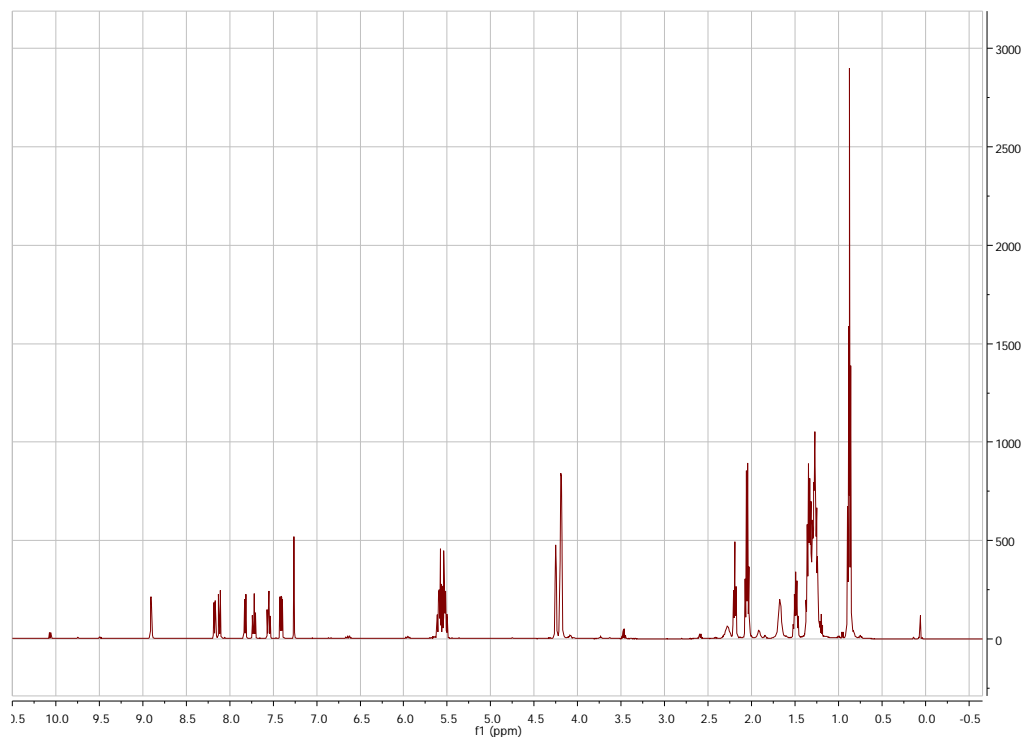


^1H NMR (500MHz, CDCl_3)

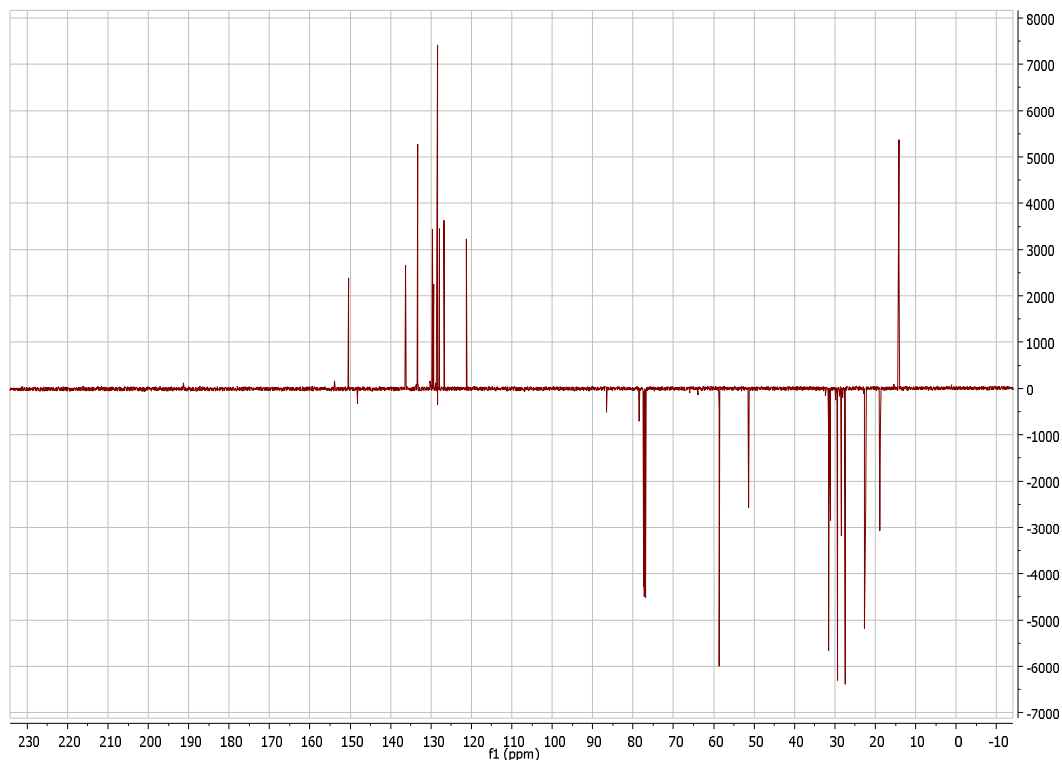


^{13}C NMR (125MHz, CDCl_3)

2-Z-octen-1-ol Synthesis (15 minutes)

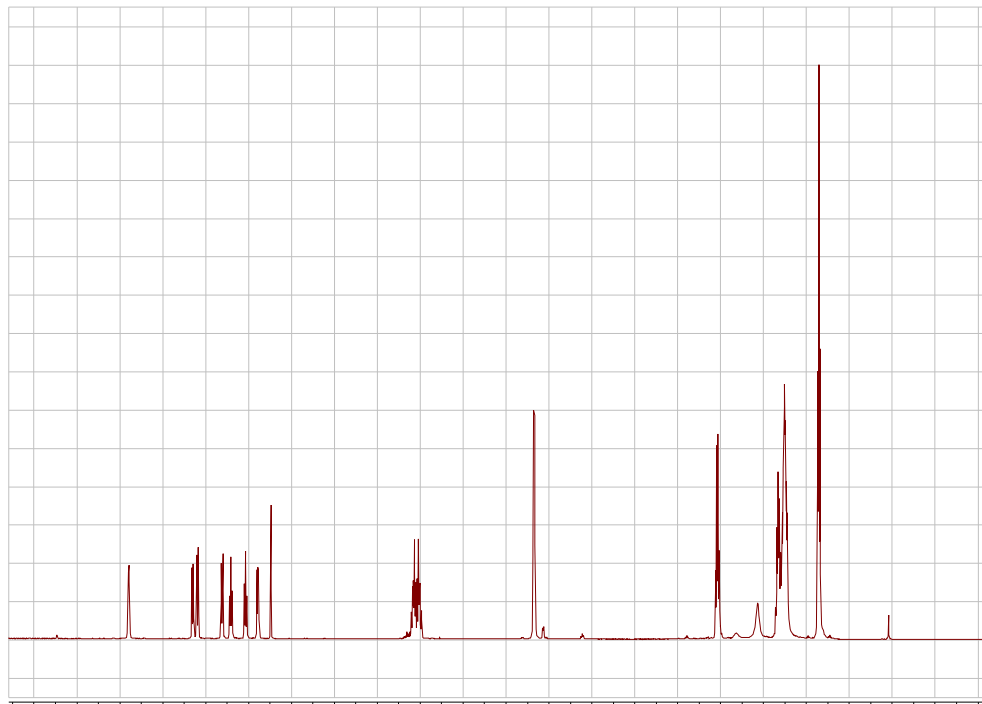


^1H NMR (500MHz, CDCl_3)

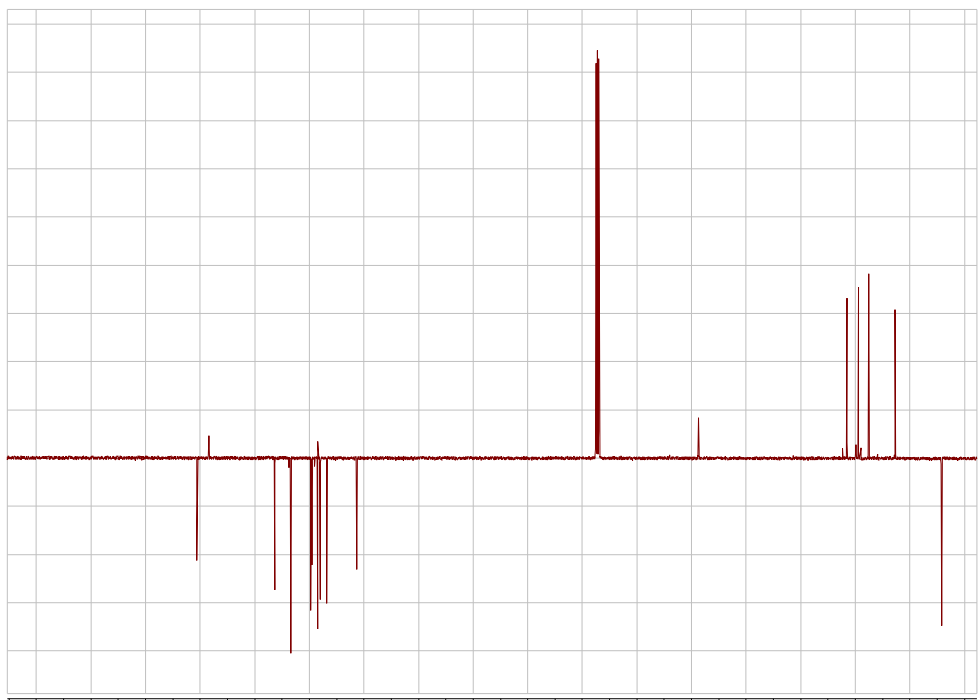


^{13}C NMR (125MHz, CDCl_3)

2-Z-octen-1-ol Synthesis (20 minutes)

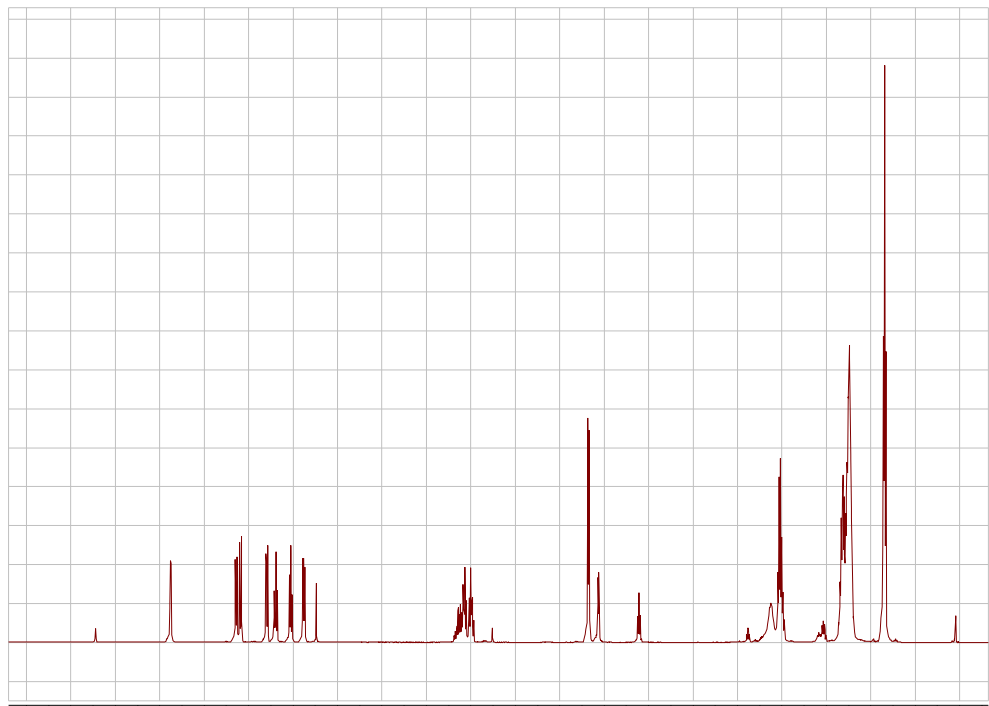


^1H NMR (500MHz, CDCl_3)

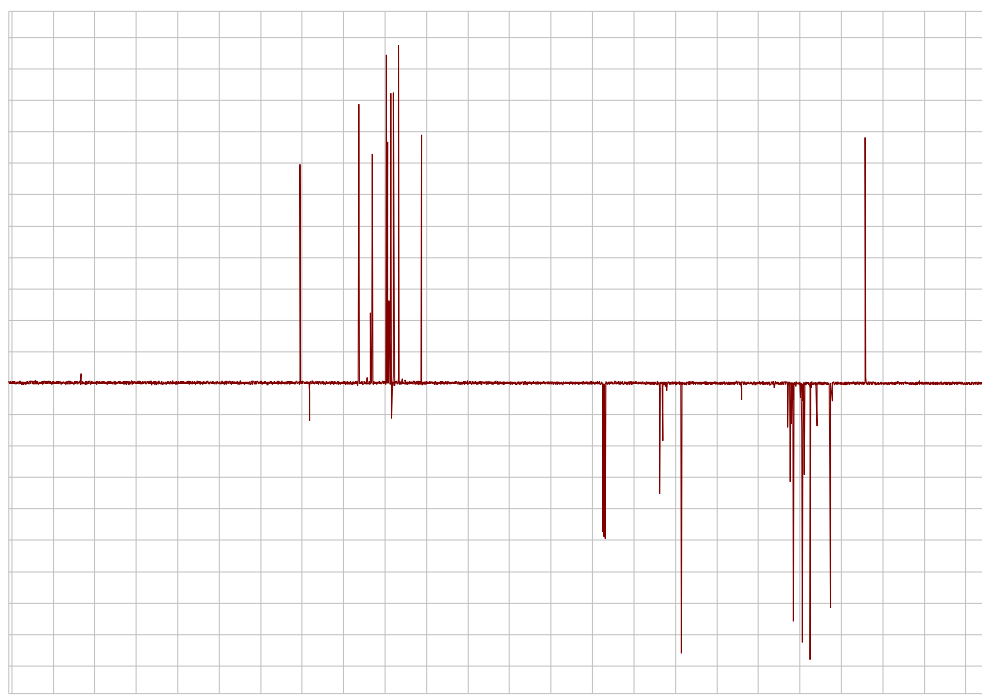


^{13}C NMR (125MHz, CDCl_3)

2-Z-octen-1-ol Synthesis (25 minutes)

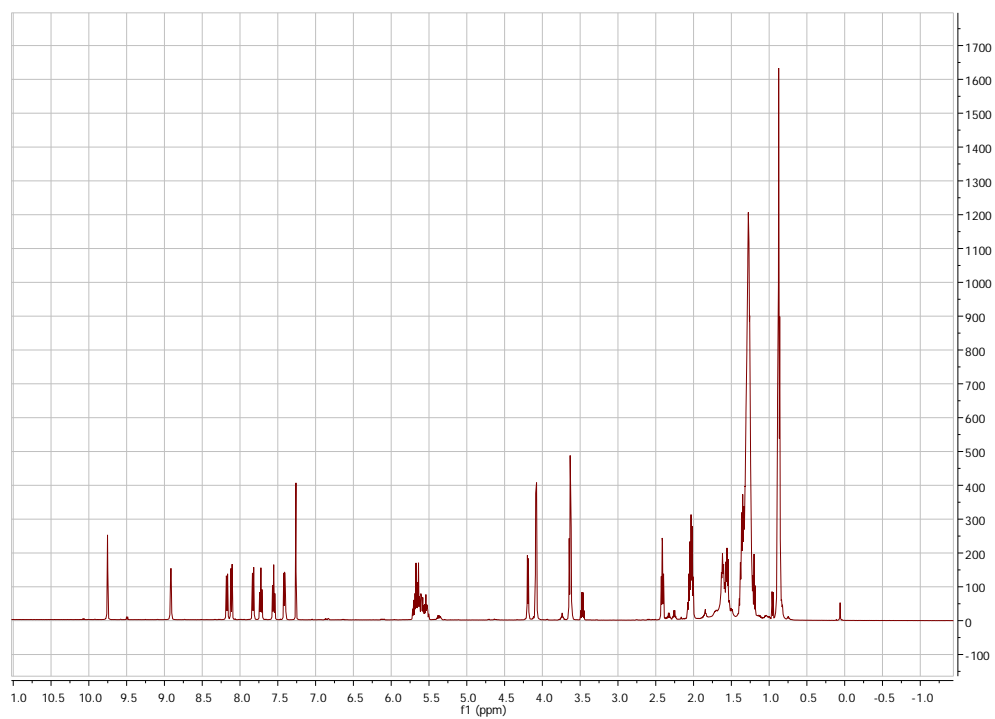


^1H NMR (500MHz, CDCl_3)

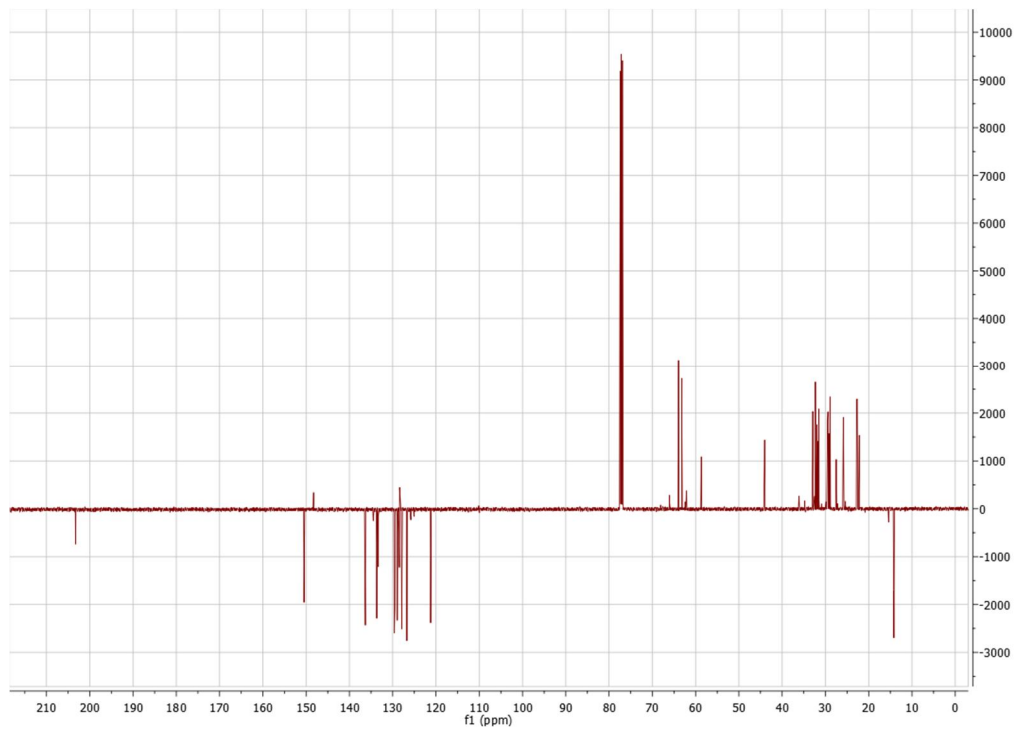


^{13}C NMR (125MHz, CDCl_3)

2-Z-octen-1-ol Synthesis (30 minutes)

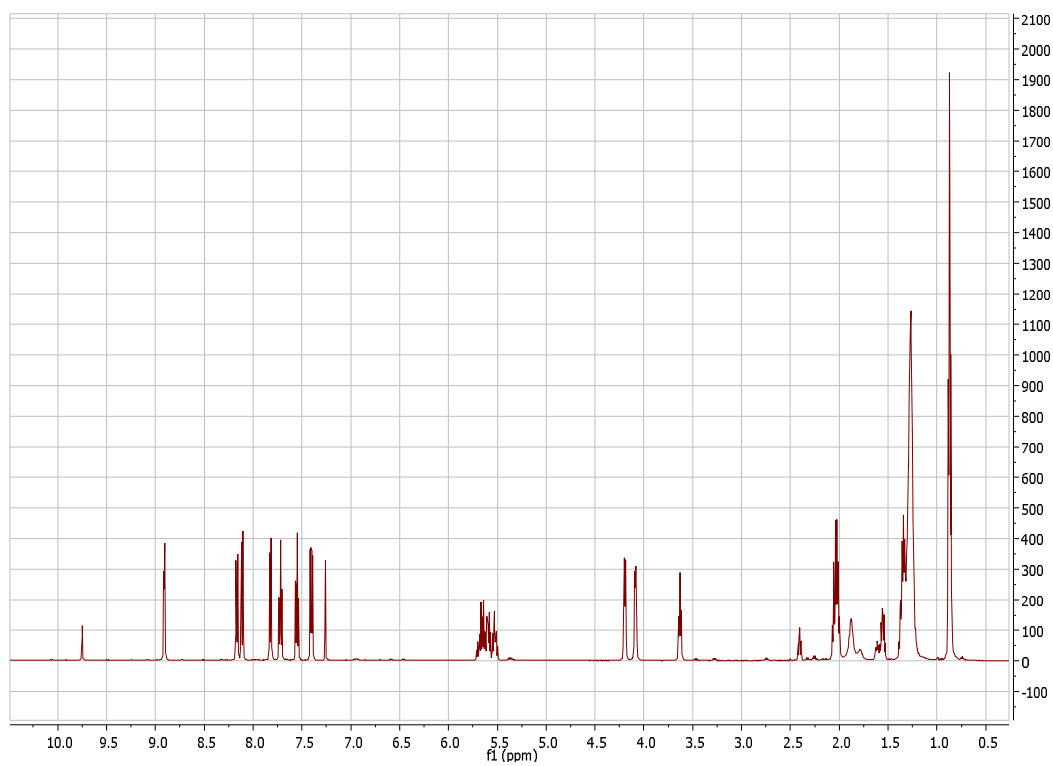


^1H NMR (500MHz, CDCl_3)

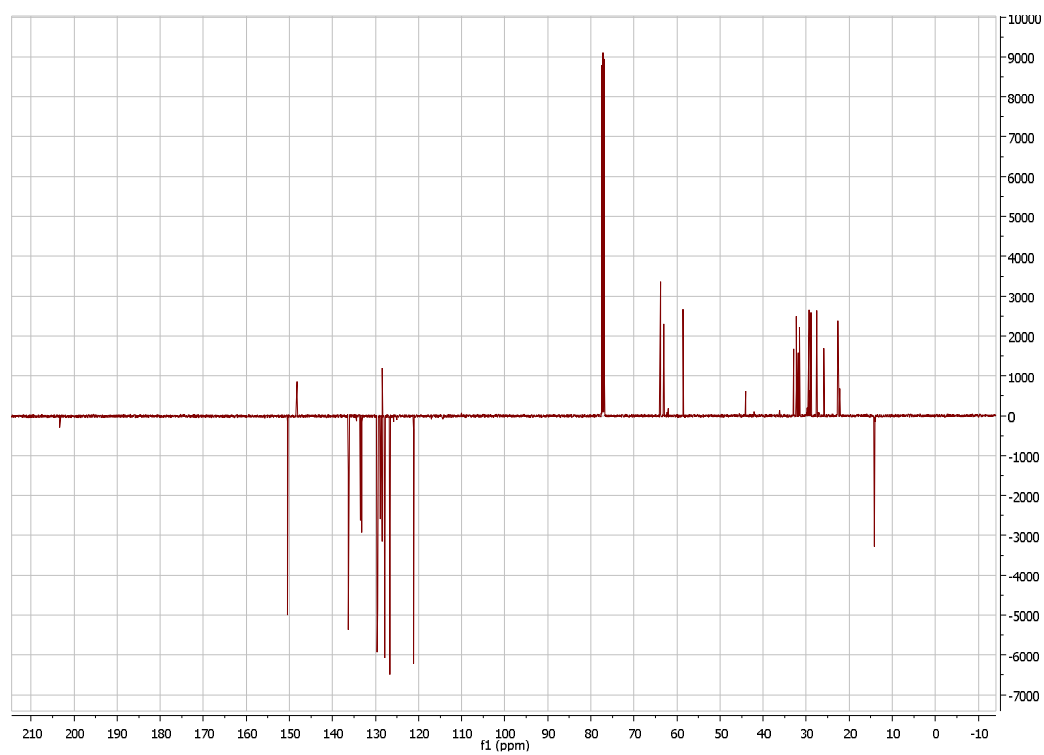


^{13}C NMR (125MHz, CDCl_3)

2-Z-octen-1-ol Synthesis (1 hour)

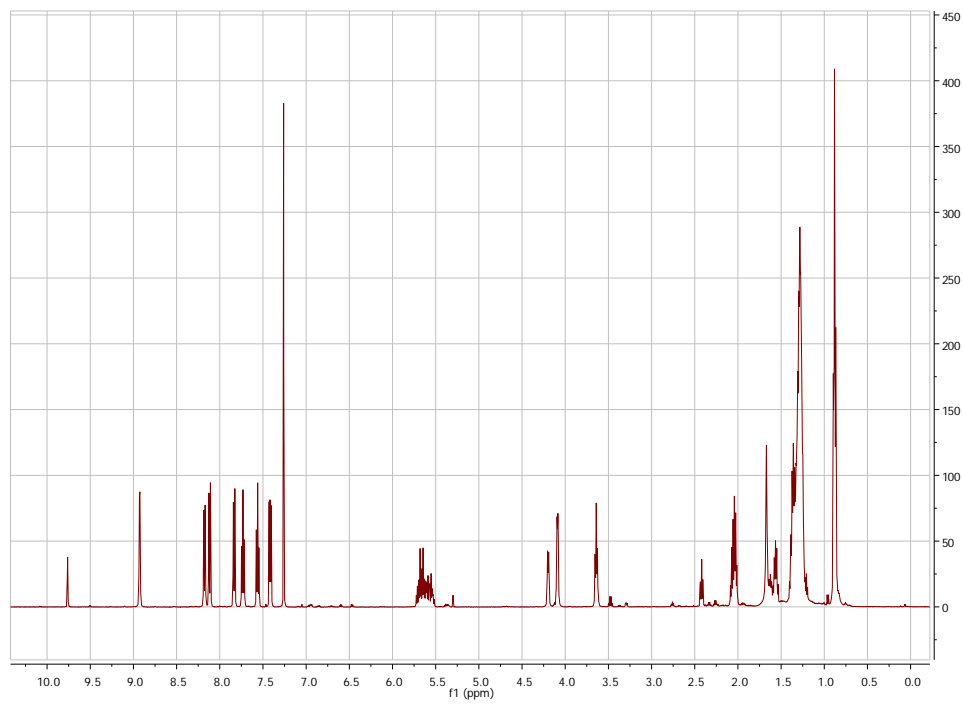


^1H NMR (500MHz, CDCl_3)

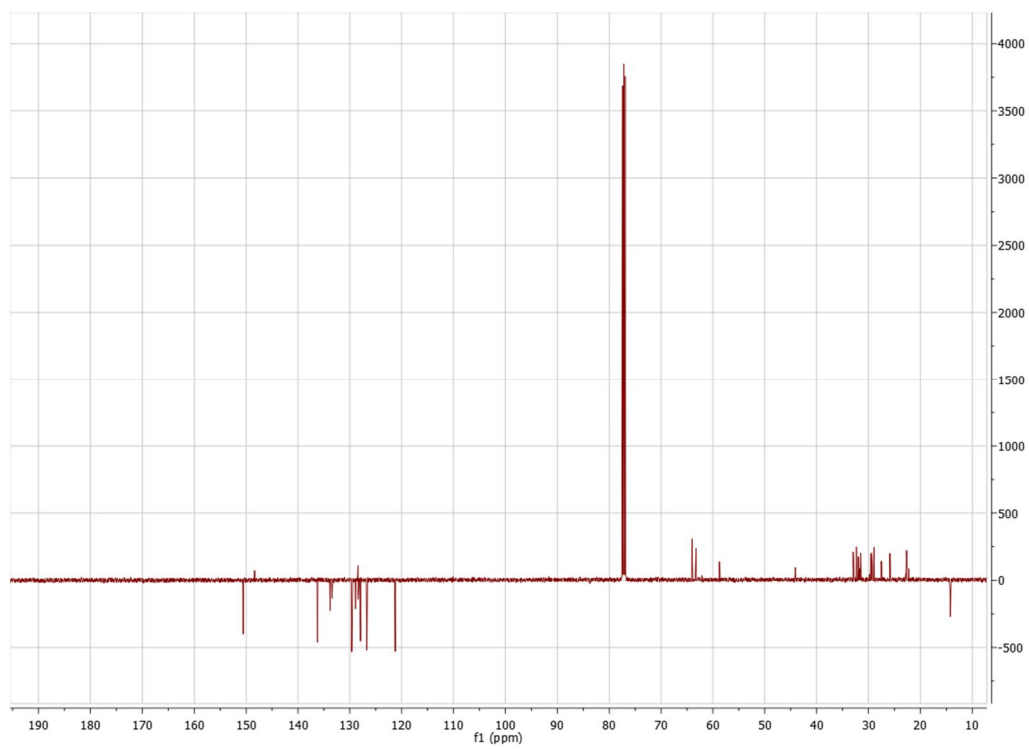


^{13}C NMR (125MHz, CDCl_3)

2-Z-octen-1-ol Synthesis (1.5 hours)

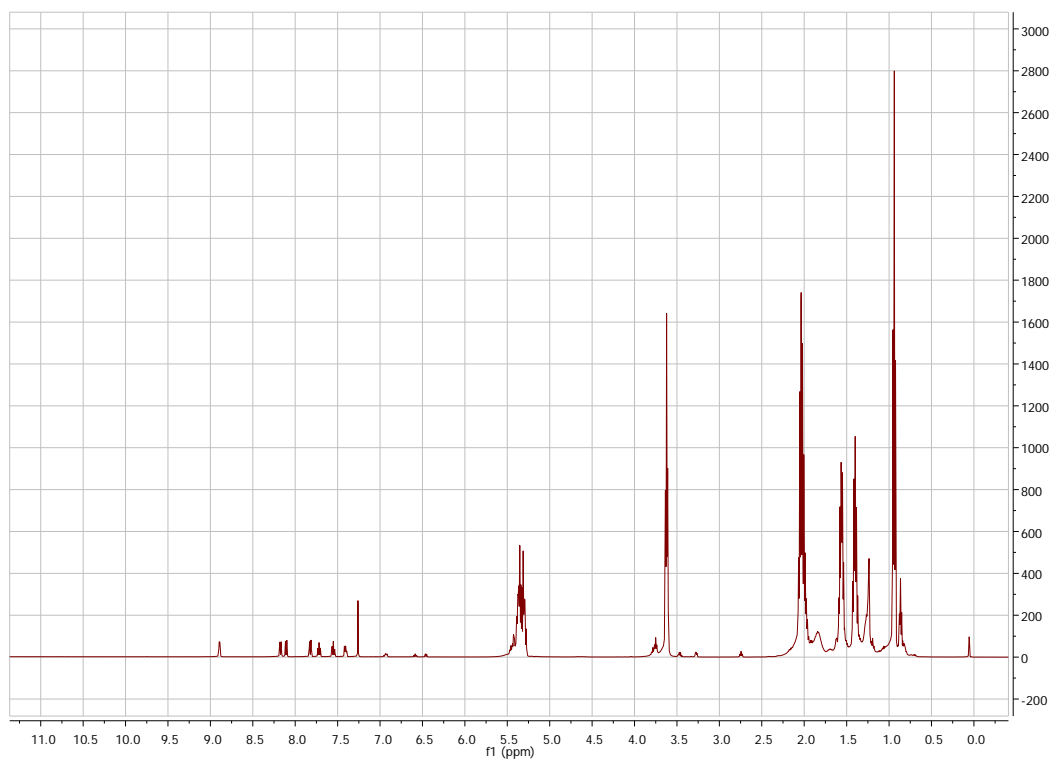


^1H NMR (500MHz, CDCl_3)

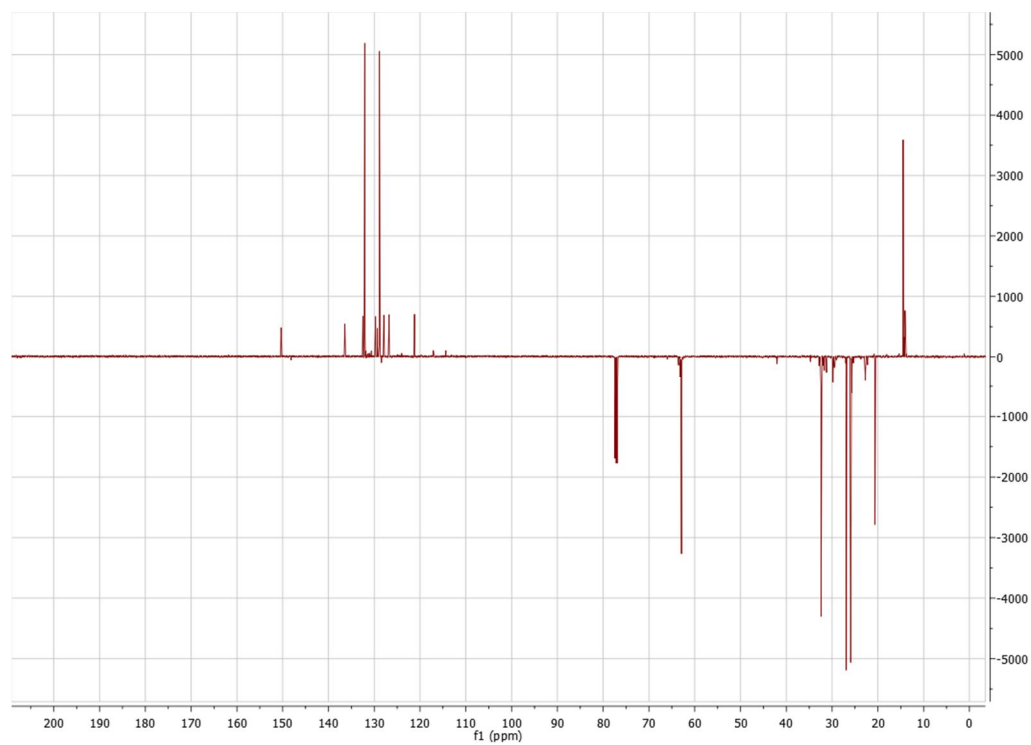


^{13}C NMR (125MHz, CDCl_3)

2-Z-octen-1-ol Synthesis (2 hours)

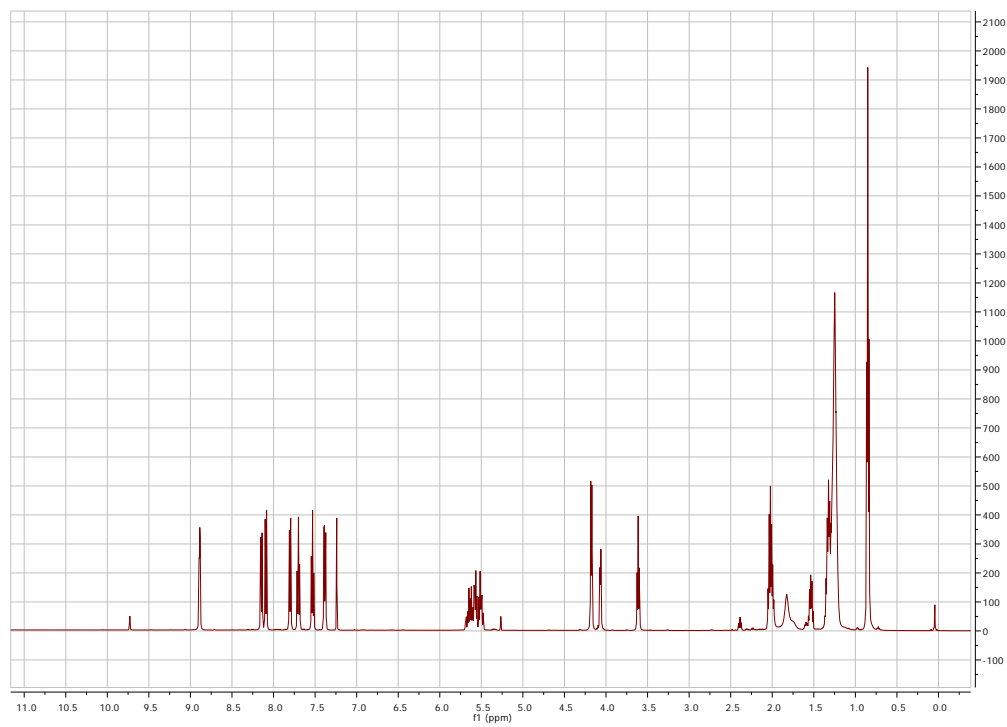


^1H NMR (500MHz, CDCl_3)

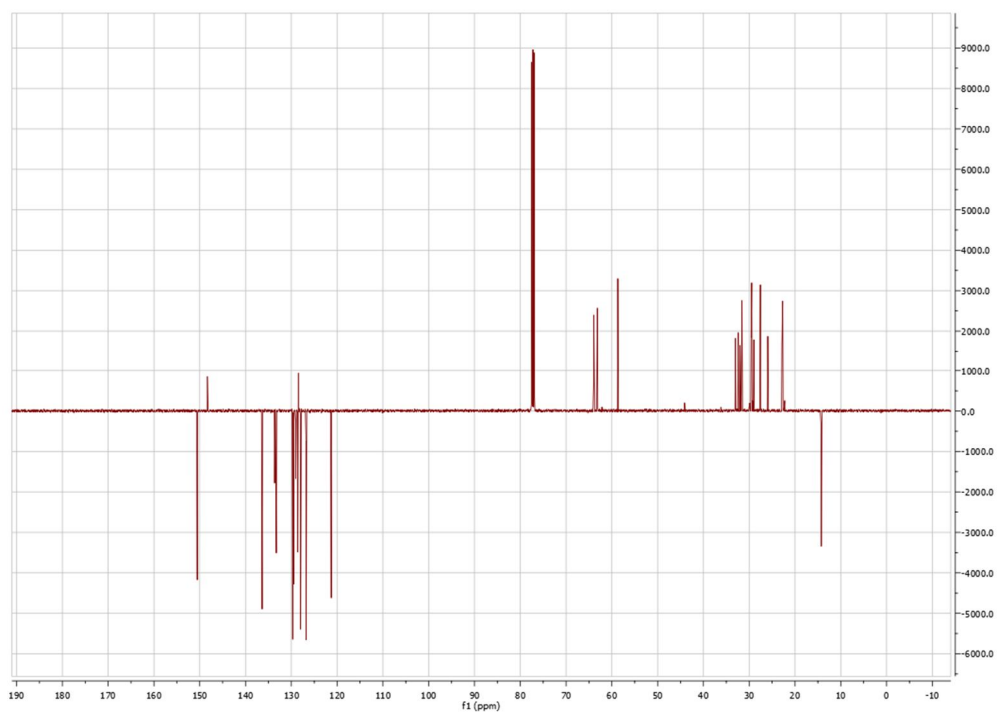


^{13}C NMR (125MHz, CDCl_3)

2-Z-octen-1-ol Synthesis (1 hour, 0°C)

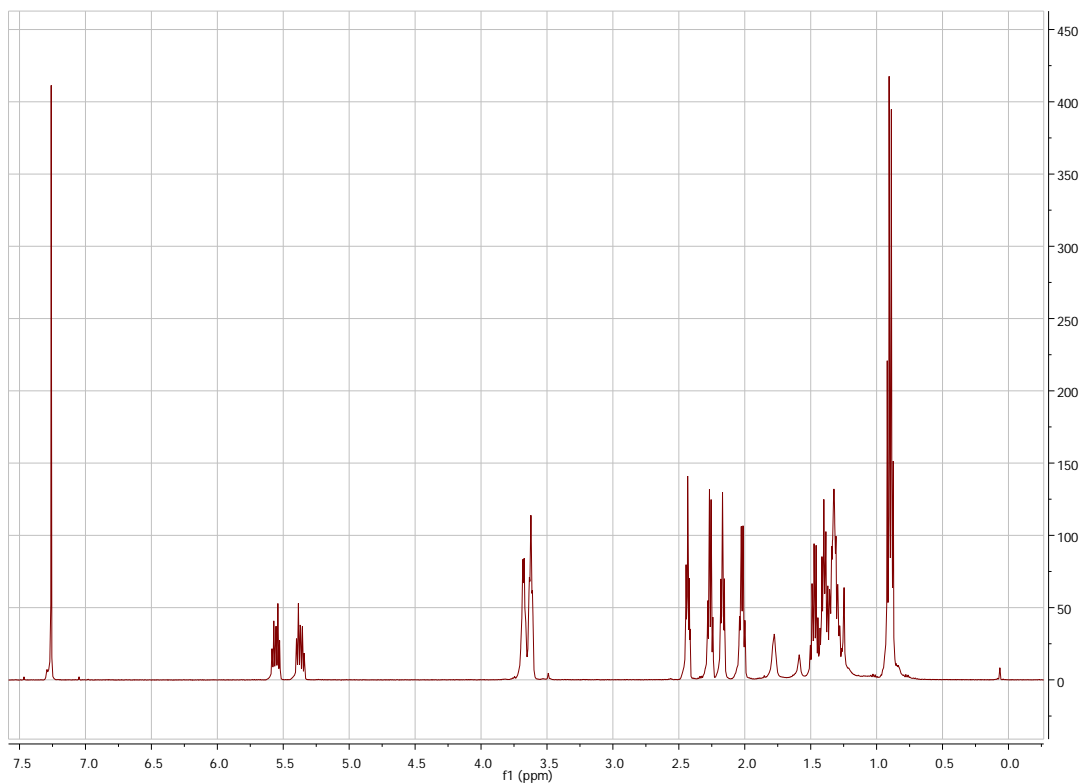


^1H NMR (500MHz, CDCl_3)

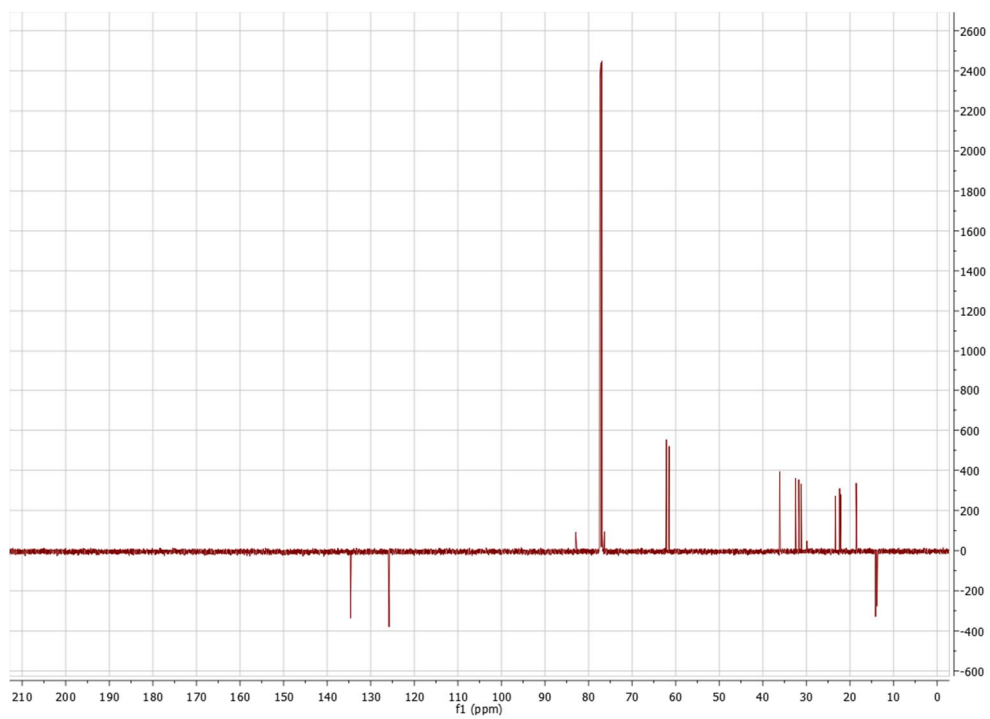


^{13}C NMR (125MHz, CDCl_3)

3-*E*-octen-1-ol Synthesis (2.5 equivalents Na^o)

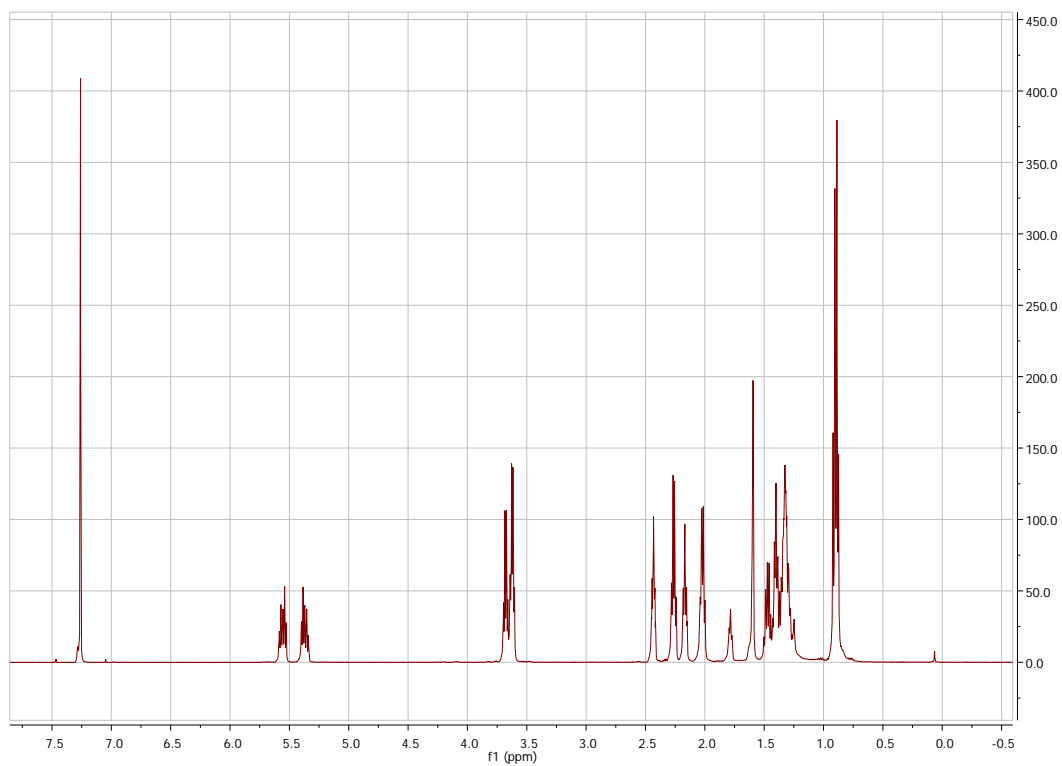


¹H NMR (500MHz, CDCl₃)

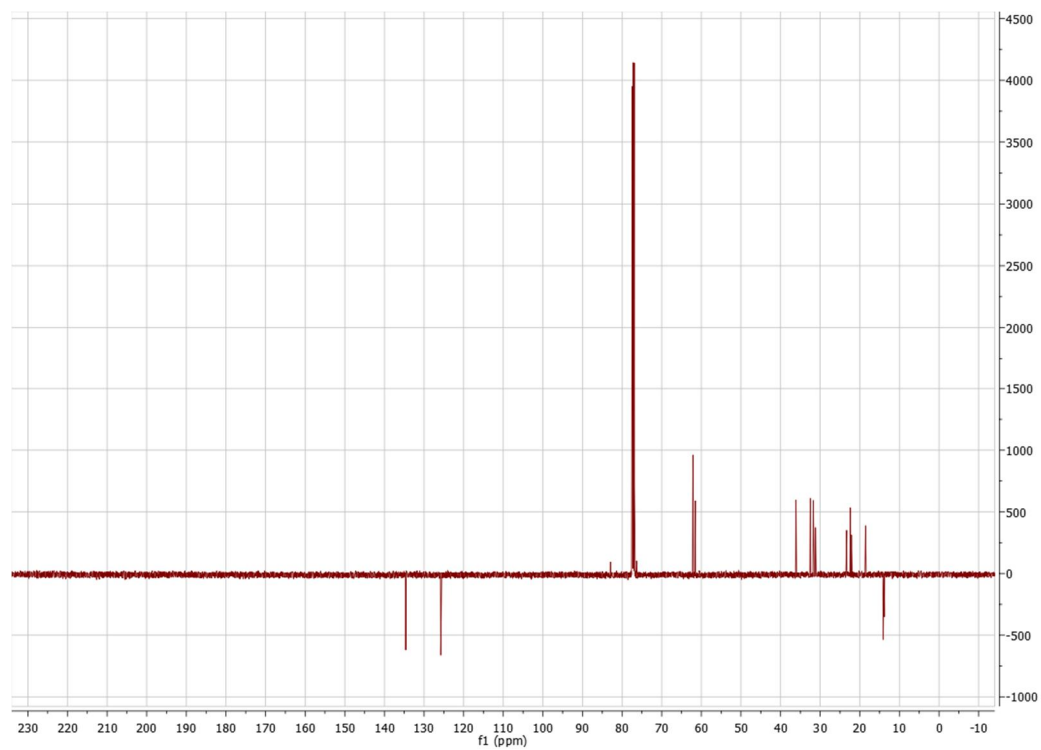


¹³C NMR (125MHz, CDCl₃)

3-*E*-octen-1-ol Synthesis (5 equivalents Na^o)

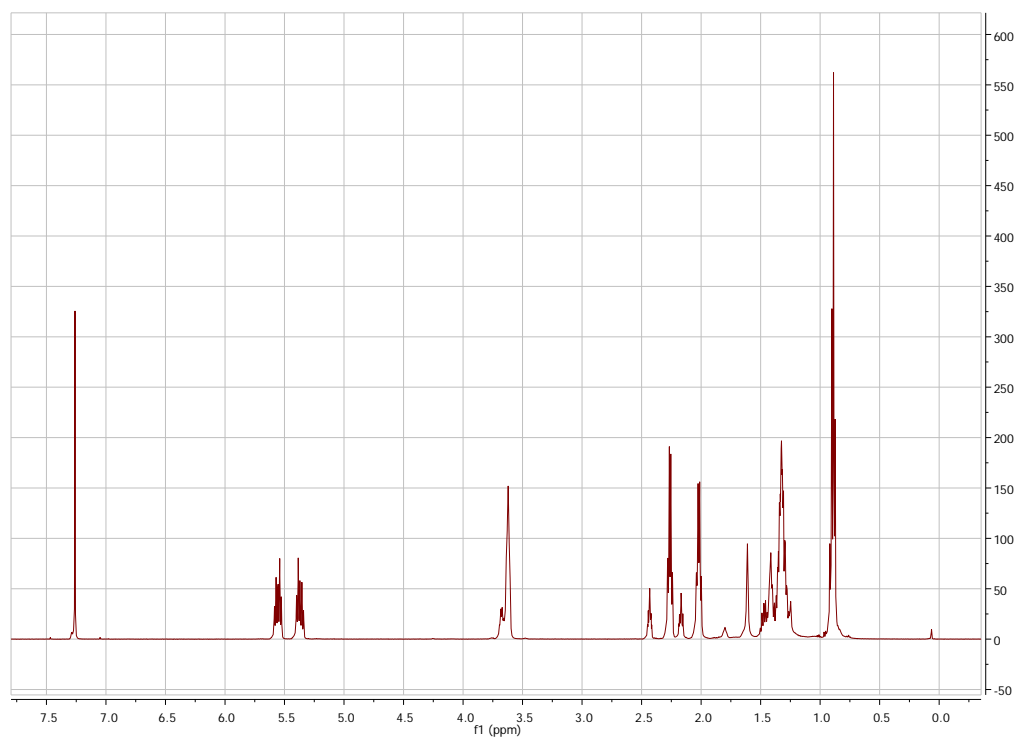


¹H NMR (500MHz, CDCl₃)

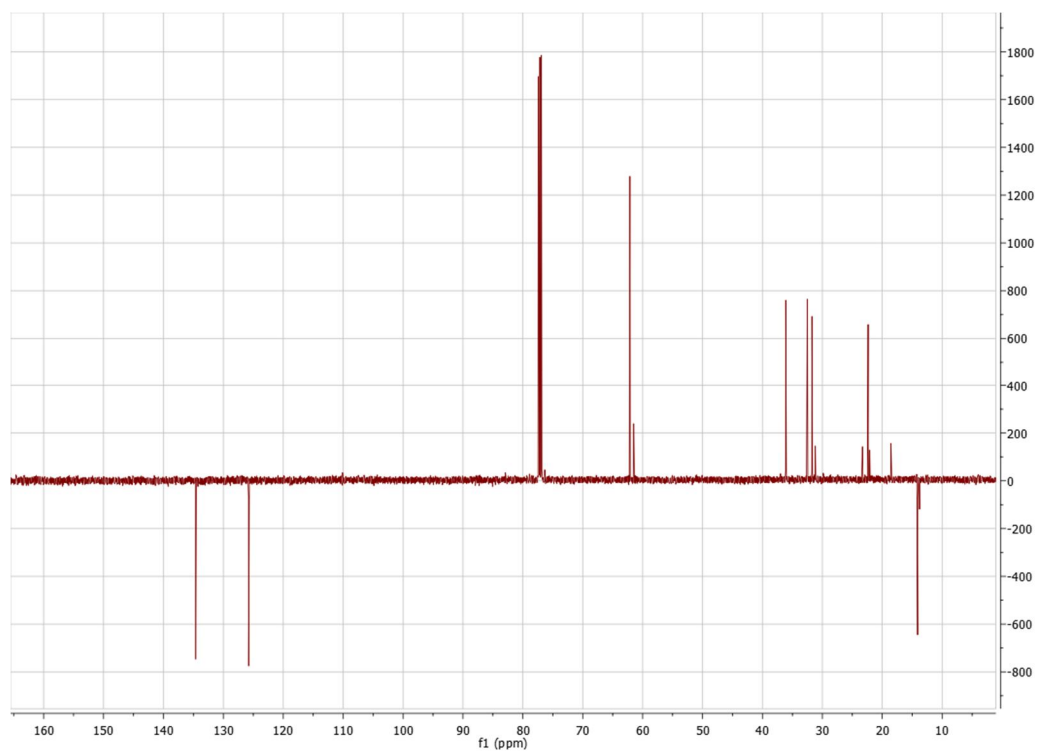


¹³C NMR (125MHz, CDCl₃)

3-*E*-octen-1-ol Synthesis (10 equivalents Na^o)

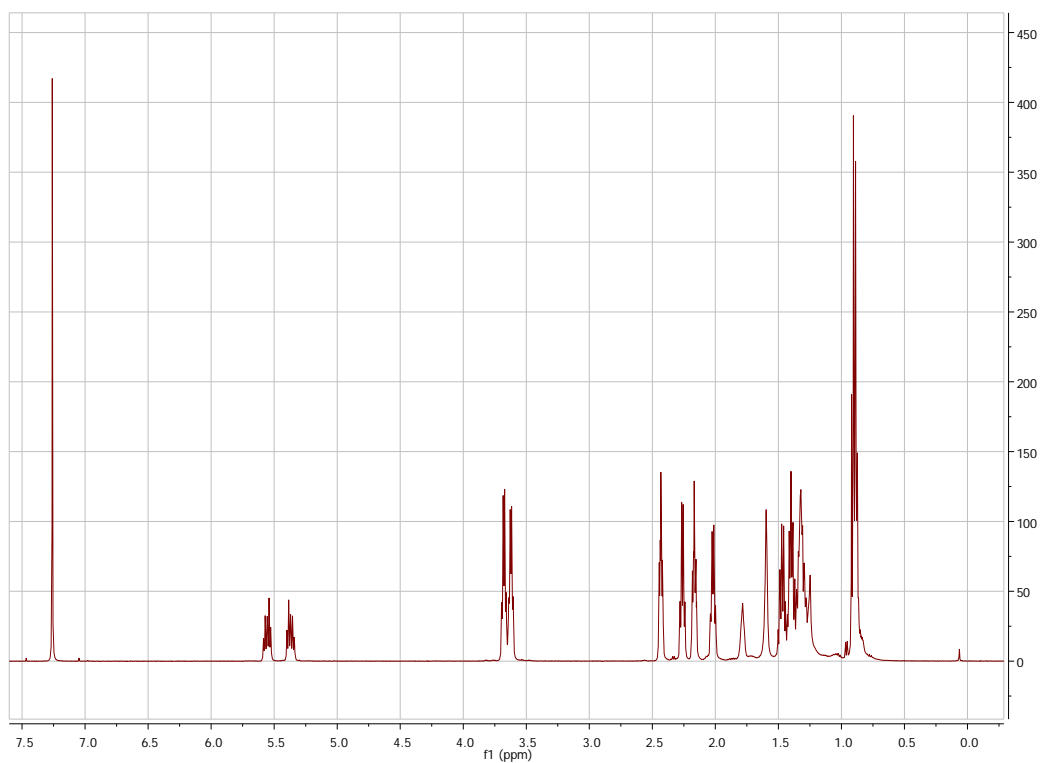


¹H NMR (500MHz, CDCl₃)

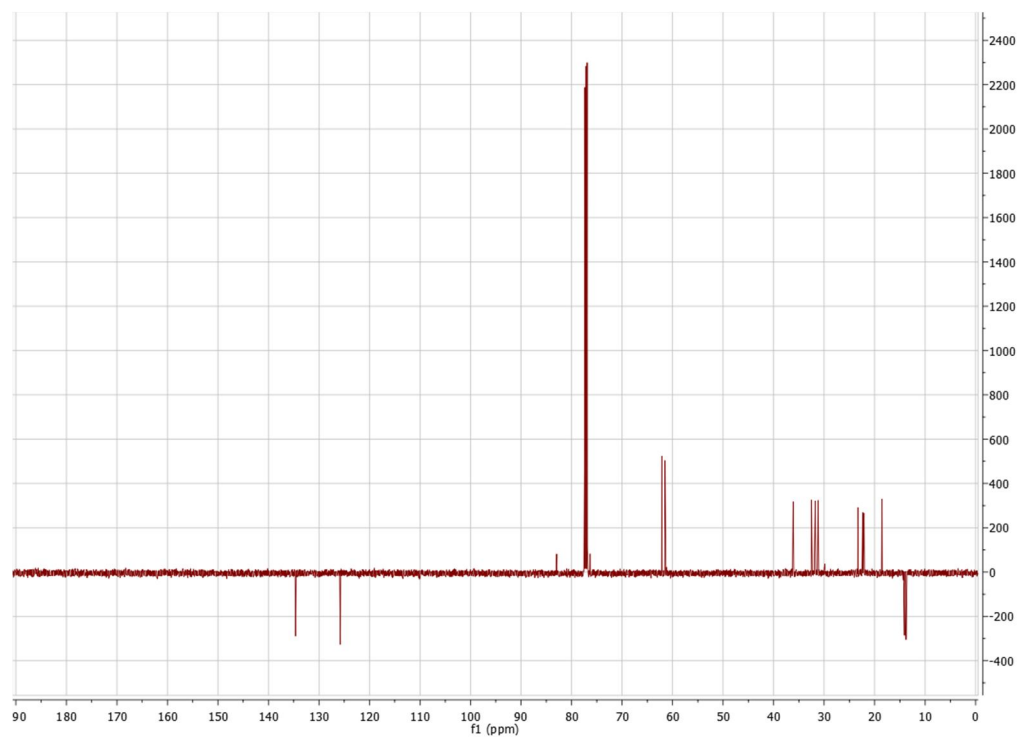


¹³C NMR (125MHz, CDCl₃)

3-*E*-octen-1-ol Synthesis (15 equivalents Na^o)



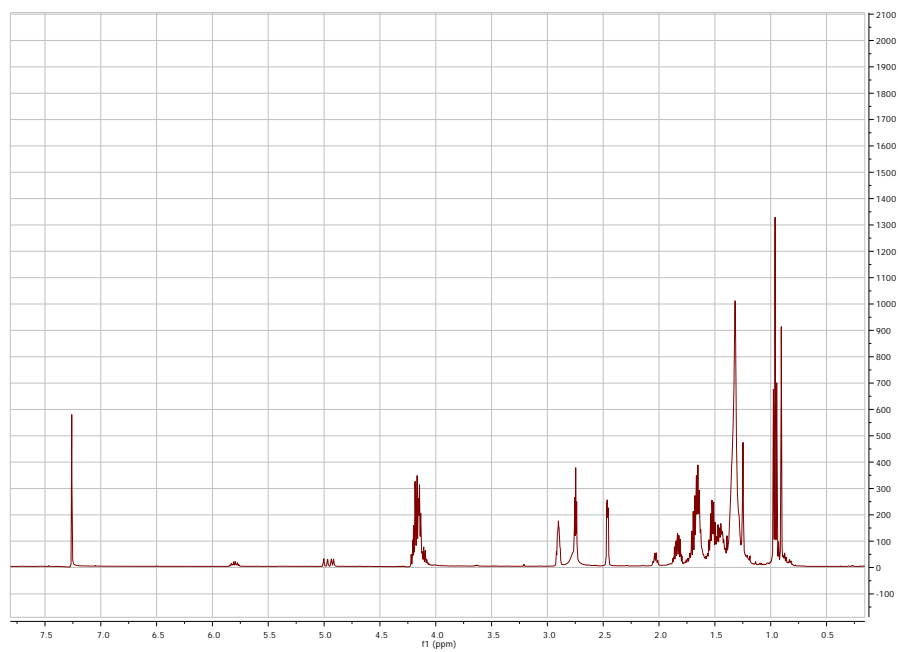
¹H NMR (500MHz, CDCl₃)



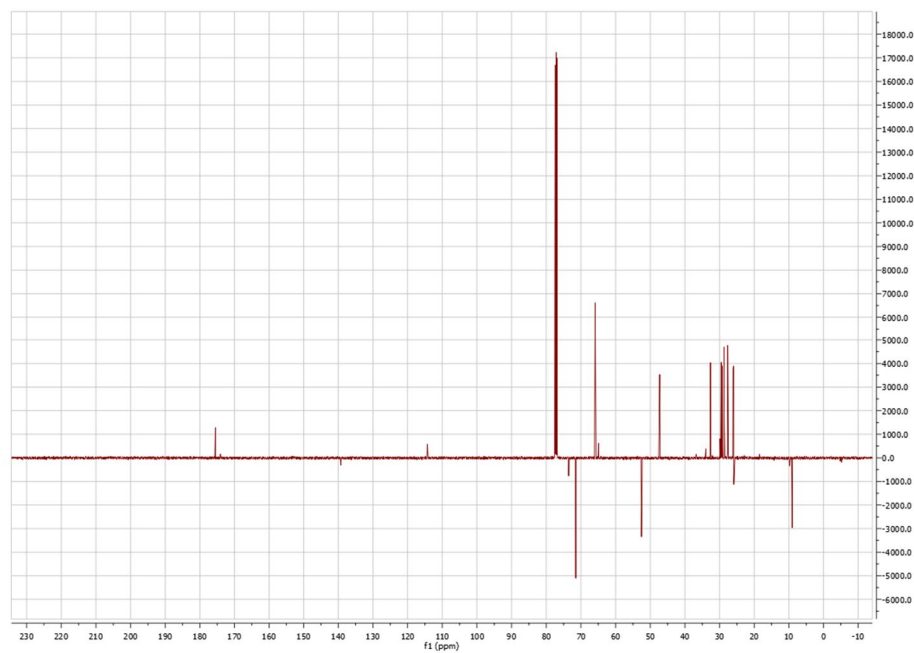
¹³C NMR (125MHz, CDCl₃)

Appendix B: Covalent Modification of *Vibrio cholerae* CqsS Spectra

Molecule 5-1

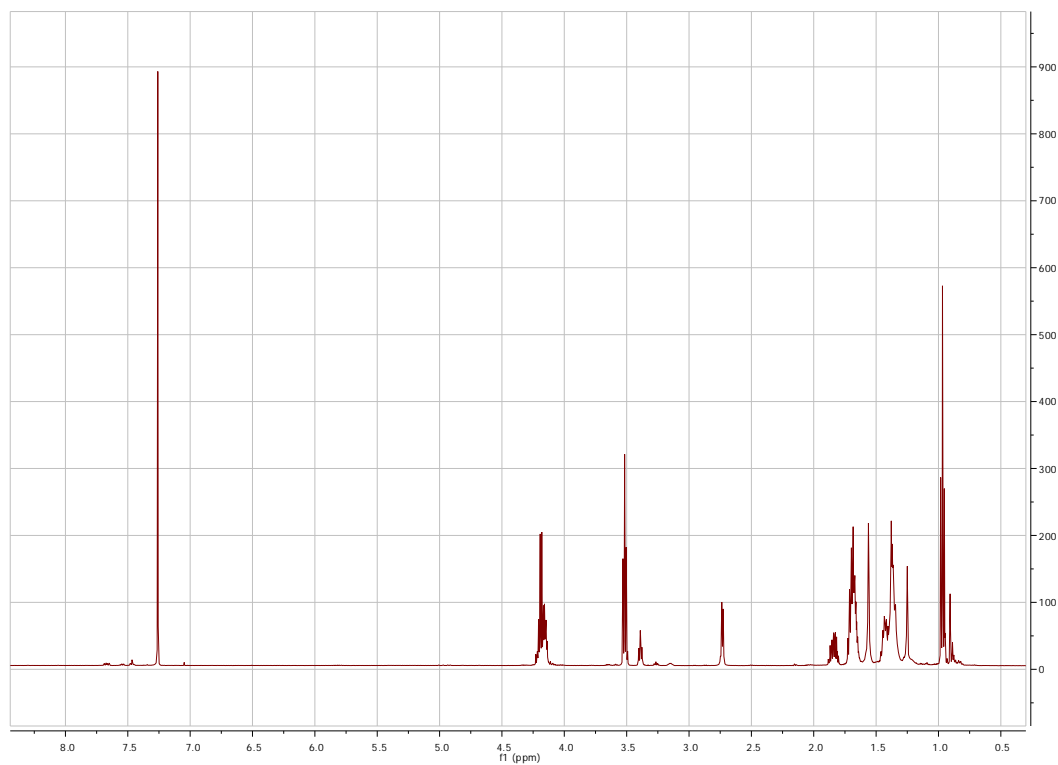


^1H NMR (500MHz, CDCl_3)

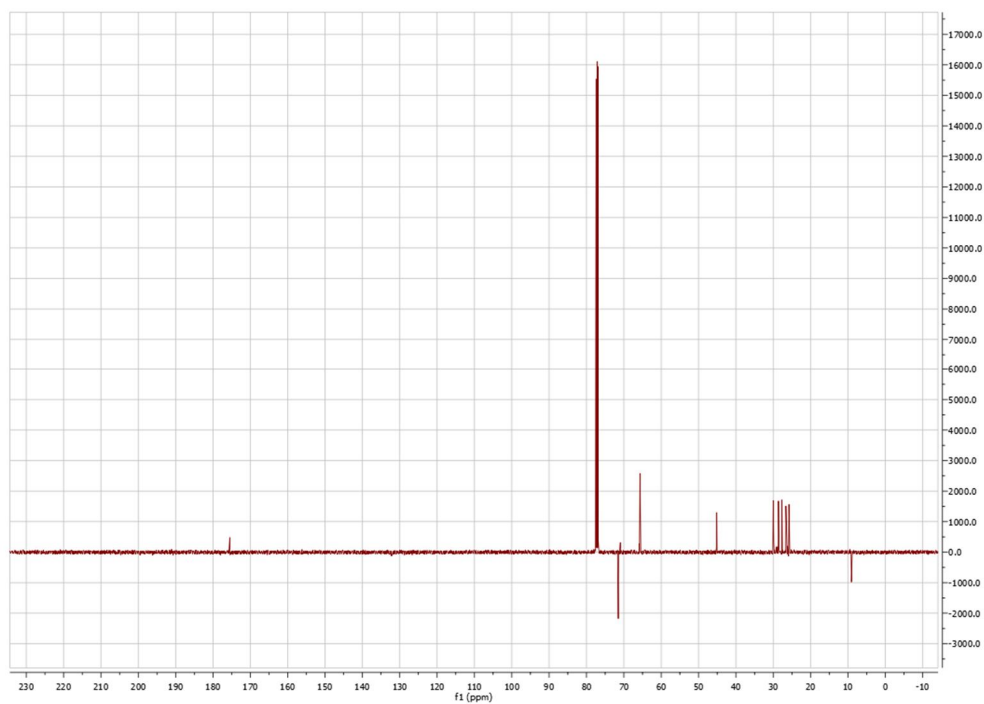


^{13}C NMR (125MHz, CDCl_3)

Molecule 5-3

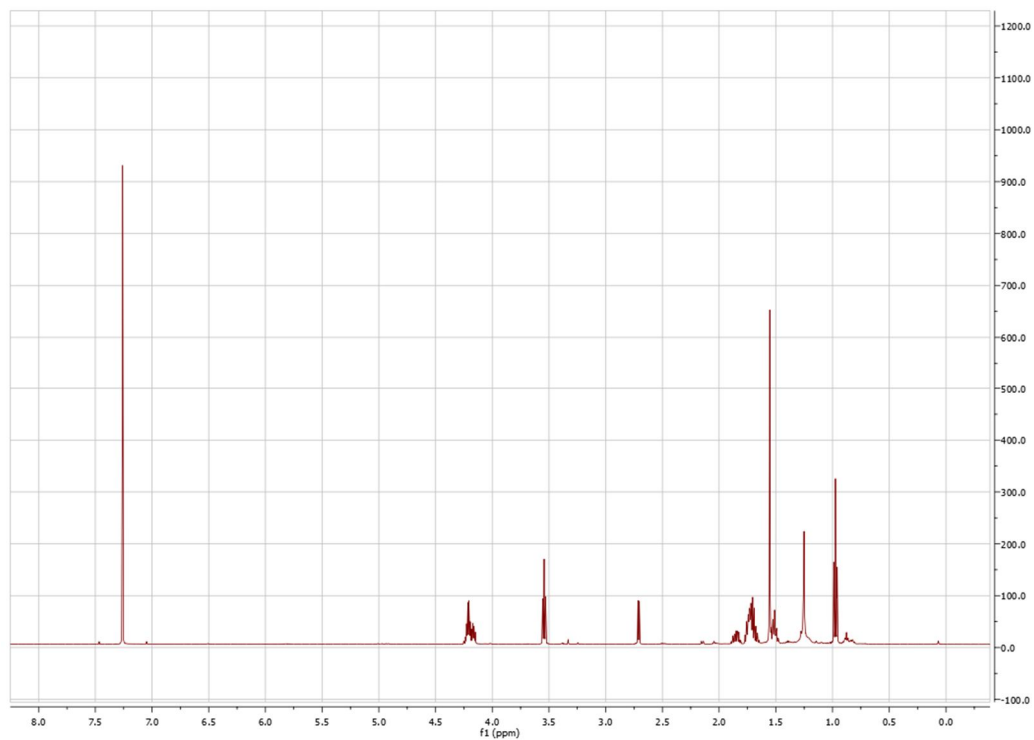


^1H NMR (500MHz, CDCl_3)

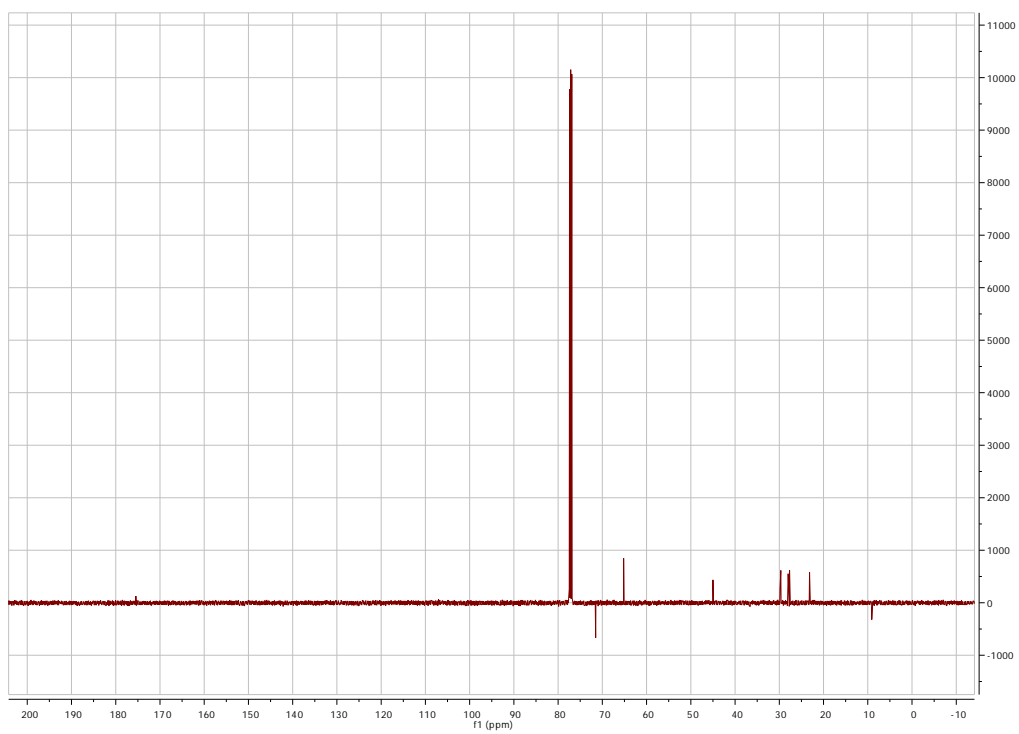


^{13}C NMR (125MHz, CDCl_3)

Molecule 5-4

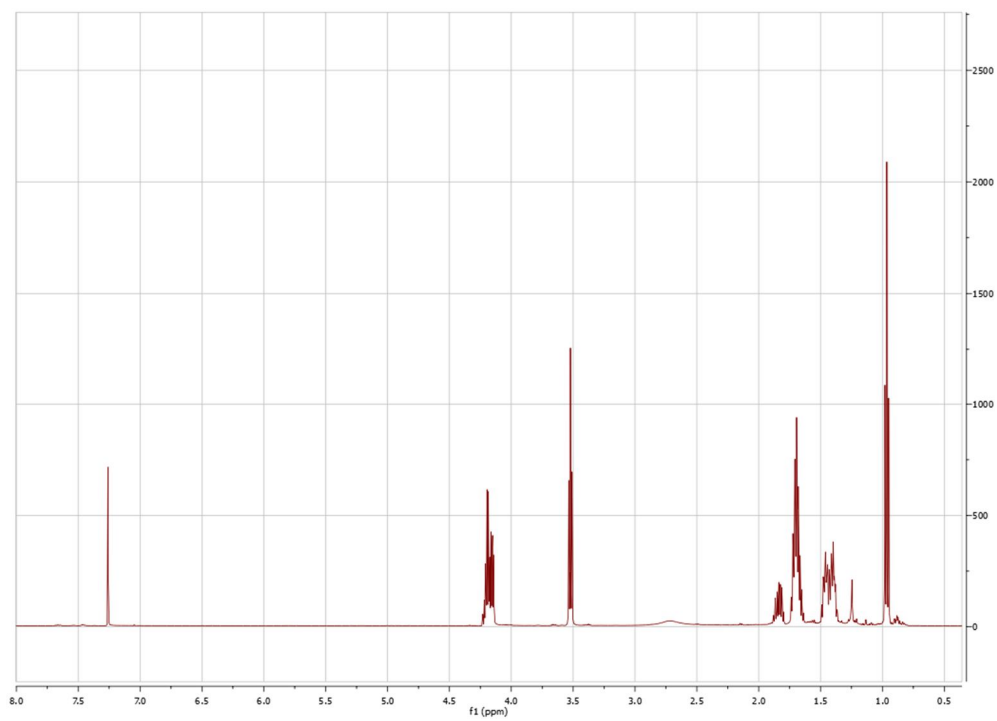


^1H NMR (500MHz, CDCl_3)

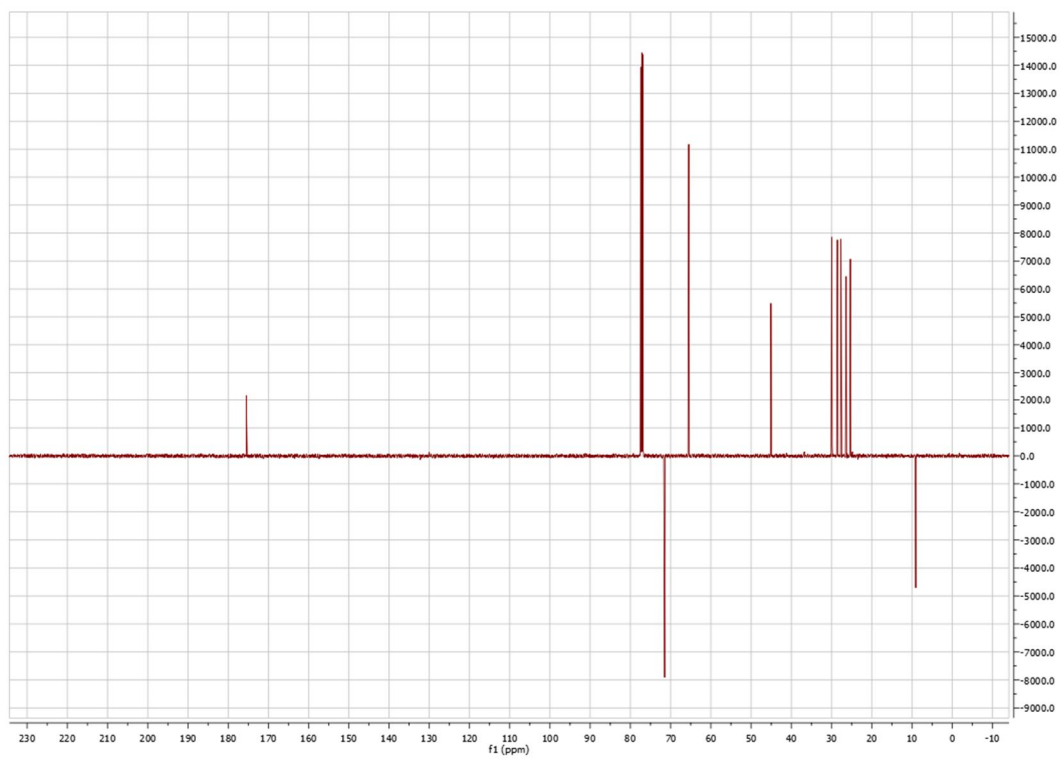


^{13}C NMR (125MHz, CDCl_3)

Molecule 5-5

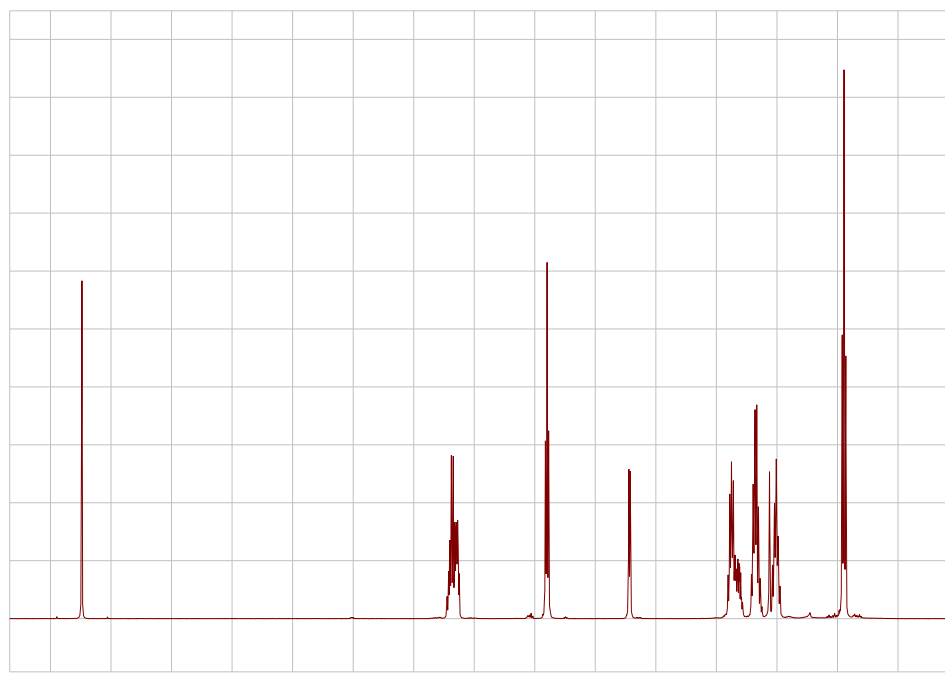


^1H NMR (500MHz, CDCl_3)

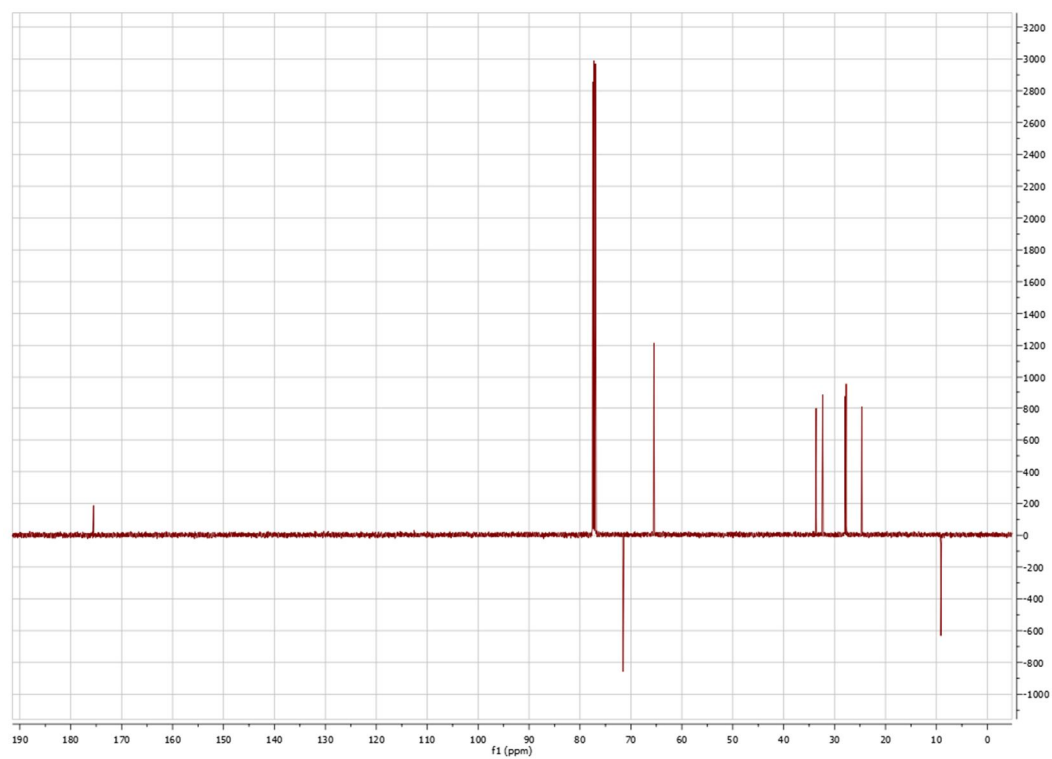


^{13}C NMR (125MHz, CDCl_3)

5-6

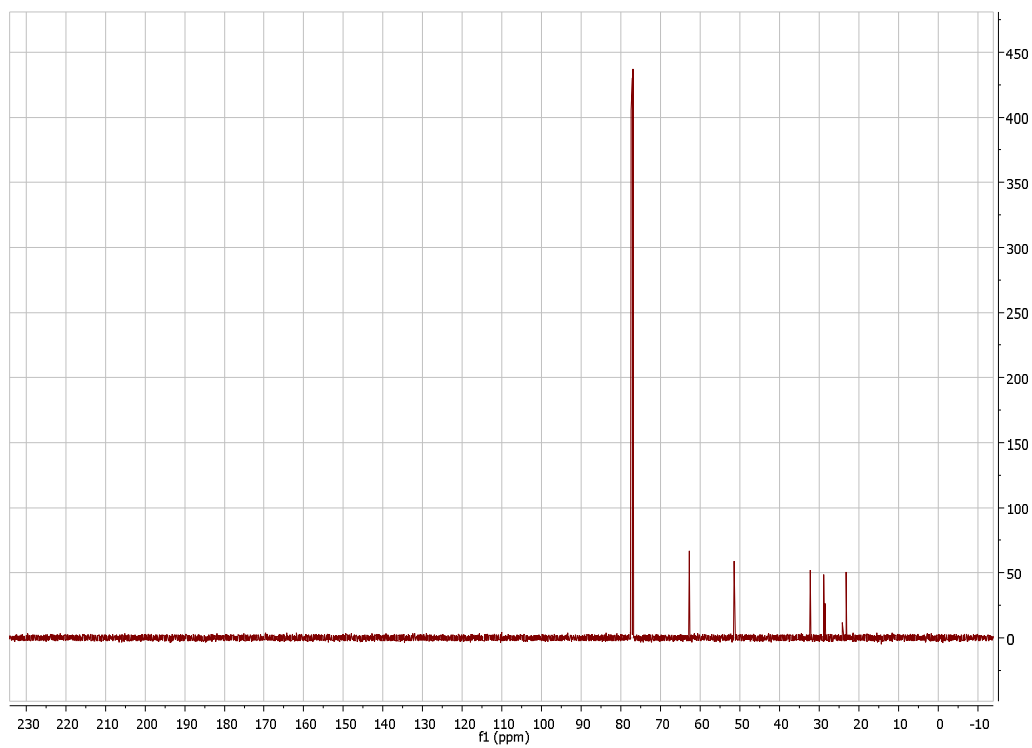
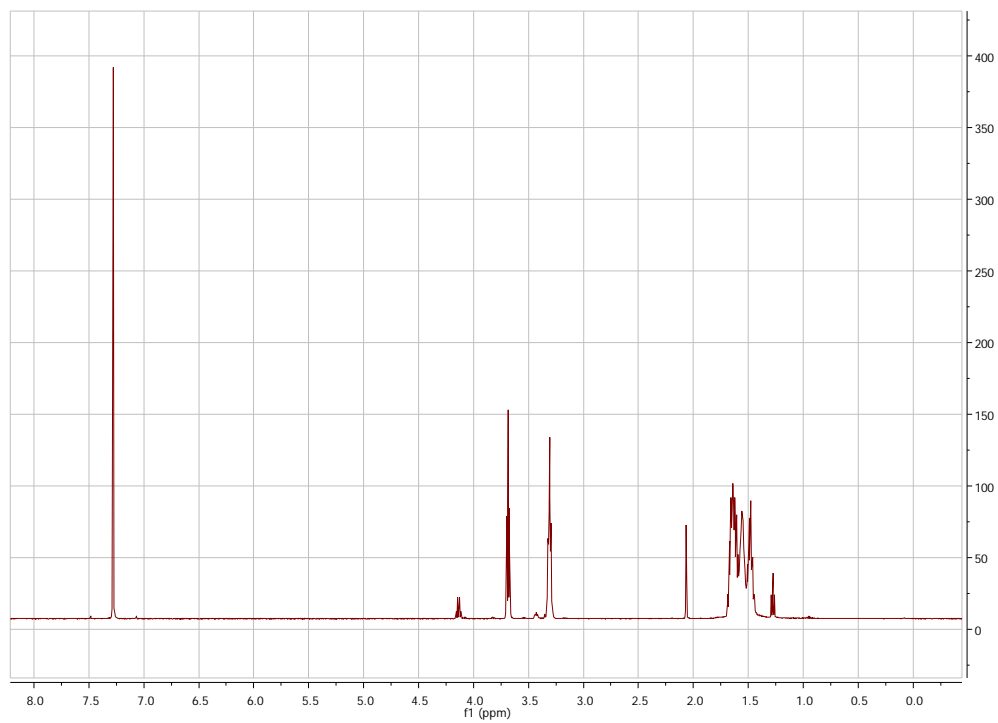


^1H NMR (500MHz, CDCl_3)

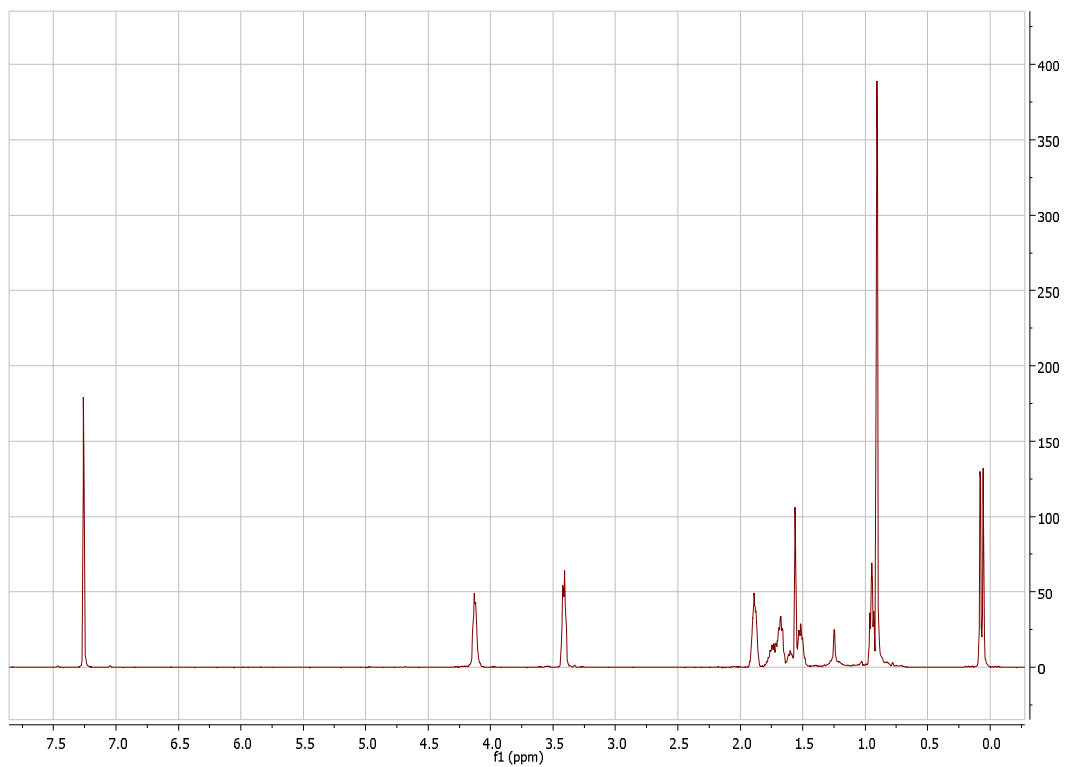


^{13}C NMR (125MHz, CDCl_3)

2-(*tert*-butyldimethylsilyoxy)butanoic acid

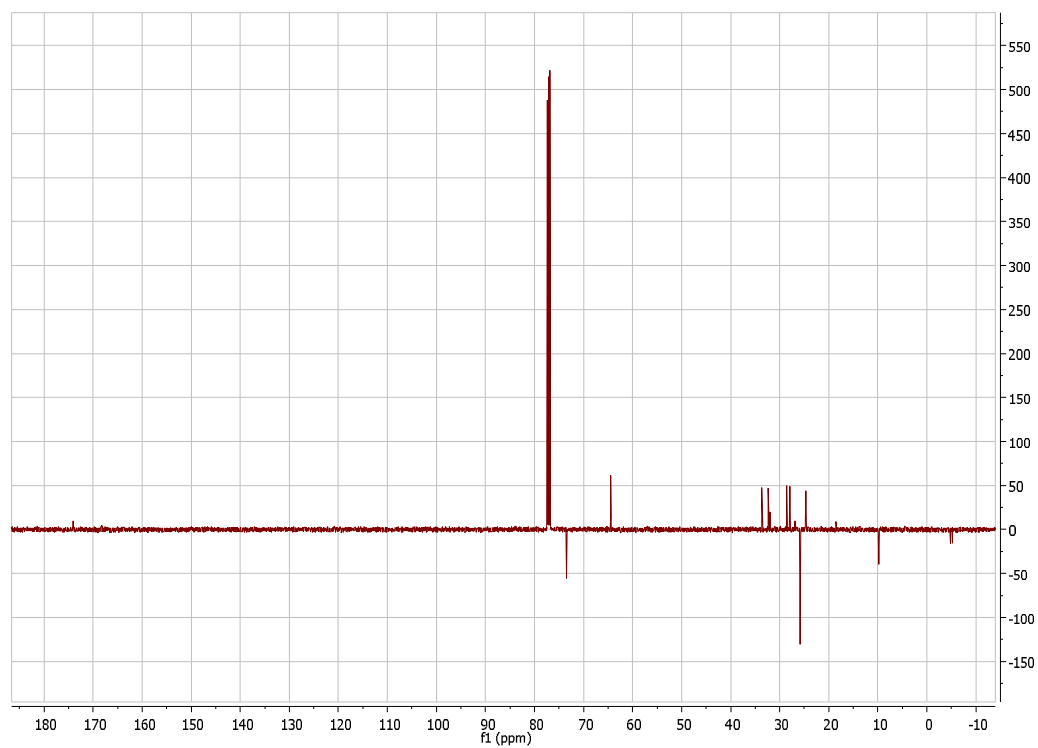


(1-(5-bromopentyloxy)butan-2-yloxy)(*tert*-butyl)dimethylsilane



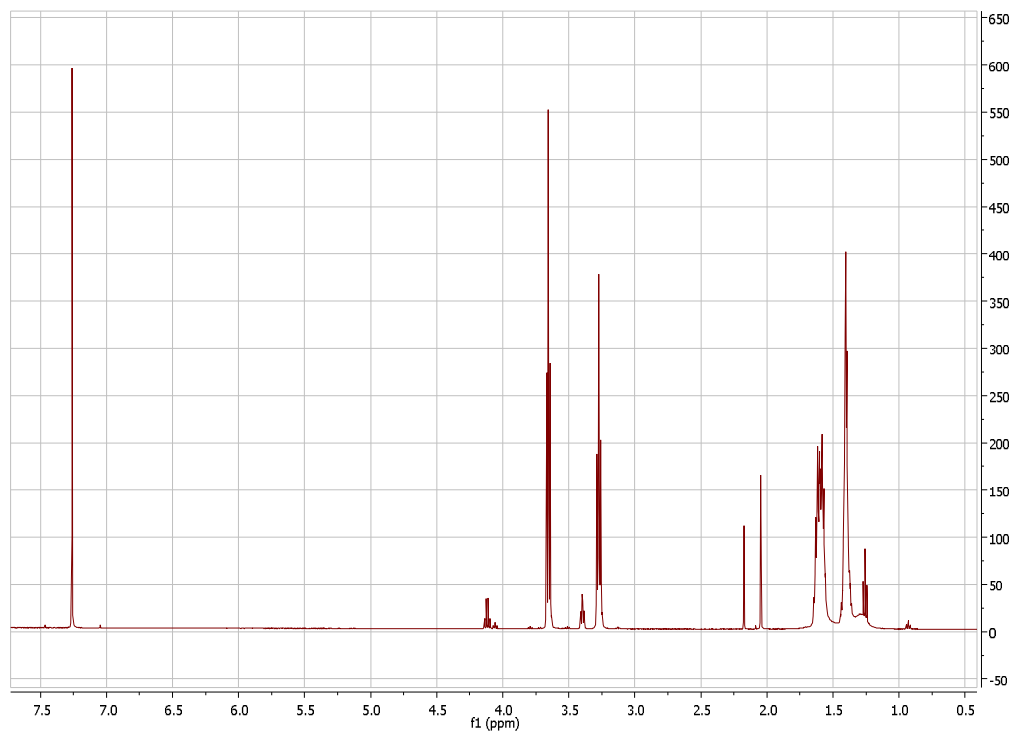
NMR (500MHz, CDCl₃)

¹H

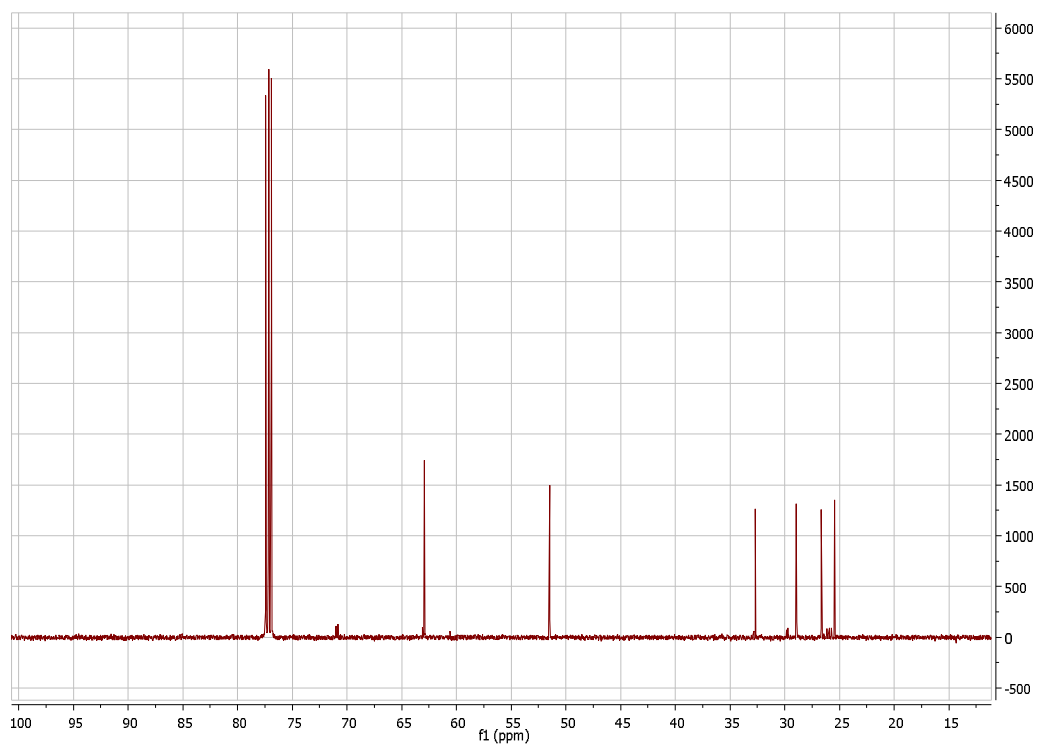


¹³C NMR (125MHz, CDCl₃)

6-azidohexan-1-ol

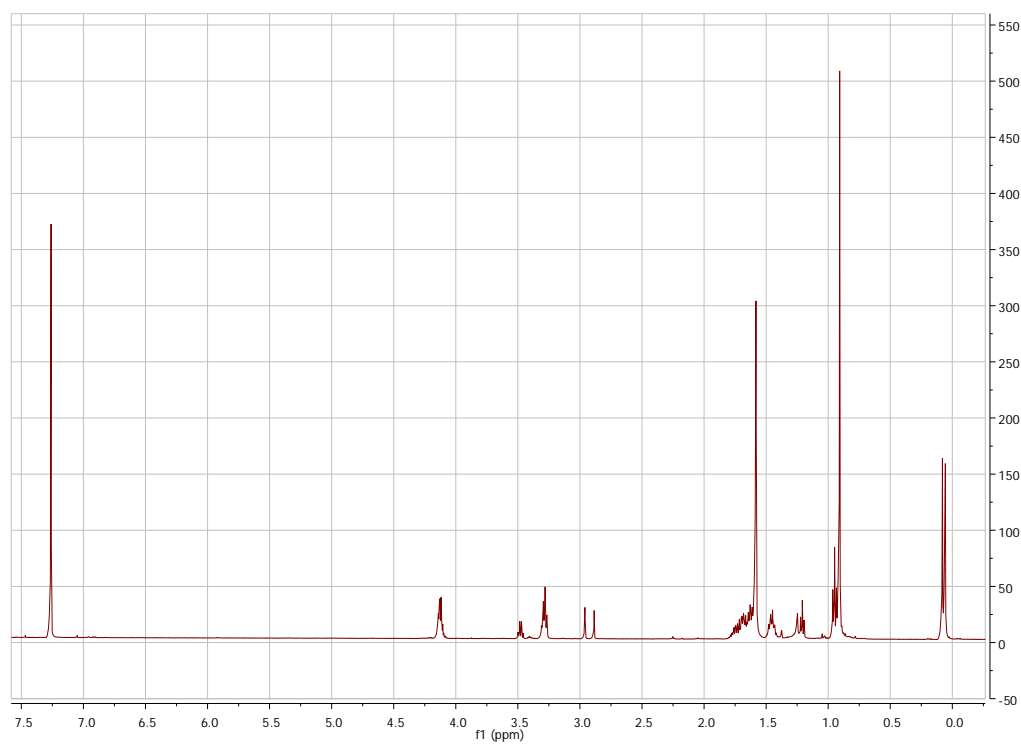


^1H NMR (500MHz, CDCl_3)

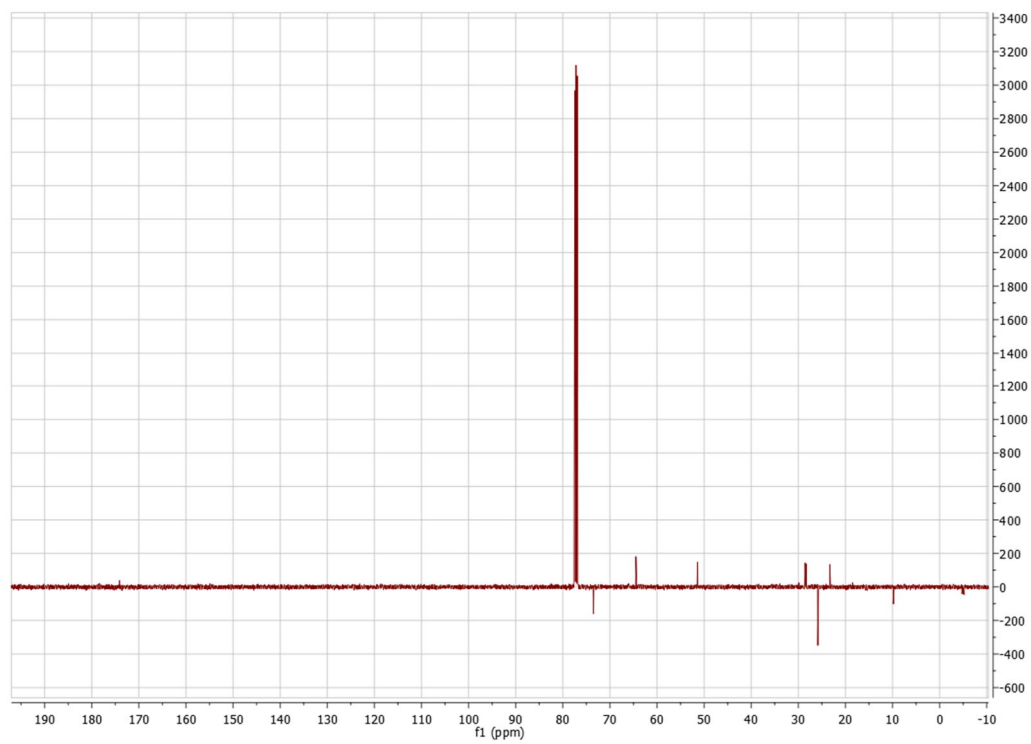


^{13}C NMR (125MHz, CDCl_3)

5-azidopentyl 2-(*tert*-butyldimethylsilyoxy)butanoate

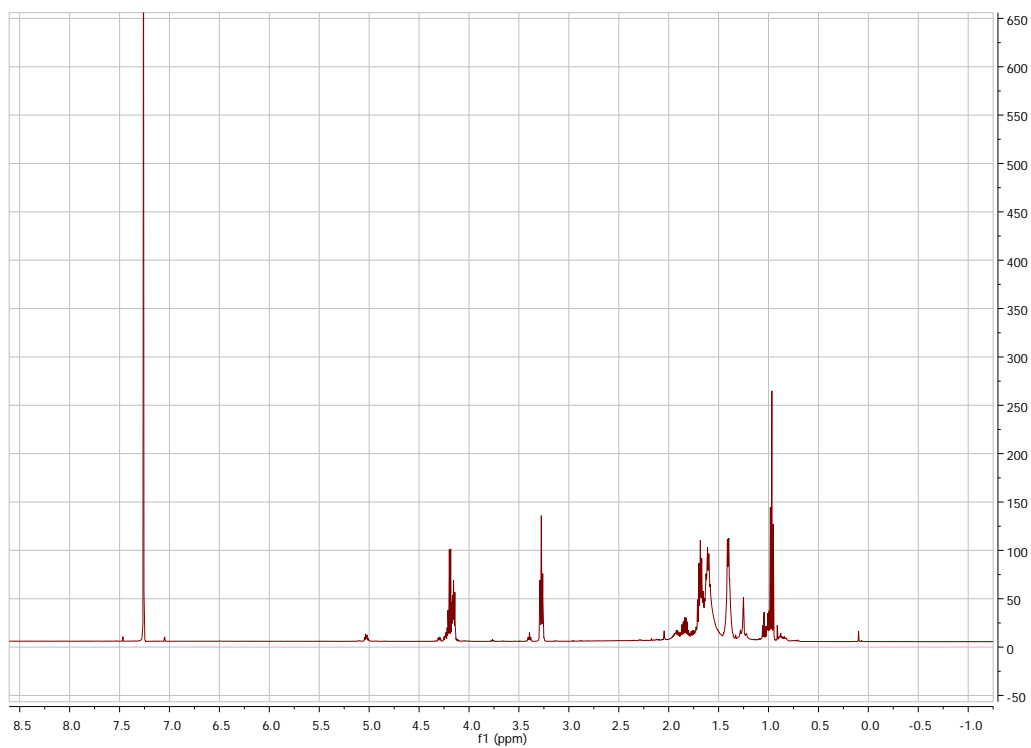


^1H NMR (500MHz, CDCl_3)

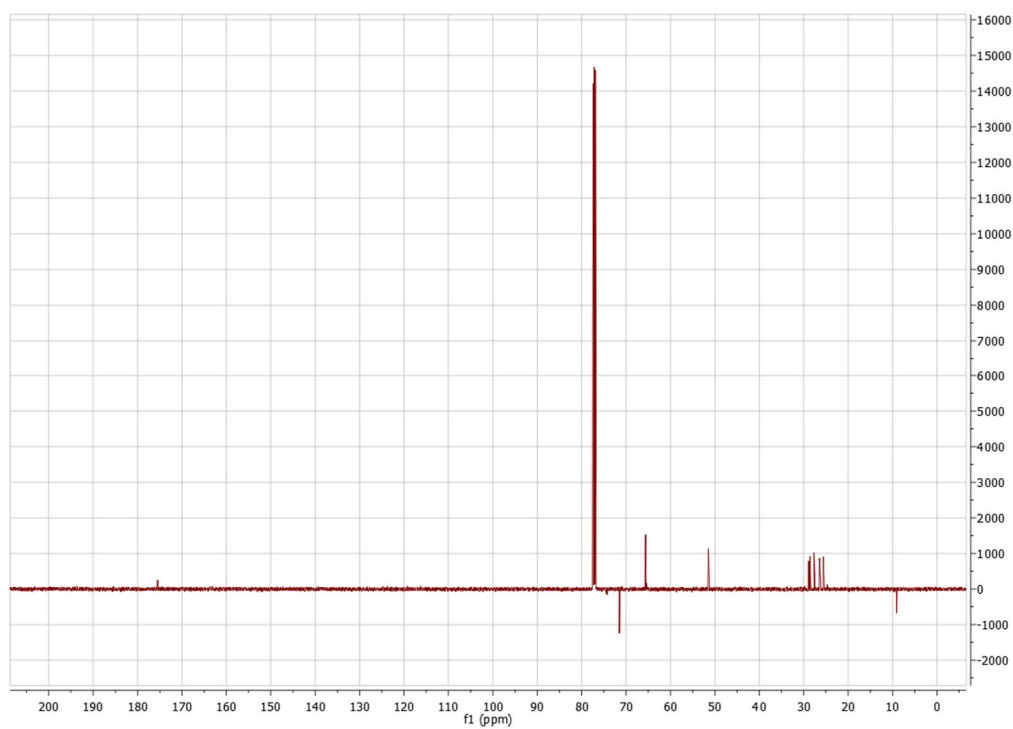


^{13}C NMR (125MHz, CDCl_3)

5-(2-chloroacetamido)pentyl 2-(*tert*-butyldimethylsiloxy)butanoate

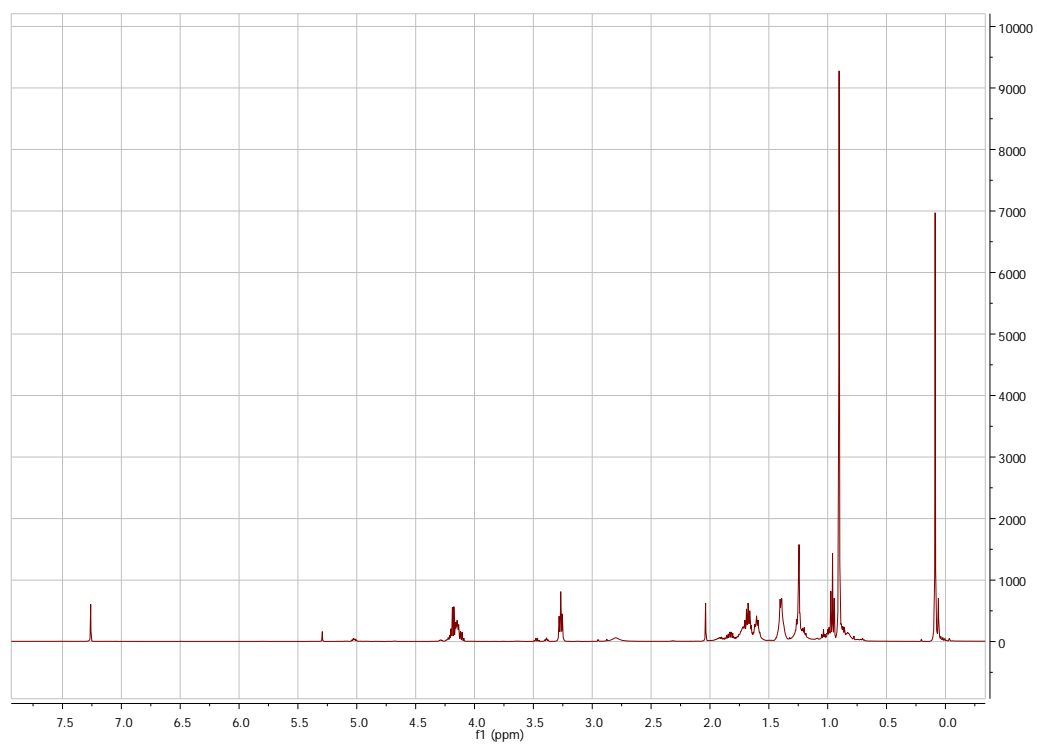


^1H NMR (500MHz, CDCl_3)

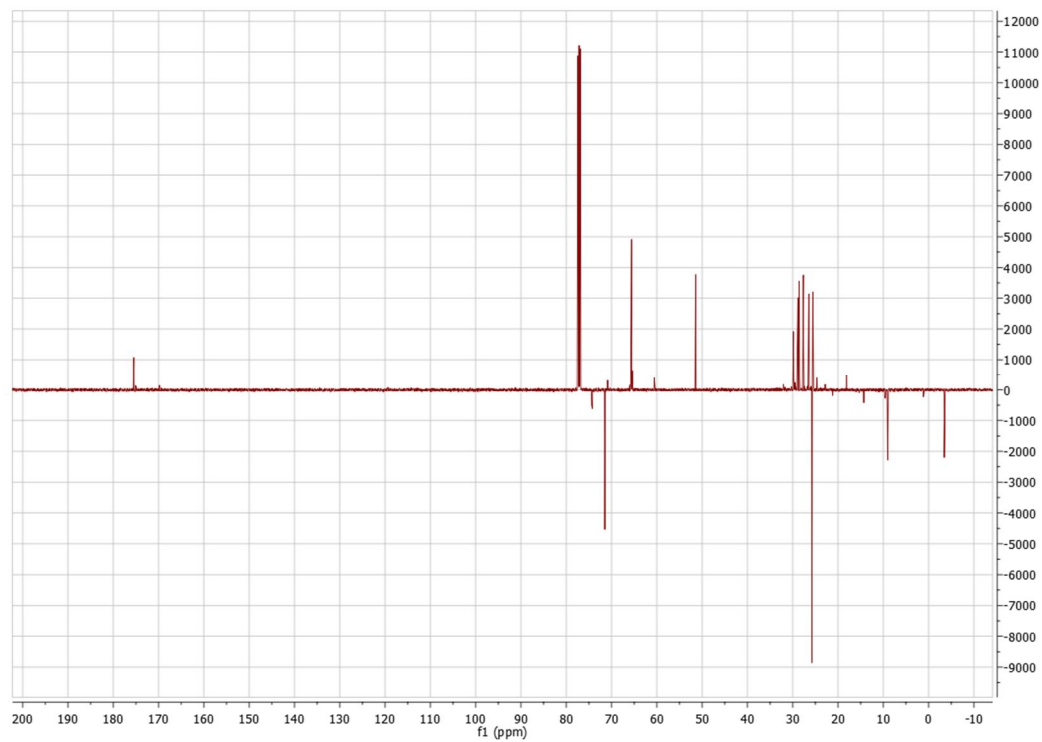


^{13}C NMR (125MHz, CDCl_3)

6-azidohexyl 2-(tert-butyldimethylsilyloxy)butanoate



^1H NMR (500MHz, CDCl_3)



^{13}C NMR (125MHz, CDCl_3)